CR 73479
AVAILABLE TO THE PUBLIC

Atmospheric Limitations On Remote Sensing Of Sea Surface Roughness By Means Of Reflected Daylight

S Q. DUNTLEY
C. F. EDGERTON
T. J. PETZOLD

SIO Ref 70-27
September 1970

Final Report
Contract NAS 12-2126
National Aeronautics and Space Administration
Ames Research Center

UNIVERSITY OF CALIFORNIA SAN DIEGO
SCRIPPS INSTITUTION OF OCEANOGRAPHY
VISIBILITY LABORATORY San Diego, California 92152

DOCUMENT CONTROL DATA - R&D

(Security classification of title, body of abstract and indexing annotation must be entered when the overall report is classified)

1 ORIGINATING ACTIVITY *(Corporate author)*
Visibility Laboratory
University of California
San Diego, California 92152

2a. REPORT SECURITY CLASSIFICATION
UNCLASSIFIED

2b. GROUP

3 REPORT TITLE

ATMOSPHERIC LIMITATIONS ON REMOTE SENSING OF SEA SURFACE ROUGHNESS BY MEANS OF REFLECTED DAYLIGHT

4 DESCRIPTIVE-NOTES *(Type of report and inclusive dates)*
Final Report

5 AUTHOR(S) *(Last name, first name, initial)*
Duntley, Seibert Q., Edgerton, Catharine F., and Petzold, Theodore J.

6 REPORT DATE
September 1970

7a. TOTAL NO OF PAGES
114

7b. NO OF REFS
16

8a CONTRACT OR GRANT NO
NAS-12-2126

b.

c.

d.

9a ORIGINATOR'S REPORT NUMBER(S)
SIO Ref. 70-27

9b OTHER REPORT NO(S) *(Any other numbers that may be assigned this report)*

10. AVAILABILITY/LIMITATION NOTICES
Distribution of this document is unlimited

11 SUPPLEMENTARY NOTES

12 SPONSORING MILITARY ACTIVITY
National Aeronautics and Space Administration
Ames Research Center

13 ABSTRACT

This report is a study of the limitations imposed by the earth's atmosphere on optical remote sensing of sea surface roughness from satellites and orbital spacecraft. It is concerned with the optical and meteorological conditions at a single ocean location and in the near infrared region of the spectrum.

There is a detailed description of the instrumentation used to make ground-based measurements of optical atmospheric data. The optical system, electronics, photocell circuit, and calibration procedures are defined.

DD FORM 1 JAN 64 1473

14 KEY WORDS	LINK A		LINK B		LINK C	
	ROLE	WT	ROLE		ROLE	WT
Optical Remote Sensing						
Vertical Path Radiance						
Vertical Beam Transmittance						
Contrast Reduction Meter						
Solar Transmissometer						
Sky Telephotometer						
Calibrations						

UNIVERSITY OF CALIFORNIA, SAN DIEGO
SCRIPPS INSTITUTION OF OCEANOGRAPHY
VISIBILITY LABORATORY
SAN DIEGO, CALIFORNIA 92152

ATMOSPHERIC LIMITATIONS ON REMOTE SENSING OF SEA SURFACE ROUGHNESS BY MEANS OF REFLECTED DAYLIGHT

S. Q. Duntley, C. F. Edgerton, and T. J. Petzold

SIO Ref. 70-27
September 1970

Final Report
Contract NAS-12-2126
National Aeronautics and Space Administration
Ames Research Center

Approved:

Seibert Q. Duntley, Director
Visibility Laboratory

Approved for Distribution:

William A. Nierenberg, Director
Scripps Institution of Oceanography

Contents

ABSTRACT

This report is a study of the limitations imposed by the earth's atmosphere on optical remote sensing of sea surface roughness from satellites and orbital spacecraft. It is concerned with the optical and meteorological conditions at a single ocean location and in the near infrared region of the spectrum.

There is a detailed description of the instrumentation used to make ground-based measurements of optical atmospheric data. The optical system, electronics, photocell circuit, and calibration procedures are defined.

INTRODUCTION

This is the final report under National Aeronautics and Space Administration Contract NAS-12-2126. The objective was to study the limitations imposed by the earth's atmosphere on optical remote sensing of sea surface roughness from aircraft and orbital spacecraft. The contract required initial studies of the optical and meteorological conditions at a single ocean location and in the near infrared region of the spectrum. The location extended from San Diego to San Clemente Island, 80 miles WNW of San Diego.

ATMOSPHERIC LIMITATIONS ON REMOTE SENSING

The principal effect of the atmosphere upon remote sensing by visible light results from the scattering of sunlight and skylight upwards toward the orbital spacecraft. Every downward-looking path of sight is luminous because of this scattering. Even if some area on the ground is completely black, i.e., has zero inherent luminosity, it appears to be luminous when viewed from space. The light in this case is entirely due to atmospheric, scattering. Measurement of the luminosity by means of an in-flight telephotometer yields a value of *path luminance*. If the measuring device responds only to monochromatic light of some wavelength, its reading denotes *spectral path radiance*. If the instrument responds to some range of wavelengths, *path radiance for that particular instrument* is measured.

Collection of appropriate in-flight optical atmospheric data is expensive and difficult, but no alternative exists with respect to the needs of designers and users of optical remote sensing systems operated in the troposphere. Data applicable to systems for use at very high altitude or in orbit can be obtained inexpensively and easily from the ground however, as will be shown in this report.

PATH RADIANCE

Typical units of spectral path radiance are watts steradian^{-1} meter^{-2} nanometer^{-1} because each unit of area in the entrance pupil of the measuring instrument receives radiant power within a defined spectral bandwidth from a specified solid angle within the field of view. Rigorously, spectral radiance is the limit approached by the ratio defined above as the solid angle, the receiving area, and the wavelength interval respectively approach zero.

Since all of the light included in the path radiance is placed there by scattering in the atmosphere, it contains no information about objects on the ground. Path radiance is ordinarily the same, moreover, for every part of any reasonably small field of view; i.e., it is usually identical in all parts of the picture.

Path radiance depends upon both the optical state of the atmosphere and the nature of the lighting on the path by the sun, the sky, and the ground. It adds to whatever image-forming light from the ground reaches the orbital spacecraft. Thus, it veils the image by reducing its apparent contrast. If the path radiance is great enough the apparent contrast of the object is below the threshold of the viewing system (eye, camera, etc.) and the object is not seen. Obviously, knowledge of path radiance is a critical requirement for the design of optical remote sensors.

TRANSMITTANCE OF THE ATMOSPHERE

Light reflected or emitted by objects on the ground carries information about these objects. Some of it departs in the direction of the orbital spacecraft but not all of that light is received. A sizeable fraction of the image-forming light coming from the ground may encounter atmospheric particles and be scattered out of the path of sight. That fraction of image-forming light which does reach the remote sensor without having experienced disruptive scattering is called the *beam transmittance* of the path of sight. Additional adjectives such as *spectral, luminous, instrumental,* etc. are used exactly as in the case of path radiance.

Beam transmittance is a property of the atmosphere but not of its lighting. In atmospheres having horizontal uniformity, beam transmittance does not depend upon the azimuth of the path of sight relative to the sun. It is always the same for a given path of sight regardless of whether the image-forming light travels upward or downward. Knowledge of beam transmittance is therefore another important requirement for the design of optical remote sensors.

HORIZONTAL UNIFORMITY

In many cases an atmosphere can be validly and usefully approximated as having horizontal uniformity; i.e., the only important optical variations are vertical. It is commonplace to think of the atmosphere as a vast assemblage of flat horizontal layers, but this is by no means always true. Minor point-to-point changes in optical atmospheric properties are often recorded by instrumented aircraft in horizontal flight. Very little reliable statistical information on the nature of this type of variability in the atmosphere exists. Fortunately, the effect appears to be nearly negligible on most of the occasions when the atmosphere is clear enough to see down from high altitudes. Consequently, horizontal uniformity in the atmosphere will be assumed here.

OTHER OPTICAL ATMOSPHERIC PROPERTIES

Several other optical atmospheric properties are defined, calculated or measured, and tabulated in the

literature[1,2]. Some of these (e.g., attenuation coefficient, attenuation length, path function, volume scattering function) are used to calculate the beam transmittance and path radiance of particular paths of sight. Others (e.g., equilibrium radiance) have special uses in atmospheric modeling[3] or in the smoothing of data. The end use of all these properties is the generation of beam transmittance and path radiance, or some function of them, for particular atmospheric paths of sight.

SELECTION OF SPECTRAL REGION

The satellite camera sees the apparent radiance of the sea which contains the space-averaged radiance of the surface of the sea plus the path radiance due to sunlight and skylight scattered toward the satellite by the atmosphere throughout the path of sight. Another component arises from the daylight which has penetrated into the depths of the sea and has been redirected upward by the scattering processes within the water. Fortunately, this scattered component can be eliminated completely if the satellite makes its observations in terms of red or infrared light. At these wavelengths the water molecule absorbs very strongly. Thus, the component of the daylight which enters the ocean is absorbed so completely that no appreciable amount of it is scattered upward toward the satellite*. The present study used the near infrared region of the spectrum for this reason.

MEASURED OPTICAL ATMOSPHERIC DATA

Measured data on the path radiance and beam transmittance of real atmospheres are not plentiful. They are collected by three means:

1. By photographic aircraft over-flying test panels set up and monitored on the ground;
2. By instrumented aircraft equipped with photoelectric recording equipment for measuring optical scattering and many aspects of the light incident on the aircraft from all directions. Suitable integration of vertical profiles of such data enables path radiance and beam transmittance to be found;
3. By ground-based instruments which measure apparent radiance at the center of the solar disk to obtain the total beam transmittance of the atmosphere and make radiance maps of the sky from which path radiance can be calculated for paths of sight through the total atmosphere.

The first two of these methods relate strictly to paths of sight from aircraft to earth. In very clear weather the obtained data can be extrapolated upward by means of standard atmosphere data. But such extrapolations are uncertain when any form of clouds, even very tenuous ones, are above the maximum altitude at which measured data are taken. The third procedure provides data which are strictly applicable only to remote sensing from orbital spacecraft or satellites. It is, by far, the easiest and cheapest source of reliable atmospheric data and is the only method with which this report is concerned.

GROUND-BASED MEASUREMENTS

Techniques developed within the Visibility Laboratory were used to construct two contrast reduction meters for this project to collect optical atmospheric data. The equipment and methods for calibration are described in the following section. Values for vertical path radiance and vertical beam transmittance

* This concept has been explained in more detail in an earlier report[4].

were derived from the ground-based measurements through methods developed[5] and validated[6] within the Visibility Laboratory.

The vertical path radiance is derived from the ground-based measurements of beam transmittance and the sky radiance as follows:

$$N^*_\infty(\infty,\theta,\phi) = N^*_\infty(0,\theta',\phi')\left[\frac{1 - T_\infty(\infty,\theta)}{1 - T_\infty(0,\theta')}\right]. \tag{1}$$

Here:

$N^*_\infty(\infty,\theta,\phi)$ is the path radiance of the downward inclined vertical path of sight θ,ϕ from the surface of the sea to any altitude outside the atmosphere, i.e., $z = \infty$, and $N^*_\infty(0,\theta',\phi')$ is the path radiance, i.e., the radiance of the sky as seen from the surface of the sea, of an upward inclined path of sight θ',ϕ' which has the same angle from the sun as does the downward inclined path of sight θ,ϕ.

The $T_\infty(\infty,\theta)$ is the vertical beam transmittance of the downward inclined path of sight θ,ϕ from the surface of the sea to any altitude outside the atmosphere (∞) and $T_\infty(0,\theta')$ is the beam transmittance from the surface of the sea to space for the inclined path of sight defined by θ' and ϕ'.

The beam transmittance for the path of sight from the surface of the sea in the direction of the sun is obtained directly from the solar transmissometer measurement of the apparent radiance of the sun ${}_sN_\infty(0,\theta_s,0)$ and the inherent radiance of the sun outside the atmosphere of the earth ${}_sN_o$ by the following equation:

$$T_\infty(0,\theta_s) = \frac{{}_sN_\infty(0,\theta_s,0)}{{}_sN_o} - \frac{N^*_\infty(0,\theta_s,0)}{{}_sN_o}. \tag{2}$$

Because the second term on the right is usually not over 1 percent of the first term it can be neglected. Then,

$$T_\infty(0,\theta_s) \approx \frac{{}_sN_\infty(0,\theta_s,0)}{{}_sN_o}. \tag{3}$$

The inherent radiance of the sun outside the atmosphere of the earth ${}_sN_o$ has been deduced from the literature [7–9].

After relative optical air mass correction[10], data from the solar transmissometer provide the two values of beam transmittance needed for Eq. (1). This is the only time that the optical air mass reference will be used; all other air mass references are to meteorological air mass types.

The values of beam transmittance required in Eq. (1) are obtained from solar beam transmittance by means of the relations

$$T_{\infty}(\infty,\theta) = T_{\infty}(0,\theta_s)^{\cos\theta_s} \tag{4}$$

and

$$T_{\infty}(0,\theta') = T_{\infty}(0,\theta_s)^{\cos\theta_s/\cos\theta'}. \tag{5}$$

The radiance of the sky as seen from the ground or the surface of the sea along the upward inclined path of sight θ' and ϕ' is measured by means of a sky telephotometer on the ground. It should be noted that normally there are a number of skyward directions for which the path of sight has the same angle from the sun as does the path of sight looking down from space to the surface of the sea. Data for any of these paths may be used in Eq. (1) and should produce the same value of $N^*_{\infty}(\infty,\theta,\phi)$. Usually the measurement is made for an upward inclined path at the azimuth 180 degrees from the sun. When the sun is at an elevation of more than 45 degrees, the path used is 90 degrees from the sun in the 180-degree azimuth. Figure 1 illustrates the position of the sky telephotometer for measuring the sky radiance at the azimuth 180 degrees from the sun, for the same angle (β) from the sun as for a satellite camera looking vertically downward. The diagram represents a plane passed through the azimuth of the sun.

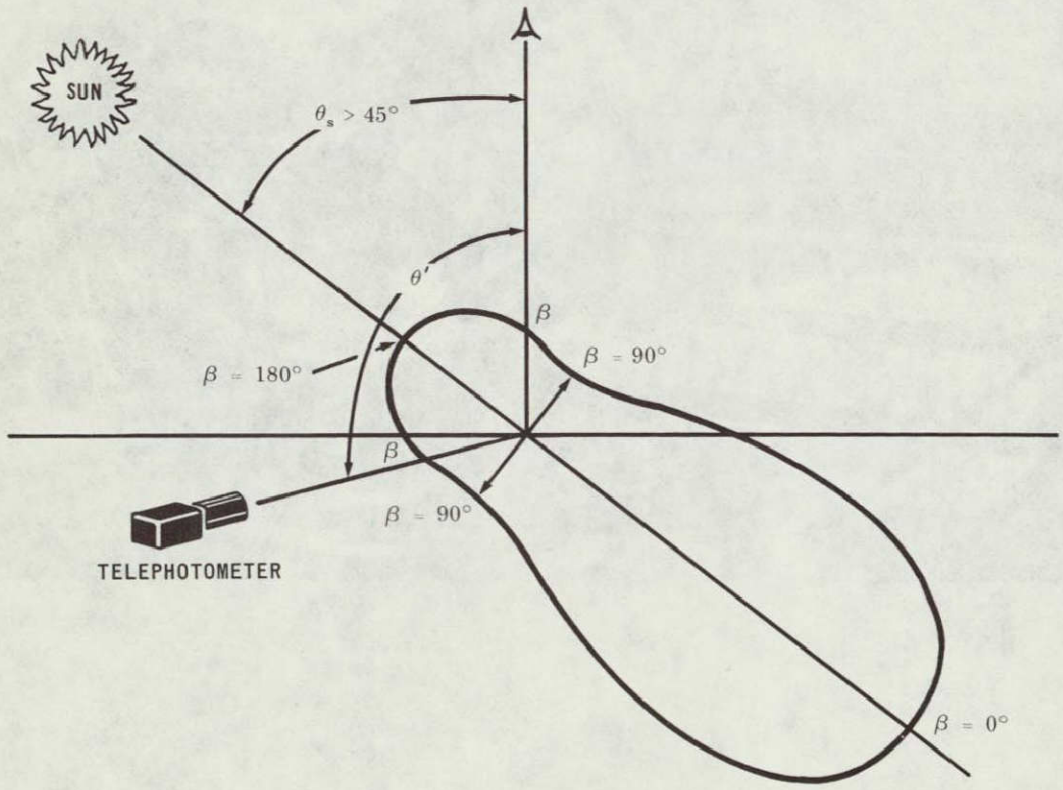

Fig. 1. Scattering Angle from the Sun (β) for Observer and Telephotometer.

If the sky contains scattered or broken clouds the measurements of sky radiance must be made in clear portions of the sky only. If no appropriate clear region of the sky can be found, the method cannot be used.

Contrast Reduction Meter

THE CONTRAST REDUCTION METER

GENERAL DEVELOPMENT OF THE CONTRAST REDUCTION METER

Over the years an instrument system has been developed at the Visibility Laboratory and used successfully on several projects both in the field and at the Laboratory site on Point Loma in San Diego. The primary function of this system, the contrast reduction meter (CRM), is to measure three radiometric quantities which result from the irradiation of the earth by the sun and from the optical properties of the atmosphere. The three quantities are: (1) apparent radiance of the central portion of the solar disk; (2) radiance of any point of the sky; and (3) irradiance arriving on a horizontal plane. The spectral region over which the measurements are made is determined by the spectral response of the photodetector used and the color filters selected. Several different models of the CRM have been fabricated at the Laboratory and the two identical models built especially for this project will be identified here as Serial No. 1 and 2.

The CRM is a marriage of three optical light collection systems with one photodetector for all three systems. The system desired is selected manually. These three optical systems are:

1. *Solar Transmissometer:* This consists of simply a telescope which uses a pinhole aperture to image the sun on a stop containing a second pinhole.
2. *Sky Telephotometer:* This is a telescope type system designed to collect light from a restricted field of view (4.4 degrees). It is at the rear of the solar transmissometer.
3. *Irradiance Collector:* This collector is designed to accept light in proportion to the cosine of the angle of incidence. It slips over the sunshade of the sky telephotometer to convert from a radiance to an irradiance type measurement system.

The optics of all the CRM's fabricated and used by the Visibility Laboratory are essentially identical except for small differences in the focal lengths of the lenses used in the sky telephotometer. In all the CRM models the sky telephotometer optical axis is 90 degrees to the optical axis of the solar transmissometer. In normal usage the CRM is mounted so that when the solar transmissometer is aimed at the sun, the sky telephotometer is looking at a point in the sky 90 degrees from the sun in the plane through the sun and the zenith point.

The major modification used for the first time on CRM's Serial No. 1 and 2 is the photometer for detecting, amplifying, and displaying the signal. All earlier versions used photomultiplier tubes for the detector. The more recent models, excluding Serial No. 1 and 2, had thermoelectric units within which the photomultiplier is installed and where its temperature is closely controlled to avoid the changes in response most photomultiplier tubes exhibit with changes in temperature. The photometer circuit used was such that the response was quasi-logarithmic and the photometer was capable of covering a range of many orders of magnitude. Because of this, it was necessary to obtain a complete calibration curve for each CRM and to apply this calibration to each data point when reducing the data. When used for its intended purpose, a large dynamic range is not required in the CRM to collect the data and it was decided that a linear response would be more convenient for the user.

The solar transmissometer presented a problem however. Calibration procedures required that it be calibrated at a level much lower than the one at which data were obtained and this span was bridged over several orders of magnitude by a relative calibration of the photometer. A review of the calibration procedures led to a revised method for calibrating the solar transmissometer and in general all absolute calibrations are now made within the range over which data are obtained.

It was also decided to investigate the possible use of a solid state detector to replace the photomultiplier. It was felt that this would greatly simplify the photometer and enhance the reliability of the CRM. A silicon solar cell was selected for study on the basis of its spectral response in the regions of interest and its good temperature stability characteristics. The detector selected did prove to be adequate for this application. Testing showed excellent stability in the visible region of the spectrum but a change in sensitivity with temperature was found in the near infrared region. A temperature-compensating circuit was therefore devised. This compensation is automatically switched into the circuit whenever data are collected within the near infrared region.

The CRM's Serial No. 1 and 2 have two filters either of which can be selected by the operator. Depending upon the filter used, the photometer response is either a visual photopic one or one in the near infrared between 700 and 1100 nanometers (10-percent points). Thus six channels of information are obtained, three in photometric units and three in radiometric units:

	Photometric (photopic)	**Radiometric (700 to 1100 nanometers)**
Solar Disk	Apparent Luminance (lumens steradian^{-1} feet^{-2})	Apparent Radiance (watts steradian^{-1} feet^{-2})†
Sky	Luminance (lumens steradian^{-1} feet^{-2})	Radiance (watts steradian^{-1} feet^{-2})
Downwelling	Illuminance (lumens feet^{-2} or foot-candles)	Irradiance (watts feet^{-2})

To help the operator check the functioning of the photometer and obtain data on the long term stability of the photometer, a stable reference source has been installed within the CRM Serial No. 1 and 2 packages. When the reference reading is taken, the filter mechanism inserts a shutter in front of the photometer, blocking all entering light, and the silicon photodetector is exposed to the flux from a small

† A value in watts steradian^{-1} feet^{-2} x 10.764 yields a corresponding value in watts steradian^{-1} meters^{-2}.

lamp which is powered by a very stable voltage source. Thus seven channels of information are obtainable. These are the three optical functions of apparent solar radiance, sky radiance, and irradiance, each in two spectral regions, and the calibration reference signal. Each of the channels has its own span or gain circuit which is automatically brought into use when the optical mode/color filter combination or reference lamp is selected by the operator. During calibration, each of these seven channels is individually adjusted so that the significant figures of the output voltage are the significant figures of the parameter being measured in absolute units. The output voltage is displayed on a digital voltmeter on the control console and is also available in digital format for recording on tape or driving a printer, should either be desired. The linear response direct readout control console has proved to be quite desirable. Both data collection and calibration procedures are simplified and less time consuming. The data read from the console are in absolute units and directly useable, without further processing, as inputs for the equations from which vertical beam transmittance and vertical path radiance are derived.

USES OF THE CRM MODELS (Refer to CRM Serial No. 1 and 2 operation manual for detailed operating instructions.)

OPTICAL TRANSMISSION PROPERTIES OF THE TOTAL ATMOSPHERE

The CRM is frequently used to obtain data from which optical transmission properties of the total atmosphere (from space to the earth's surface) can be computed. Specifically, the information obtained can be used to compute the amount that the contrast of objects on the surface is reduced by the passage of the optical signal through the atmosphere, hence the name contrast reduction meter. Later sections of this report discuss the use of the data in detail.

MOUNTING

The CRM is usually placed on a sturdy astronautical type equatorial mount adapted to this use. It is a good practice to have the equatorial mount firmly secured to a rigid support such as a large diameter pipe imbedded vertically in a concrete pad or bolted to a solid platform.

EQUATORIAL COORDINATE

If continuous data of apparent sun radiance are desired, it is convenient to set up the mount as would be done for a telescope, with the equatorial axis aligned with the north/south axis of the earth. This facilitates tracking of the sun. Occasionally a clock drive has been used successfully and then only infrequent adjustments are necessary to correct for drift of the sun in declination at certain seasons of the year when this drift is most rapid and for atmospheric refraction during early and late periods of the day.

ELEVATION AZIMUTH

If data are taken infrequently, an elevation azimuth coordinate procedure may be more convenient. The equatorial axis is placed horizontally as the axis for elevation and the vertical axis of the mount is used for rotation in azimuth. This method allows the elevation and azimuth of the sun to be read from dials on the mount at the time the solar transmissometer is aligned with the sun's disk. A further advantage is that the CRM can be more easily placed in a horizontal position to obtain the irradiance reading.

SKY-MAPPING

The CRM has provision for rotation about the axis of the solar transmissometer. If this axis is placed horizontally, the sky telephotometer can be scanned through a vertical plane which passes through the zenith. An analog voltage which represents the scan position is available and by using an X-Y chart recorder a plot of sky radiance in a plane through the zenith is produced. By repeating this in various azimuth planes, data for a map of sky radiance can be obtained. An attenuator switch with X1, X0.1, and X0.01 positions allows readings to be taken in the area near the sun. A range of radiance values of 10^4 can be covered by using this attenuator switch.

SCAN OF SUN'S DISK

By aligning the solar transmissometer on a point ahead of the sun's apparent motion and allowing the sun to pass through the field of view of the CRM, a scan of the apparent radiance across the disk of the sun can be obtained.

RADIANCE AND DIRECTIONAL REFLECTANCE

Occasionally the sky telephotometer has been used to measure the directional radiance of natural terrains, manmade surfaces, large grey scales, etc. By making a comparison measurement with a surface of known directional reflectance, values of directional reflectance under the existent lighting conditions can be obtained.

DESCRIPTION OF THE CRM SERIAL NO. 1 AND 2

OPTICAL SYSTEM (See Fig. 2 for schematic of the CRM collection optics.)

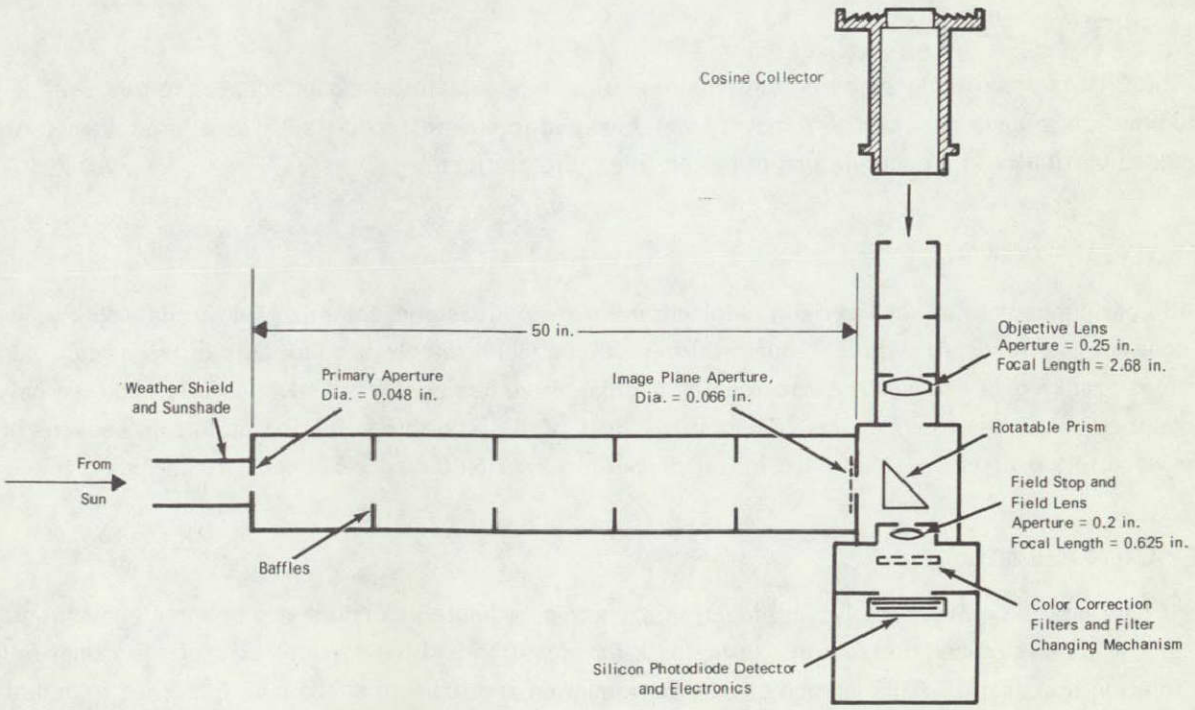

Fig. 2. Schematic of Collection Optics for Contrast Reduction Meter.

Solar Transmissometer. (See "A" in Fig. 3.) The collection optics of the solar transmissometer consist of two small holes separated by 50 inches. No lenses are used to reduce the stray light which is always a concern when making measurements of high intensity sources. Stray light is of particular concern when the transmissometer is used to measure radiance values of the aureole surrounding the sun. The two small apertures are carefully machined to have sharp knife-edge openings which are held to close diameter tolerances. The sizes of these apertures are also carefully held to maintain consistency among CRM models. But, more important, the size of the forward primary aperture must be known accurately since the square of its diameter is a constant which is used during calibration. These apertures are mounted at the ends of a long cylinder. Within this cylinder are knife-edged baffles strategically located to block internal reflections. A small cylinder is mounted in front of the forward primary aperture to shield it from most of the off-axis sky light and the weather. The diameter of the forward primary aperture is 0.048 inches and the diameter of the rear aperture 0.066 inches. These dimensions were arrived at by considering the resolution desired on the sun's disk to avoid limb darkening influencing the measurement and to keep the effect of diffraction below a significant level.

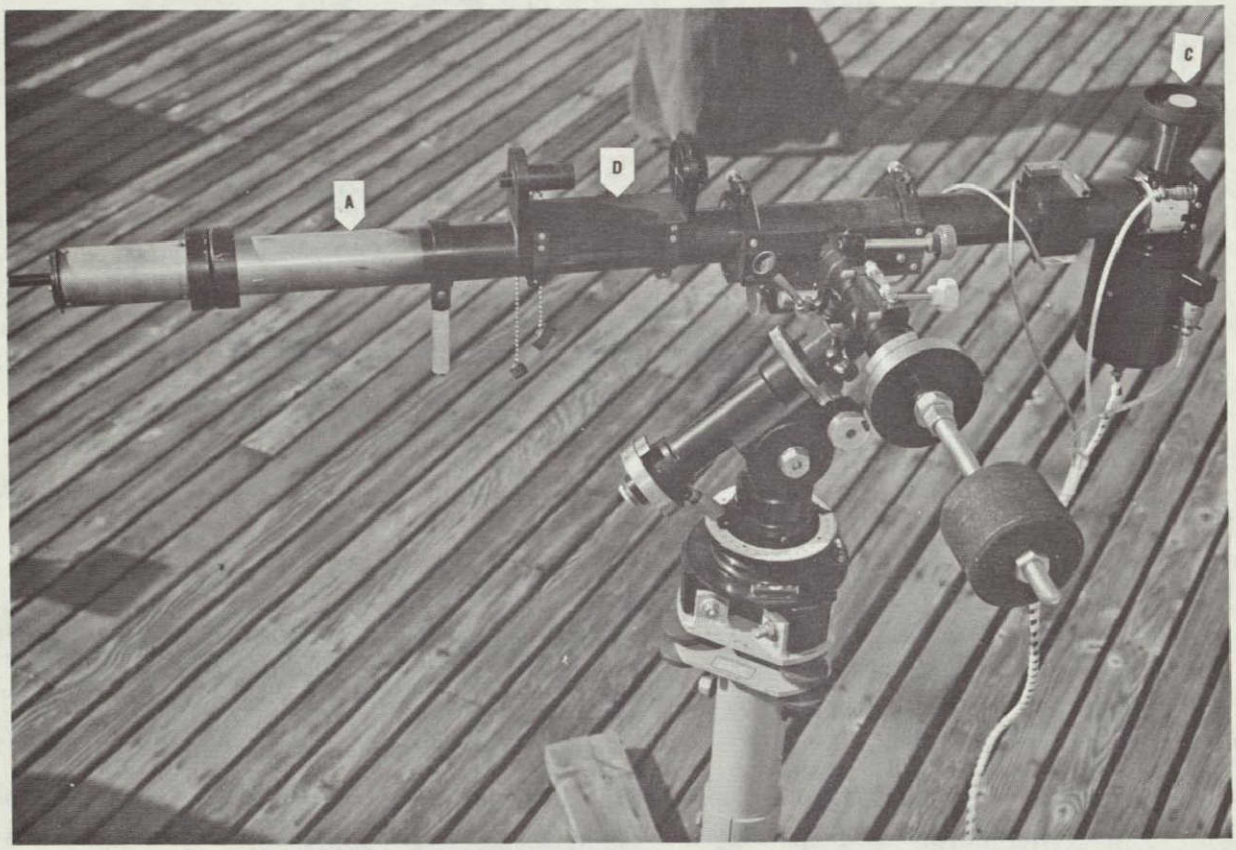

Fig. 3. A View of the Contrast Reduction Meter.

When the CRM is properly aligned with the sun an "image" of the sun is formed at the plane of the rear aperture with the rear aperture in the exact center of this "image." The energy arriving from the central portion of the sun's disk passes through the rear aperture, is deviated 90 degrees by a prism, passes through a collection lens (which is also the field lens for the sky telephotometer), and arrives at the photodetector. The field of view of this type of system is not sharply defined and vignetting occurs at the edges. A point on the forward aperture has an acceptance angle, determined by the rear aperture, of

0.00132 radians (4.54 minutes). But, for each point on the area of the forward aperture, the axis of this acceptance angle is positioned differently with respect to the optical centerline. The net result is that the CRM responds equally to all rays entering the forward aperture at angles less than 0.655 minutes from the optical axis. When the angle of an entering ray increases beyond 0.655 minutes, the sensitivity of the CRM decreases until it reaches zero at 3.88 minutes, beyond which no light is accepted. Figure 4 shows this graphically as the theoretical relative response of the CRM when a point source at a great distance is scanned across the field of view of the solar transmissometer.

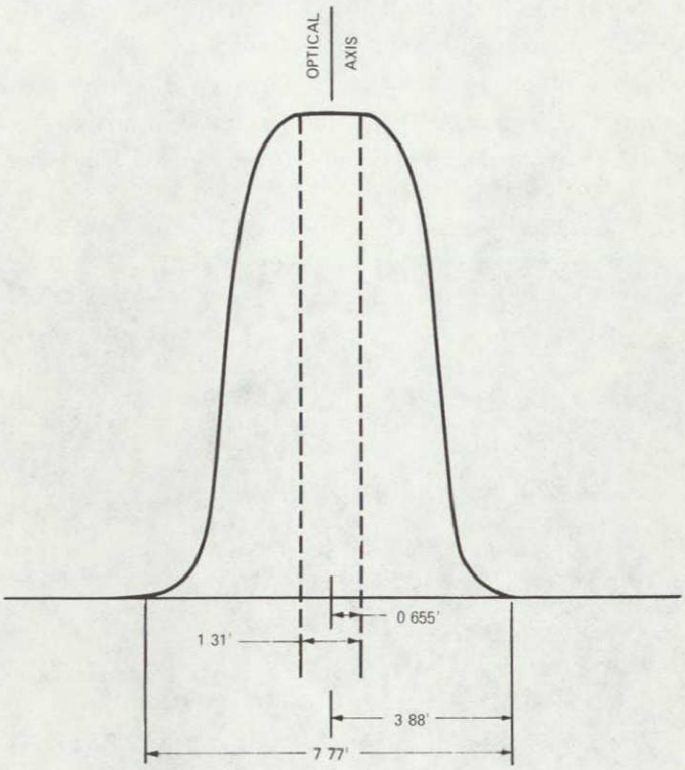

Fig. 4. Theoretical Relative Response of the Solar Transmissometer to a Point Source Scanning through the Field of View.

Sky Telephotometer. (See "B" in Fig. 5.) The sky telephotometer is mounted at the rear of the solar transmissometer with its optical axis 90 degrees to the axis of the transmissometer. When using the telephotometer the prism used to relay the light from the transmissometer is rotated out of position. The light from the solar transmissometer is blocked and the light entering the sky telephotometer is allowed to pass straight through to the photodetector. The telephotometer has an entrance aperture of 6.35 millimeters and an achromatic objective lens with a focal length of 68 millimeters. The focal length of the lenses varies slightly on the different CRM models. Mounted in front of the objective lens is a sunshade with internal baffles to reduce stray light. In the focal plane of the objective lens is a field stop which limits the field of view to about 4.4 degrees. Behind the field stop is a field lens which images the entrance aperture on the surface of the photodetector.

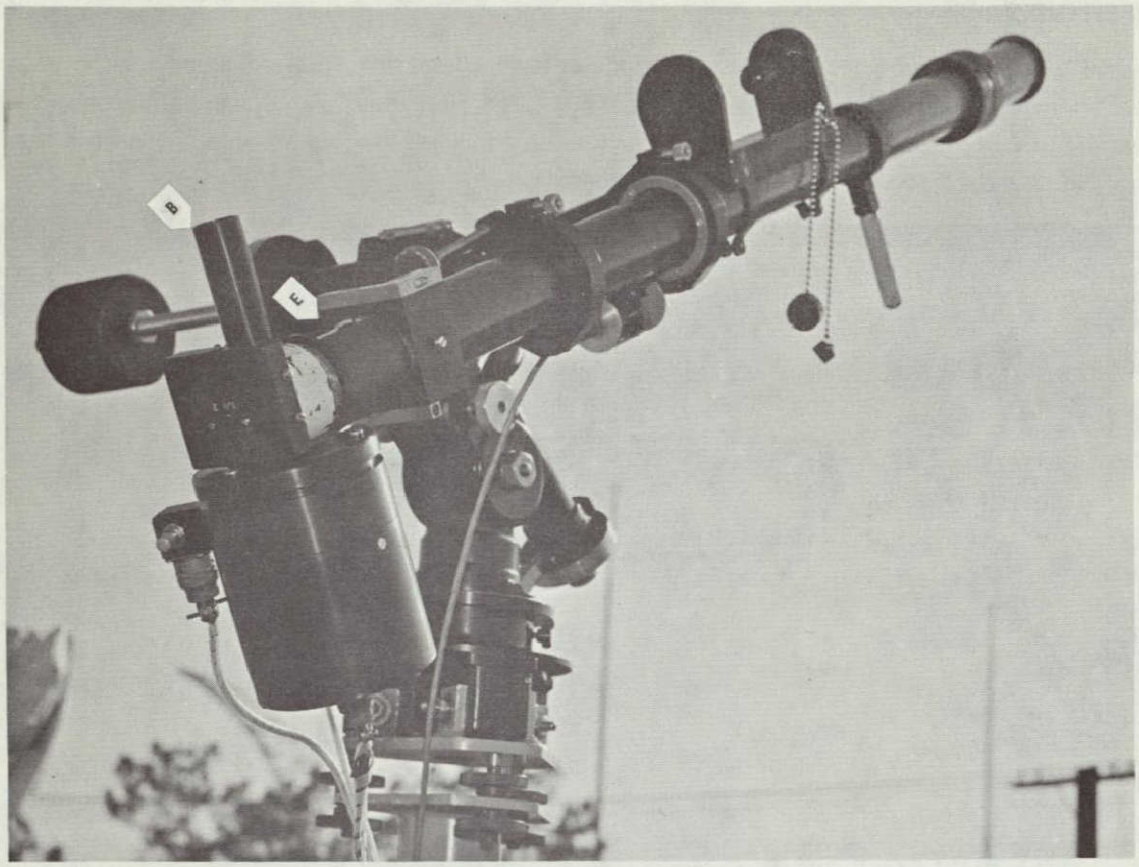

Fig. 5. Another View of the Contrast Reduction Meter.

Irradiance Cap. (See "C" in Fig. 3.) The irradiance cap is a device designed to collect and transmit light in correspondence with the cosine of the angle of incidence of the arriving light. This cap slips over the sunshade of the sky telephotometer and converts it from a system which makes a radiance measurement to one which makes an irradiance measurement. With this cap in place the optics of the telephotometer simply collect the light from the back of the irradiance cap and relay it to the photodetector.

Alignment Sight. (See "D" in Fig. 3.) The alignment sight is mounted on the side of the transmissometer barrel and is used in aiming the transmissometer at the sun. It is a small diameter telephoto lens with an effective focal length of about 26 inches which produces a 0.250-inch diameter image of the sun on a surface located about 10 inches behind the lens. This surface is open to view and has crosslines and a circle engraved upon it the size of the image of the sun. The sight is aligned with the solar transmissometer so that when the image is centered on the crosslines and circle, the image of the sun within the transmissometer is also centered on the rear aperture. Verification of alignment is achieved by direct examination through a viewing port (see "E" in Fig. 5) of the image at the rear aperture of the solar transmissometer. A circle which matches the image size is engraved on the surface around this aperture to facilitate observation. The alignment sight is frequently used to "find" the sun and final alignment is accomplished by looking through the view-port.

THE CRM ELECTRONICS

The CRM electronics are packaged into four modular assemblies, the filter changing assembly, prism assembly, photocell assembly, and the control console. The first three are mechanically connected together and electrically connected to the control console. All four assemblies are interchangeable between CRM Serial No. 1 and 2. See Fig. 6 for the control console.

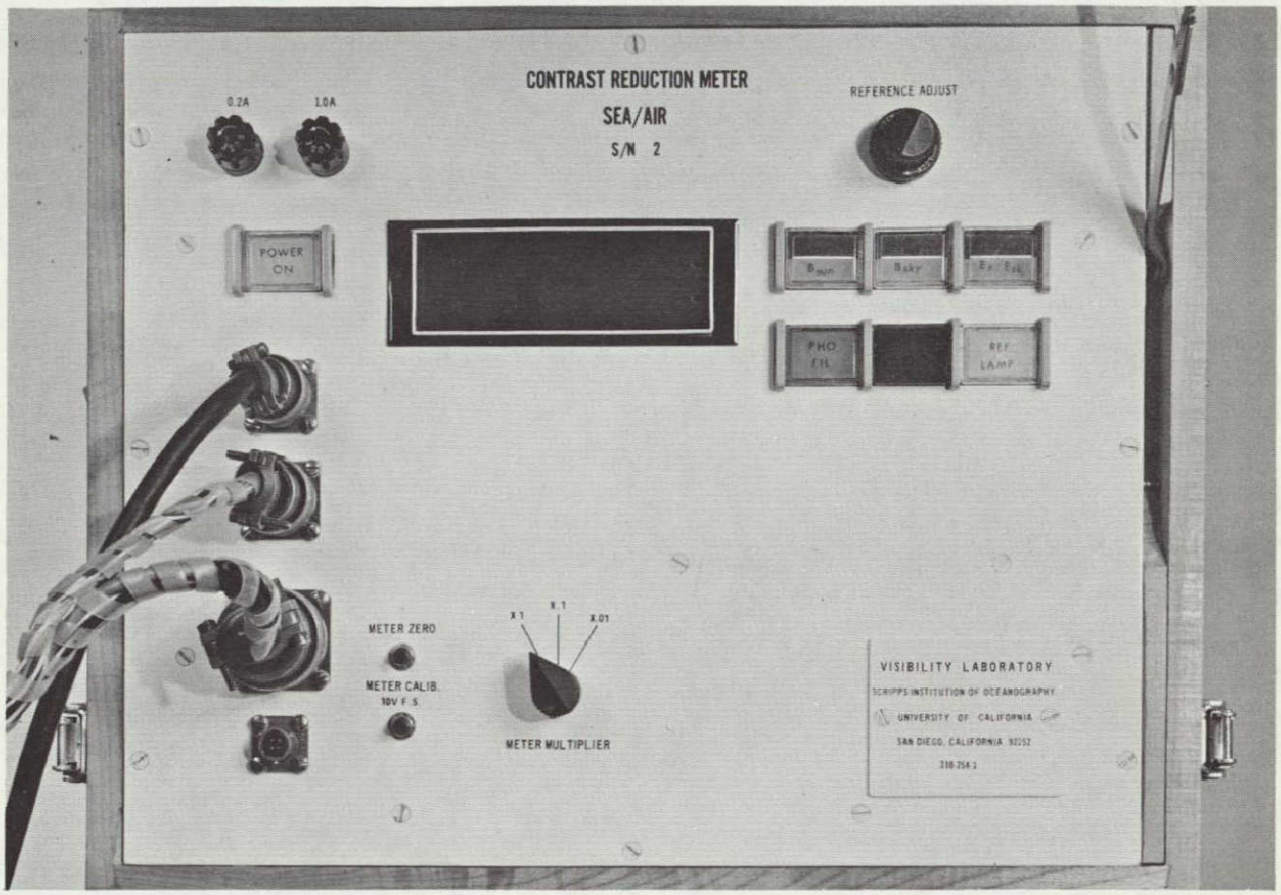

Fig. 6. Control Console.

The filter changing assembly places a photopic filter, a red filter, or a blank paddle in the light path when the corresponding pushbutton switch on the control panel is energized. The blank paddle interrupts the incoming light to the photocell when the reference lamp switch is pushed. Verification switches in the filter assembly confirm each of the operations by causing the proper control panel switch to be illuminated when a filter or blank paddle is in the correct position.

The prism assembly mechanically selects one of three measurement modes. They are:

1. Horizontal irradiance (H_t) or illuminance (E_t)
2. Apparent sun radiance (N_{sun}) or luminance (B_{sun})
3. Sky radiance (N_{sky}) or luminance (B_{sky}).

Verification switches in the prism assembly assure that the prism is in position by illuminating the corresponding control panel switch.

The photocell assembly contains the photocell, input amplifier, temperature-compensation network, gain changing circuit, and reference lamp.

The control console houses the second amplifier, calibration circuit, gain switch, digital readout, and other electronics.

Photocell Circuit. (Refer to circuit diagram, Fig. 7.) The input flux is received by a Sensor Technology Inc. silicon solar cell P1. Illumination causes a linear variation of the photocell short-circuit current. The output current developed into a load is a function of illumination level, load resistance, and cell photosensitive area. The chopper-stabilized high gain amplifier A1 inverts the photocell signal and presents a low impedance (roughly 0.1 ohm) to the photocell.

The reed relays SW1, SW2, SW3, and SW4 apply feedback resistors around amplifier A1. When the meter multiplier switch on the control panel is positioned to X1, SW3 is in the normally closed position and resistor R5 (100K ohms) or R6 is in the feedback loop. Resistor R6 is a temperature-compensating thermistor network coupled to the photocell and is placed in the feedback loop whenever SW4 is activated. Relay SW4 is energized when the red filter or the reference lamp pushbutton switch on the control panel is pushed. Figures 8 and 9 show the photocell before and after temperature compensation. It was found that no compensation was needed in the photopic region of the photocell spectral sensitivity. When position X.1 is selected, SW2 and SW3 are activated placing resistors R3 and R4 in the feedback loop. Resistors R3 and R4 are adjusted to reduce the output of amplifier A1 by a factor of 10. Selecting position X.01 activates SW1 and SW3 and reduces the output of A1 by a factor of 100.

Lamp L1 is an unbased miniature lamp with an unsupported filament manufactured by LAMP, Inc. It is powered from a regulated supply and operated at its design voltage of 5.0 volts and design current of 0.060 amperes. It is physically located so that it illuminates the photocell at the same time the filter changer blank paddle occults the incoming flux. This occurs when the reference lamp control panel pushbutton switch is pushed. Resistor R7 is a zero offset potentiometer which adjusts the offset voltage of amplifier A1. The function of capacitor C1 is to reduce the high frequency response of A1 and prevent any oscillations.

Control Console Circuit. The positive output voltage of amplifier A1 is dc coupled to the second chopper-stabilized amplifier A2. The gain of amplifier A2 is determined by the ratio of any one of the seven calibration feedback resistors to the 1 K resistor R8. Resistor R8 is the load for A1 and R23 is the load for A2. Resistor R9 is the zero offset potentiometer for A2 and C9 limits the high frequency response. Relays SW5 through SW11 are individually activated by the six illuminated pushbutton switches on the control panel. These switches are equipped with holding coils and are interconnected in two groups of three. Each group is wired so that the pressing of one button automatically releases any of the other two buttons previously held down by the magnetic detent. The red filter, photopic filter, and reference lamp switches are in one group, while the $N_{sky} - B_{sky}$, $N_{sun} - B_{sun}$, and $H_t - E_t$ switches are in the other group. The lights in the switches act as verification indicators and will light only if the prism assembly is in the proper position and the chosen filter has flipped into place. Small microswitches mounted in the filter changing assembly and the prism assembly are wired to the control panel switches to activate the verification indicators. These are not shown on the circuit diagram.

The output of the second amplifier is attenuated by R23 and displayed on the digital voltmeter on the control console. Relay SW12 is a normally closed pushbutton panel switch (10V F.S. on the control console) which, if activated, applies a preset −10 volts (from R24) to the meter. Resistor R24 is connected

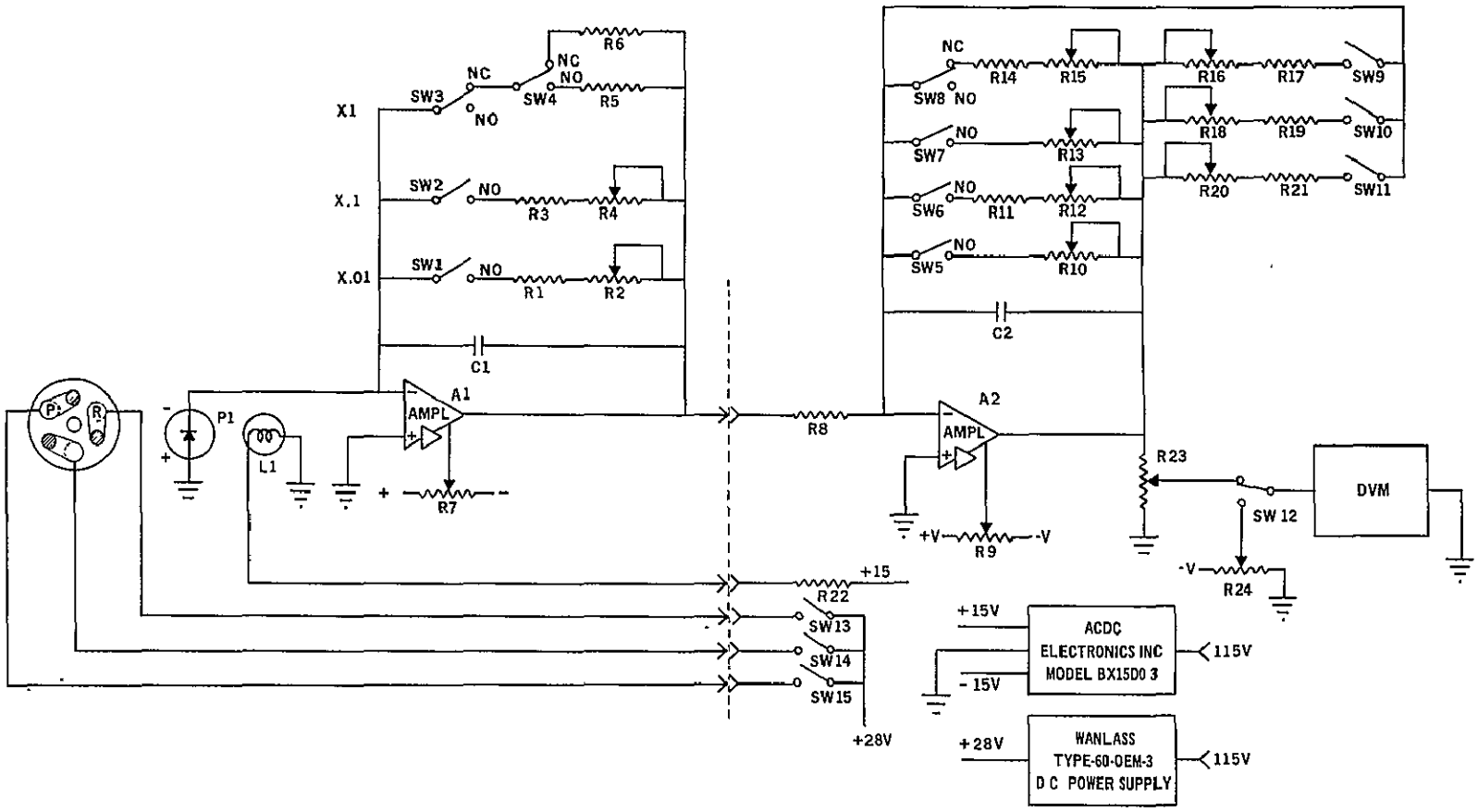

Fig. 7. Circuit Diagram.

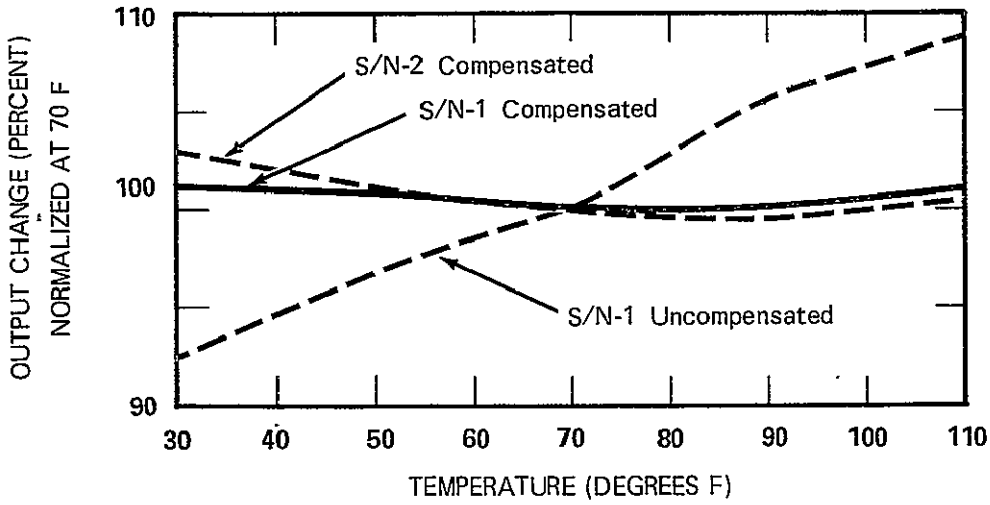

Fig. 8. Temperature Stability of Contrast Reduction Meter Near Infrared Response (700 to 1100 nm)

Fig. 9. Temperature Stability of Silicon Solar Cell Visible Region

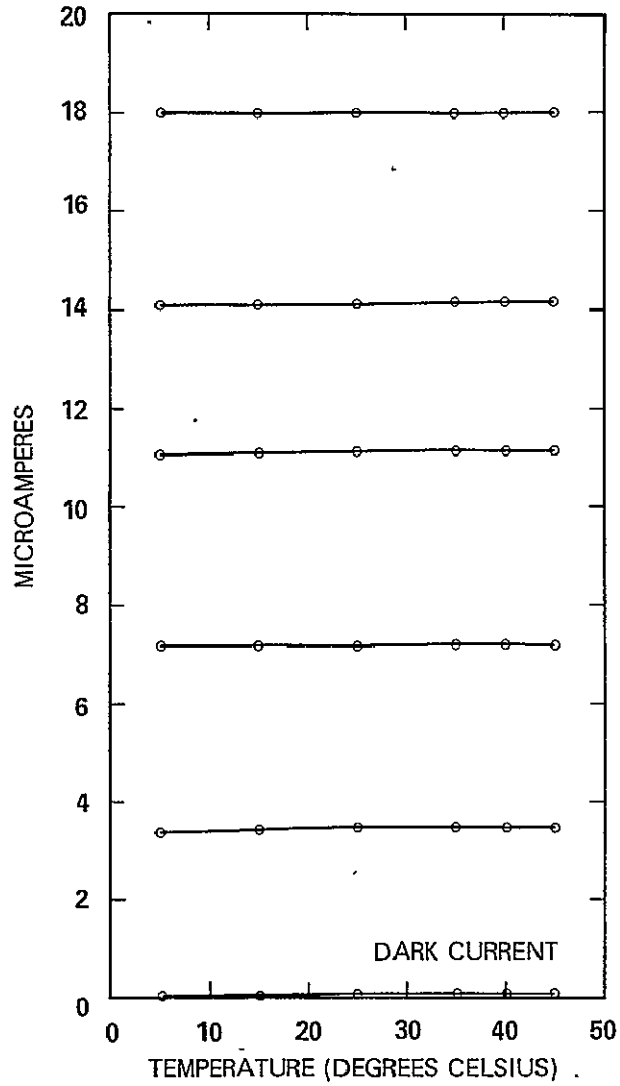

across the −15 volt power supply and is preset to −10 volts within ±0.05 percent. The ACDC Electronics Inc. power supply BX15D-0.3 provides the positive and negative 15-volt power to the circuit. It is regulated within ±0.01 percent for line voltage changes of 105 to 125 volts and load changes of 0 to 0.3 amperes.

The Wanlass 60-OEM-3 power supply provides 28-volt power to the reed relays, filter solenoids, lamps, and switch-holding coils. It is regulated within ±1 percent for line voltage changes of 105 to 125 volts and load changes of 0 to 2 amperes.

CALIBRATION OF THE CRM SERIAL NO. 1 AND 2

SOLAR TRANSMISSOMETER

Calibration of the solar transmissometer presents an interesting problem since the radiance of the sun which is measured with this system is many orders of magnitude above levels normally achievable using standard sources. In one method used, the forward aperture is replaced by a much larger opening which increases the light-gathering power by a factor of 1000. With this larger aperture in place, the system is calibrated on a photometric bar using a plaque of known reflectance, such as Mg 0_2, and a standard lamp of known intensity. Even with the gain of 1000 the level reached is well below the level at which the measurement is made. The photometer must have a dynamic range large enough to bridge the remaining span between calibration level and data level. To avoid having a large photometer range only for calibration purposes, an alternate calibration procedure has been devised allowing the use of a solid state detector and making the photometer less cumbersome. This procedure requires, as did the other method, that the size of the forward aperture and the separation between the forward and rear apertures be accurately known. No intermediate calibration aperture is required and the energy level at the photometer is in the range over which data are taken. The following is a description of the calibration procedure now used for the solar transmissometer.

1. When used to examine the solar disk the collection optics of the transmissometer consist of two small holes separated by 50 inches with a small aperture and a small field of view. The defining dimensions are shown in the sketch below.

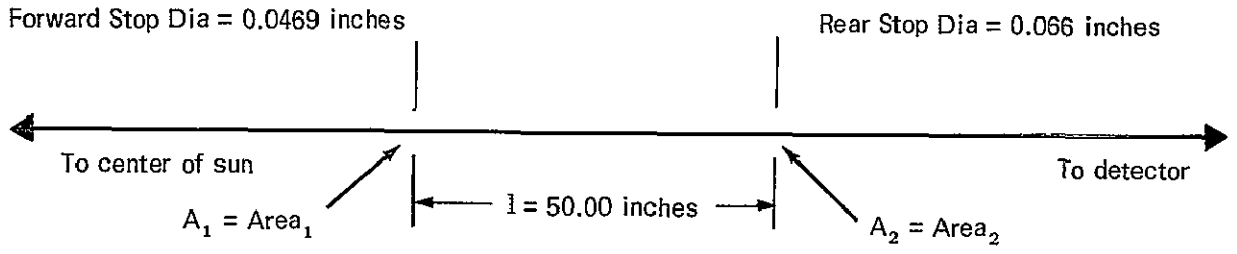

2. Looking at a source of uniform radiance over the field of view of the instrument, the power arriving at the detector for this type of system will be

$$P = N_s T A_1 A_2 / l^2 \text{ (watts)}, \tag{6}$$

where:

N_s = Radiance of the source (sun) (watts steradian^{-1} feet^{-2})

T = Transmission of any filters used

A_1 = Area of forward aperture (feet^{-2})

A_2 = Area of rear aperture (feet^{-2})

l = Distance between A_1 and A_2 (feet).

The signal generated by the detector will be

$$V_s = \left[CS_p \int_0^\infty N_{s(\lambda)} T_{(\lambda)} S_{(\lambda)} \, d\lambda \right] \frac{A_1 A_2}{l^2} \text{ (volts)}, \tag{7}$$

where:

C = A constant determined by the gain of the electronics

S_p = Peak radiant sensitivity of the detector

$N_{s(\lambda)}$ = Spectral radiance of source (watts steradian^{-1} feet^{-2} nanometer^{-1})

$T_{(\lambda)}$ = Absolute spectral transmission of filters used

$S_{(\lambda)}$ = Relative spectral response of detector normalized to peak response.

3. The forward aperture and all housings, baffles, etc. forward of the rear aperture are removed and the rear aperture is placed normal to the axis of a standard source of radiant intensity, as shown below.

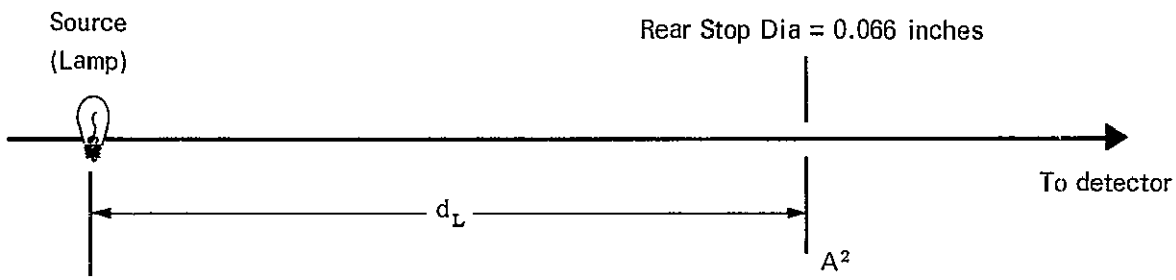

The power arriving at the detector will be

$$P = J_L \left(\frac{A_2}{d_L^2} \right) \text{(watts)}.$$

The signal generated will be

$$V_L = \left[CS_p \int_0^\infty J_{L(\lambda)}\, T_{(\lambda)}\, S_{(\lambda)}\, d\lambda \right] \frac{A_2}{d_L^2} \text{ (volts)}, \tag{8}$$

where

$J_{L(\lambda)}$ = Spectral radiant intensity of the lamp (watts steradian^{-1} nanometer^{-1})

d_L = Distance to standard lamp during calibrations (feet).

4. Dividing Eq. (8) by Eq. (7) gives the ratio

$$\frac{V_L}{V_S} = \frac{l^2}{A_1\, d_L^2} \cdot \frac{\int_0^\infty J_{L(\lambda)}\, T_{(\lambda)}\, S_{(\lambda)}\, d\lambda}{\int_0^\infty N_{s(\lambda)}\, T_{(\lambda)}\, S_{(\lambda)}\, d\lambda}. \tag{9}$$

Let

$$N_{s(T\lambda S\lambda)} = \int_0^\infty N_{s(\lambda)}\, T_{(\lambda)}\, S_{(\lambda)}\, d\lambda$$

and change the integrals to summations. Then

$$N_{s(T\lambda\, s\lambda)} = \left(\frac{V_s}{V_L} \right) \left(\frac{l^2}{A_1\, d_L^2} \right) \Sigma J_{L(\lambda)}\, T_{(\lambda)}\, S_{(\lambda)}\, \Delta\lambda \tag{10}$$

(watts steradian^{-1} feet^{-2}).

If the absolute spectral radiant intensity output distribution ($J_{L(\lambda)}$) of the lamp is known, this expression suffices.

5. The spectral radiant intensity of the lamp is

$$J_{L(\lambda)} = \left(\frac{A_L}{\pi}\right) W_{L(\lambda)} , \tag{11}$$

where:

$J_{L(\lambda)}$ = Spectral radiant intensity of the lamp as a function of wavelength (watts steradian^{-1} feet^{-2})

$W_{L(\lambda)}$ = Spectral radiant emittance of the lamp, which is a function of wavelength, determined by the absolute temperature of the filament and the emittance ϵ of tungsten at this temperature (watts steradian^{-1} feet^{-2})

A_L = Projected area of the lamp filament.

The luminous intensity of the lamp is

$$I_L = \frac{680\, A_L}{\pi} \int W_{L(\lambda)}\, \bar{Y}_{(\lambda)}\, d\lambda$$

and

$$A_L = \frac{\pi\, I_L}{680} \quad \frac{1}{\Sigma W_{L(\lambda)}\, \bar{Y}_{(\lambda)}\, \Delta\lambda} . \tag{12}$$

Substituting Eq. (11) into Eq. (10),

$$N_{s\,(T_\lambda S_\lambda)} = \left(\frac{V_s}{V_L}\right)\left(\frac{l^2}{A_1\, d_L^2}\right)\left(\frac{A_L}{\pi}\right) \Sigma W_{L(\lambda)}\, T_{(\lambda)}\, S_{(\lambda)}\, \Delta\lambda . \tag{13}$$

Substituting Eq. (12) into Eq. (13) and indicating normalized functions with a bar,

$$N_{s\,(T\lambda S\lambda)} = \left(\frac{V_s}{V_L}\right)\left(\frac{l^2}{A_1\, d_L^2}\right)\left(\frac{I_L}{680}\right)\left(\frac{\Sigma \overline{W_{L(\lambda)}}\ \overline{T_{(\lambda)}\, S_{(\lambda)}}\ \Delta\lambda}{\Sigma \overline{W_{L(\lambda)}}\ \bar{Y}_{(\lambda)}\, \Delta\lambda}\right) \tag{14}$$

(watts steradian^{-1} feet^{-2}) .

Since $W_{L(\lambda)}$ appears in the numerator and denominator, it is not necessary to use absolute values but it is the custom to normalize this function at 555 nanometers, the peak of the $\bar{Y}_{(\lambda)}$ function (the spectral response of the standard observer). The product $\overline{T_{(\lambda)} S_{(\lambda)}}$ is normalized to its peak value as is $\bar{Y}_{(\lambda)}$.

6. Where the actual $S_{(\lambda)} T_{(\lambda)}$ response does not agree exactly with the desired function, a color-match correction factor,

$$F_c = \frac{\Sigma \overline{N_{s(\lambda)}}\ \overline{T_{(\lambda)} S_{(\lambda)}}\ \Delta\lambda \text{ (Ideal)}}{\Sigma \overline{N_{s(\lambda)}}\ \overline{T_{(\lambda)} S_{(\lambda)}}\ \Delta\lambda \text{ (Actual)}},$$

is applied and Eq. (14) becomes

$$N_{s(T_\lambda S_\lambda)} = \left(\frac{V_s}{V_L}\right)\left(\frac{1^2}{A_1 d_L^2}\right)\left(\frac{I_L}{680}\right)\left(\frac{\Sigma \overline{W_{L(\lambda)}}\ \overline{T_{(\lambda)} S_{(\lambda)}}\ \Delta\lambda \text{ (Actual)}}{\Sigma \overline{W_{L(\lambda)}}\ \bar{Y}_{(\lambda)}\ \Delta\lambda}\right)\left(\frac{\Sigma \overline{N_{s(\lambda)}}\ \overline{T_{(\lambda)} S_{(\lambda)}}\ \Delta\lambda \text{ (Ideal)}}{\Sigma \overline{N_{s(\lambda)}}\ \overline{T_{(\lambda)} S_{(\lambda)}}\ \Delta\lambda \text{ (Actual)}}\right) \quad (15)$$

(watts steradian^{-1} feet^{-2}).

7. For photopic response

$$\overline{T_{(\lambda)} S_{(\lambda)}} = \bar{Y}_\lambda$$

and if we assume a perfect color match, Eq. (15) becomes

$$N_{s(\bar{Y}_\lambda)} = \left(\frac{V_s}{V_L}\right)\left(\frac{1^2}{A_1 d_L^2}\right)\left(\frac{I_L}{680}\right) \text{ (watts steradian}^{-1} \text{ feet}^{-2}) \quad (16)$$

or

$$= \left(\frac{V_s}{V_L}\right)\left(\frac{1^2}{A_1 d_L^2}\right) I_L \quad \text{(lumens steradian}^{-1} \text{ feet}^{-2}). \quad (17)$$

The expression given in Eq. (15) is of a form frequently used. However, it was found convenient to use the radiant intensity function ($J_L\lambda$) for the lamp rather than the radiant emittance ($W_L\lambda$). Also, if the spectral response of the system does not exactly match the desired response, two color correction factors may be applied. One factor corrects for the mismatch when using the calibrating source. The second factor corrects for the error the mismatch causes when data are taken.

Rewriting Eq. (15) in terms of the radiant intensity of the calibrating lamp $J_{L(\lambda)}$ and including both color correction factors we have:

$$N_{(S_\lambda T_\lambda)} = \left(\frac{V_s}{V_L}\right)\left(\frac{1^2}{A_1 d_L^2}\right) I_L \left[\Sigma \left(\frac{J_{L(\lambda)}}{I_L}\right) \overline{S_\lambda T_\lambda}\ \Delta\lambda\right] F_1 F_2 \quad (18)$$

and

$$F_1 = \text{Color correction factor for calibrating lamp}$$

$$= \frac{\Sigma J_{L(\lambda)}\, S_\lambda T_\lambda\, \Delta_\lambda \text{ (Actual)}}{\Sigma J_{L(\lambda)}\, S_\lambda T_\lambda\, \Delta_\lambda \text{ (Ideal)}}$$

$$F_2 = \text{Color correction factor for measured source}$$

$$= \frac{\Sigma \overline{W_{s(\lambda)}}\ \overline{S_{(\lambda)} T_{(\lambda)}}\ \Delta_\lambda \text{ (Ideal)}}{\Sigma \overline{W_{s(\lambda)}}\ \overline{S_{(\lambda)} T_\lambda}\ \Delta_\lambda \text{ (Actual)}},$$

where:

$N_{s_\lambda T_\lambda)}$ = Radiance within spectral function defined by $S_\lambda T_\lambda$ (watts steradian^{-1} feet^{-2})

V_s = Voltage signal from photometer when solar transmissometer is looking at the sun

V_L = Voltage signal from photometer when system is calibrated with standard lamp

l = Distance between entrance aperture and rear aperture of transmissometer (feet)

A_1 = Area of entrance aperture (feet^2)

d_L = Distance to standard lamp during calibration (feet)

I_L = Intensity of calibration lamp (candelas)

$\frac{J_{L(\lambda)}}{I_L}$ = Normalized spectral radiant intensity of calibration lamp (watts steradian^{-1} nanometer^{-1} candela^{-1})

S_λ = Spectral response of photodetector

T_λ = Spectral transmission of optical system and filters used

$\overline{S_\lambda T_\lambda}$ = Normalized product

$\overline{W_{s(\lambda)}}$ = Normalized radiant emittance of sun.

A discussion of the color correction filters and the methods used to determine the spectral functions and color correction factors is given in the following section. For the measurement in the red region, the response obtained was considered to be the desired response and no color correction factors were applied. For the photopic response the color correction product $F_1 \times F_2$ was determined to be 1.043. The forward apertures of both CRM's Serial No. 1 and 2 were carefully measured and the optical constant l^2/A_1 was computed to be 1.369×10^6 steradian^{-1} for CRM Serial No. 1 and 1.384×10^6 steradian^{-1} for CRM Serial No. 2. The average value of $l^2/A_1 = 1.3767 \times 10^6$ steradian ($\pm$ 0.56 percent) was used for both CRM models. As discussed in the section on color functions, the summation

$$\Sigma \left(\frac{J_{L(\lambda)}}{I_L} \right) \overline{S_\lambda T_\lambda} \, \Delta_\lambda$$

was computed and found to have a value of 0.01134 watts steradian^{-1} candela^{-1}. Inserting these constants into Eq. (15) gives the following relationships:

A. For the red region

$$N_{(s_\lambda T_\lambda)} = 0.0156 \times 10^6 \left(\frac{V_s}{V_L} \right) \left(\frac{I_L}{d_L^2} \right) \text{ (watts steradian}^{-1} \text{ feet}^{-2}\text{).}$$

The photometer has a linear response, $(1/V_L)(I_L/d_L^2)$ is a constant, and $N_{(s_\lambda T_\lambda)} = f(V_s) = KV_s$. Then

$$V_L = (0.01561 \times 10^6) \left(\frac{1}{K} \right) \left(\frac{I_L}{d_L^2} \right) \text{ (calibration)}$$

and

$$N_{(s_\lambda T_\lambda)} = KV_s \text{ (watts steradian}^{-1} \text{ feet}^{-2}\text{) (data),}$$

where

K = A constant determined by the overall gain of the system.

During calibration the gain is adjusted to make the constant K some multiple of 10 and the voltage output can be read directly in radiance units.

B. For the photopic region the luminance (B) is

$$B = \left(\frac{V_s}{V_L} \right) \left(\frac{l^2}{A_1 d_L^2} \right) (I_L) \, F_1 F_2 .$$

Substituting $F_1 F_2 = 1.043$ and $l^2/A_1 = 1.376 \times 10^6$,

$$B = 1.436 \times 10^6 \left(\frac{V_s}{V_L}\right)\left(\frac{I_L}{d_L^2}\right).$$

Let

$$V_s = B/K$$

so

$$B = KV_s \text{ lumen steradian}^{-1} \text{ feet}^{-2}) \text{ (data)}$$

and

$$V_L = 1.436 \times 10^6 \left(\frac{1}{K}\right)\left(\frac{I_L}{d_L^2}\right) \text{ (calibration).}$$

And again the gain is adjusted during calibration to make K a multiple of 10 and the voltage output can be read directly in luminance units.

SKY TELEPHOTOMETER

Unlike the solar transmissometer the sky telephotomer can be calibrated directly because the sky radiance levels to be measured can be easily reached in the laboratory. The procedure, illustrated in the sketch below, is to illuminate a plaque of known reflectance with a standard lamp at a known distance and aim the telephotometer so its field of view is well within the area of the illuminated plaque. A surface of pressed $BaSO_4$ was used for the reflectance standard and the distances were such that no cosine correction was necessary.

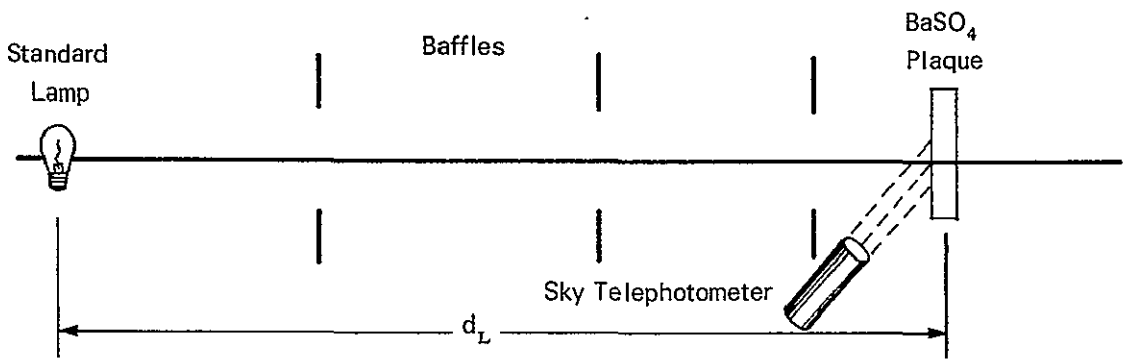

For the red region the expression which relates to the calibration of the sky telephotometer is:

$$N_{(S_\lambda T_\lambda)} = \left(\frac{V_s}{V_L}\right)\left(\frac{I_L R}{\pi d_L^2}\right) \Sigma \left(\frac{J_{L(\lambda)}}{I_L}\right) \overline{S_\lambda T_\lambda}\, \Delta_\lambda ,$$

where:

$N_{(S_\lambda T_\lambda)}$ = Radiance of sky (watts steradian^{-1} feet^{-2}) within spectral function $S_\lambda T_\lambda$

V_s = Voltage signal from photometer in response to sky radiance $N_{(S_\lambda T_\lambda)}$

V_L = Voltage signal from photometer when calibrating with standard lamp

I_L = Intensity of standard lamp (candelas)

d_L = Distance of standard lamp from reflectance plaque (feet)

R = Reflectance of plaque over spectral region $S_\lambda T_\lambda$

$\frac{J_{L(\lambda)}}{I}$ = Normalized spectral intensity of lamp used (watts steradian^{-1} nanometer^{-1} candela^{-1})

$\overline{S_\lambda T_\lambda}$ = Normalized spectral response of instrument including S_λ = spectral response of detector and T_λ = spectral transmission of the optical system and filters used.

Computations gave

$$\Sigma \frac{J_{L(\lambda)}}{I_L} (S_\lambda T_\lambda) \Delta_\lambda = 0.01134$$

and

$$N_{(S_\lambda T_\lambda)} = 0.003610 \left(\frac{V_s}{V_L}\right)\left(\frac{I_L}{d_L^2}\right) R$$

if

$$V_s = \frac{N_{(S_\lambda T_\lambda)}}{K} .$$

Then

$$V_L = \frac{1}{K}(3.610 \times 10^{-3})\ \frac{I_L R}{d_L^2}\ \text{(calibration)}$$

and

$$N_{(s_\lambda\, \tau_\lambda)} = KV_s\ \text{(watts steradian}^{-1}\ \text{feet}^{-2})\ \text{(data)}.$$

As with the solar transmissometer the gain is adjusted during calibration to make the constant K a multiple of 10 and the voltage output V_s can be read directly in absolute radiance units.

The photopic sky radiance measurement is determined in luminance units. It is not necessary to know the spectral distribution of the calibrating source except for computing the color correction factor. The relationship which applies to calibration is:

$$B = \left(\frac{V_s}{V_L}\right)\left(\frac{I_L R}{\pi\, d_L^2}\right) F_1 F_2\ ,$$

where

$$B = \text{Luminance (lumens steradian}^{-1}\ \text{feet}^{-2})$$

and all other symbols are as previously defined.

The color correction factor product $F_1 F_2$ was determined to be 1.065 and

$$B = 0.3390\left(\frac{V_s}{V_L}\right)\left(\frac{I_L R}{d_L^2}\right).$$

Let

$$V_s = B/K$$

then

$$V_L = 0.3390\left(\frac{1}{K}\right)\left(\frac{I_L R}{J_L^2}\right)\ \text{(calibration)}$$

and

$$B = KV_s \text{ (lumens steradian}^{-1} \text{ feet}^{-2}\text{) (data).}$$

During calibration the gain of the photometer is adjusted to make the constant K an even multiple of 10 and the data signal V_s can be read directly in absolute units.

IRRADIANCE COLLECTOR

The cosine collector system, used to obtain irradiance and illuminance data, is calibrated by exposing it directly to radiation from a standard source as illustrated below.

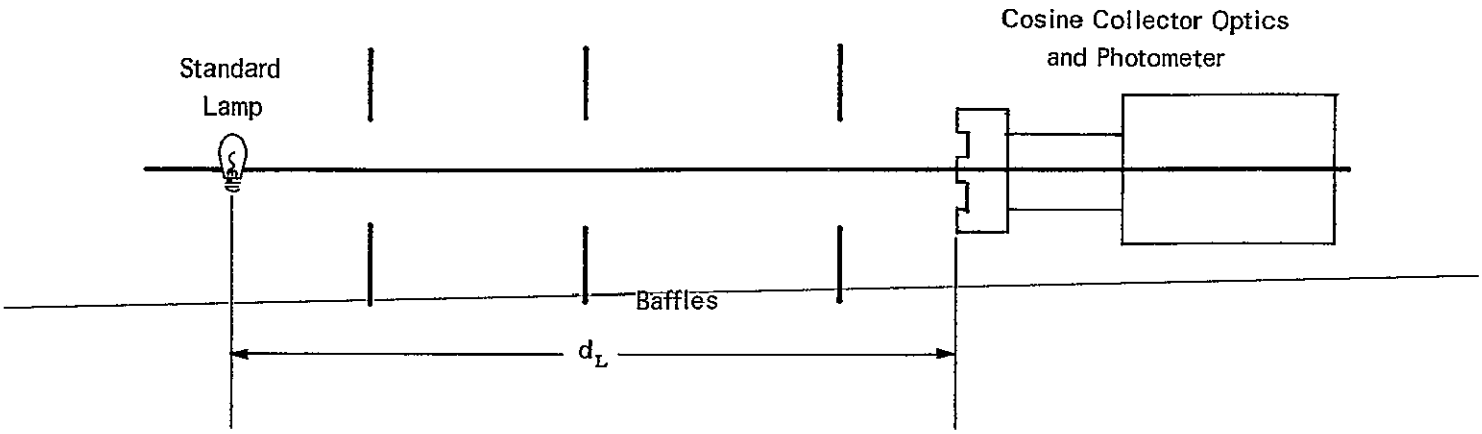

For the irradiance calibration the applicable expression is

$$H_{(s_\lambda \tau_\lambda)} = \left(\frac{V_s}{V_L}\right)\left(\frac{I_L}{d_L^2}\right) \Sigma \frac{J_{L(\lambda)}}{I_L} \overline{S_\lambda T_\lambda} \Delta_\lambda .$$

where

$H_{(s_\lambda \tau_\lambda)}$ = Irradiance (watts feet^{-2}) within the spectral function $\overline{S_\lambda T_\lambda}$.

All other symbols are as previously defined.

The spectral summation for the lamp $\Sigma\left(J_L/I_L\right)\overline{S_\lambda T_\lambda}\Delta_\lambda$ was found to be 0.0110 watts steradian^{-1} nanometer^{-1} candela^{-1} and

$$H_{(s_\lambda \tau_\lambda)} = 0.0110\left(\frac{V_s}{V_L}\right)\left(\frac{I_L}{d_L^2}\right) .$$

Let

$$V_s = \frac{H_{(s_\lambda \tau_\lambda)}}{K}$$

then

$$V_L = 0.0110\left(\frac{1}{K}\right)\left(\frac{I_L}{d_L^2}\right) \text{ (calibration)}$$

and

$$H_{(s_\lambda \tau_\lambda)} = KV_s \text{ (watts feet}^{-2}\text{) (data).}$$

For the illuminance (photopic) response calibration, the applicable expression is

$$E = \left(\frac{V_s}{V_L}\right)\left(\frac{I_L}{d_L^2}\right) F_1 F_2 ,$$

where

E = Illuminance (lumens feet^{-2} or foot-candles).

The color correction factor product $F_1 F_2$ was found to be 1.06 and

$$E = 1.06\left(\frac{V_s}{V_L}\right)\left(\frac{I_L}{d_L^2}\right).$$

Let

$$V_s = E/K$$

then

$$V_L = 1.06\left(\frac{1}{K}\right)\left(\frac{I_L}{d_L^2}\right) \text{ (calibration)}$$

and

$$E = KV_s \text{ (lumens feet}^{-2}\text{) (data) .}$$

During calibration the gain is adjusted to make the constant K an even multiple of 10 and the data signal V_s can be read directly in the units of the function measured.

LINEARITY

The photometer was checked on a photometric bar for linearity of response. This was done for all six channels. In all cases the linearity was within one resolution element of the readout digital voltmeter over the range used during data collection.

TEMPERATURE STABILITY

Temperature tests were run on the photometer head over the region from 32 to 110F. With the photometer spectral sensitivity corrected for photopic response the temperature coefficient is essentially zero. With the photometer filtered to respond in the near infrared region an overall drift with temperature of about 15 percent was found. Addition of a temperature-compensating circuit greatly improved the temperature stability. This compensation is automatically switched into the circuit whenever the "red" filter is used. After the compensating circuit was added, testing showed the drift to be within 1 percent from 50 to 110F and to be + 1.3 percent for CRM Serial No. 1 and + 3 percent for CRM Serial No. 2 at 30F. The results of these tests are shown in Figs. 8 and 9.

LONG TERM STABILITY

As an indication of the overall CRM stability, a summary of the calibration history of CRM Serial No. 2 is given in Table 1 below. The calibrations were made through the collection optics of the instrument.

Calibration Date	Sun Disk		Sky		Irradiance	
	Radiance (700 to 1100 nm)	Luminance (Photopic)	Radiance (700 to 1100 nm)	Luminance (Photopic)	Irradiance (700 to 1100 nm)	Illuminance (Photopic)
20 Aug 69			Initial Calibration			
28 Oct 69	−0.9%	−5.5%	−0.5%	−7.0%	0	0
21 Jan 70	+0.6%	−6.1%	+4.8%	−11.0%	−4.7%	−10.0%
11 May 70	−3.2%	0	−4.2%	+9.0%	0	0
5 Jun 70	+0.6%	+4.2%	+0.5%	+2.0%	−1.5%	+6.5%
Net Change	−2.9%	−7.4%	+0.6%	−7.0%	−6.2%	−3.5%

Table 1. Percent Change in Calibration for CRM Serial No. 2

RADIOMETRIC STANDARDS

All of the radiometric data are reported in absolute units. The techniques and equipment used for making secondary standards and for operating incandescent standard lamps purchased from the Bureau of Standards were developed with great care over a period of several years.

In preparation for building the best possible facility for operating primary standard lamps and making secondary standards, an experienced Visibility Laboratory engineer, thoroughly versed in the theory and practice of lamp standardization, photometry, and radiometry, visited the National Bureau of Standards in Washington, D.C. to observe the equipment and procedures used there. He then visited the corresponding government standardizing laboratories of Canada, Great Britain, France, and Germany to learn firsthand the techniques employed by those countries as well. The lamp standardization facilities subsequently set up at the Visibility Laboratory were based upon all this information. These facilities represent the best ones presently achievable for visible spectrum radiometric calibration.

It is important to note that all radiometric calibrations involved in the measurements were based on incandescent standard lamps and attenuations by means of inverse square law techniques involving every precaution and refinement. Both CRM models had absolute calibrations at levels within operating range and linearity checks at 0.1 log intervals. The reliability of the data is believed to be excellent with respect to both linearity and absolute calibration.

SPECTRAL CONSIDERATIONS

Color Correction Filters and Computation of $\overline{S_\lambda T_\lambda}$ Function. The $\overline{S_\lambda T_\lambda}$ is the relative spectral response of the CRM as a function of wavelength (λ). The S_λ is the spectral sensitivity of the silicon detector and T_λ is the spectral transmission of the optical system and color correction filters used. Many combinations of filters were investigated before a final selection was made. For the near infrared region a Wratten No. 89B filter is used. To obtain a photopic response a Schott No. BG-18 and Wratten Filter No. 9 are used. The spectral transmission of the filters used on the CRM Serial No. 1 and 2 was measured on a Cary model 14 spectrophotometer. The spectral transmissions of the clear plastic used as cover plates to mount the color filters and the diffusing plastic used in the irradiance cap were also measured on the spectrophotometer. These measurements were combined by multiplication at 10-nanometer intervals and the result normalized. For the near infrared region:

$\overline{S_\lambda T_\lambda}$ = $\overline{S_\lambda}$(silicon detector) x T_λ(Wratten 89B filter) x T_λ(clear plastic) x T_λ(diffusing plastic) for the irradiance measurement.

For the photopic region:

$\overline{S_\lambda T_\lambda}$ = $\overline{S_\lambda}$(silicon detector) x T_λ(Wratten No. 9 filter) x T_λ(Schott BG-18 filter) x T_λ(clear plastic) x T(diffusing plastic) for the illuminance measurement.

These measurements and computations were made for each of the six optical system/filter combinations used (sun radiance, sky radiance, irradiance, sun luminance, sky luminance, and illuminance) for both CRM models used in this project. The spectral response of the two models is so nearly identical that correction for spectral mismatch between models is not required. Also the spectral effect of the diffusing plastic used for the irradiance and illuminance measurement, although included in the computations, is very

subtle. The overall spectral response $\overline{S_\lambda T_\lambda}$ is shown in Fig. 10 for the near infrared and in Fig. 11 for the visible region.

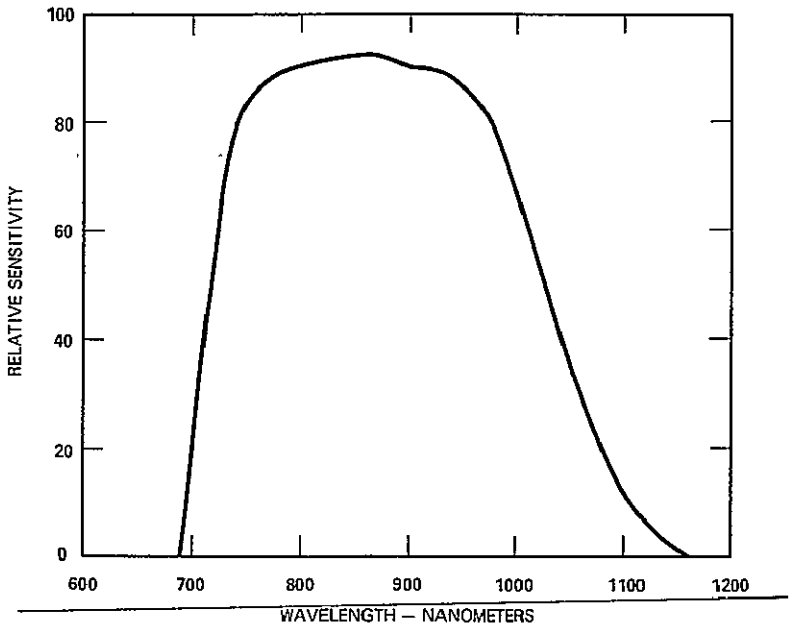

Fig. 10. Spectral Response Near Infrared

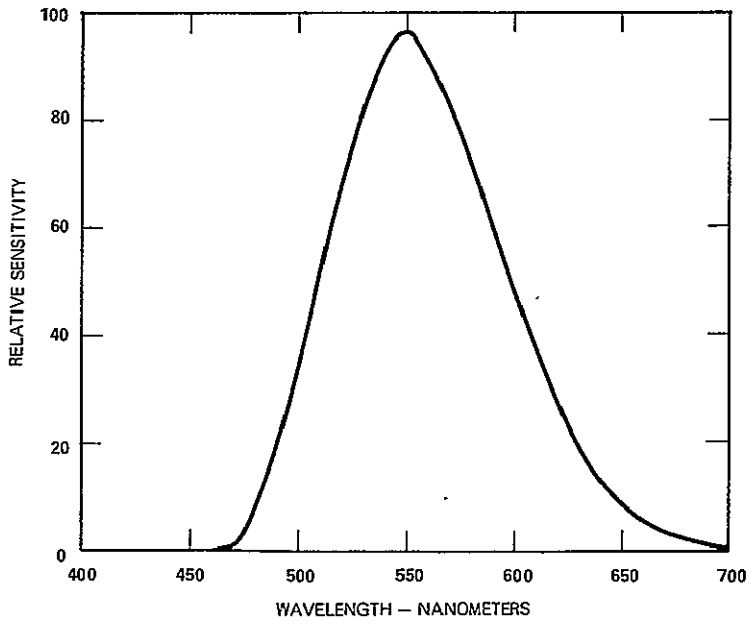

Fig. 11. Spectral Response Visible

Determination of Spectral Output of the Calibration Lamp. In order to obtain an absolute calibration of the CRM and to compute the color correction factors, it is necessary to know the output of the standard source used as a function of wavelength. The section on the calibration of the solar transmissometer explains in detail how the spectral output of the calibration source is used.

The calibration lamps used at the Visibility Laboratory are, in general, standards of luminous intensity at a specified color temperature. A method proposed by Barbrow[11] was used to compute the spectral radiant intensity of the calibration lamp used. This procedure gives the spectral intensity J_λ in the units of watts steradian^{-1} nanometer^{-1} candela^{-1}. It is assumed that the spectral radiant intensity of a blackbody at an absolute temperature equal to the color temperature of the tungsten source will closely approximate the spectral intensity of the tungsten source. Using the blackbody spectral function for the color temperature of the lamp is a way of accounting for a tungsten filament not being an ideal blackbody emitter and circumvents the need to know the absolute temperature and spectral emissivity of the tungsten filament.

The color temperature of the lamp used is 2854 K. From Table 75 of the Smithsonian Physical Tables[12], the luminous intensity of a blackbody at 550 nanometers and 2854 K is found to be 0.08569 lumens steradian^{-1} 10 nanometer^{-1}. The peak luminous efficacy is 680 lumens watt^{-1} and the luminous efficiency at 550 nanometers is 0.995. The radiant intensity at 550 nanometers is then

$$J_{(\lambda = 550)} = \frac{0.08569}{680 \times 0.995} = 126.7 \times 10^{-6} \text{ watts steradian}^{-1}\ 10 \text{ nanometer}^{-1} \text{ candela}^{-1}.$$

The spectral radiant intensities at other wavelengths are then found by using tables of relative spectral blackbody functions[13].

The validity of this computational procedure was verified by comparing the spectral output of the lamp used with a calibrated standard of spectral radiance. A spectral radiometer with a dual monochromator was used for the intercomparison of the two lamps. The measured values of spectral intensities and the computed values agreed within 5 percent over the 350 to 750 nanometer region measurable with the spectral radiometer.

Summation Function. From the values computed for the spectral intensity of the lamp, J_λ/I_L watts steradian^{-1} 10 nanometer^{-1} candela^{-1}, and the relative spectral response $\overline{S_\lambda T_\lambda}$ of the CRM, the summation $\Sigma (J_L/I_L)\, \overline{S_\lambda T_\lambda}\, \Delta_\lambda$ can be calculated. This summation was calculated to be 0.01134 watts steradian^{-1} candela^{-1} for the radiance measurements and 0.0110 watts steradian^{-1} candela^{-1} for the irradiance measurements. How these numbers are used is described in the preceding section on calibration.

Color Correction Factors. If the spectral response of the CRM used to make the radiometric measurements is not identical with the spectral function desired, an error in the measurement will exist. If the spectral distribution of the energy in the source being measured and the spectral response of the CRM are known, the error caused by this spectral mismatch can be computed. In a similar manner, if there is a spectral mismatch, an error will occur during calibration. This source of error is compensated for by applying color correction factors during calibration as discussed in the section on calibration. The spectral data for the sky, the sky plus sun, and the sun which were used to compute these factors were obtained from *The Science of Color*[14].

No correction is required for the radiometric measurements in the near infrared since the spectral response of the CRM is taken to be the desired response. The spectral response of the CRM in the visible region under sky plus sun illumination is shown in Fig. 11 and the spectral response of the standard observer ($\bar{Y}$) under the same conditions of illumination is shown in Fig. 12. The functions are very similar, with the worst mismatch occuring between 425 and 480 nanometers. Color correction factors (F_c) were computed and used for the apparent sun luminance measurement ($F_c = 1.043$), the sky luminance measurement ($F_c = 1.065$), and the illuminance measurement ($F_c = 1.060$).

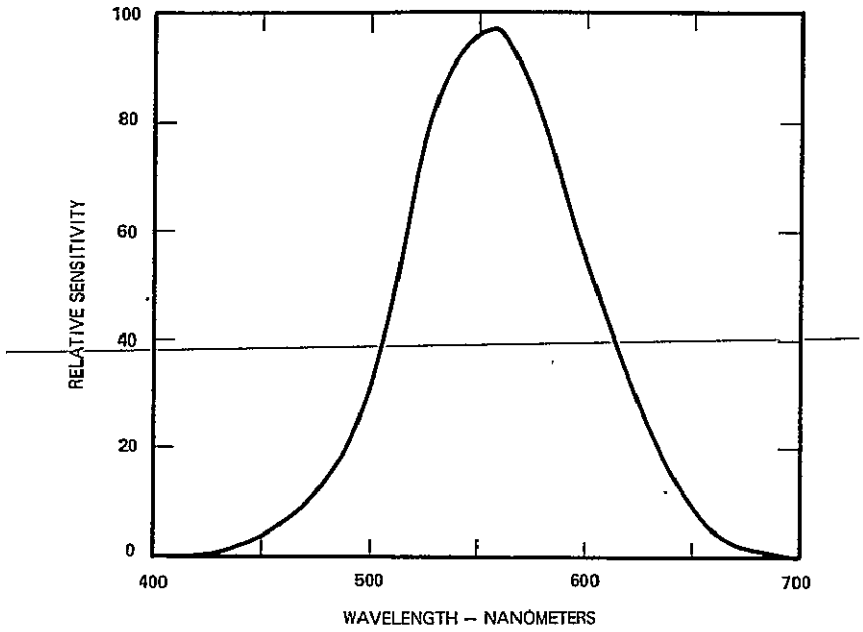

Fig. 12. Spectral Response of the Eye ($\bar{Y}$) in Sun and Sky Illumination.

DATA COLLECTION

OPTICAL DATA

On 30 October 1970 both models of the CRM were set up on the roof of a building at the Visibility Laboratory to compare readouts under real data-taking conditions. When intercompared, the models were essentially alike on all six channels. This indicated that any differences in the readouts should be real atmospheric changes and not instrumental.

A Laboratory request was approved through the Fleet Weather Facility at North Island for personnel of the Naval Weather Service Environmental Detachment (NWSED) at San Clemente Island to operate one of the CRM models. An operation manual was prepared to assist these personnel in the equipment operation. Technicians from the Laboratory delivered the CRM Serial No. 2 and instructed the personnel in its operation in early November. At the same time these arrangements were made with NWSED, the Laboratory asked that they obtain data during daylight hours when the skies were mostly clear. This limitation was not imposed on the data collection at the Laboratory and data were collected here under partly cloudy and thin overcast conditions. It was also requested that they make the time of measurement coincidental with the regular meteorological observations, stressing that parallel data were important. Sheets for recording the data were provided and mailed to the Laboratory weekly. This was done for several reasons. The Laboratory hoped to ascertain how much variance there was in conditions and also to become aware of instrument malfunctions so that a Laboratory technician could service the gear. Both the CRM at San Clemente Island and the one on the roof at the Visibility Laboratory were set up so that the field of view was free of any major obstructions above the horizon. It is particularly important that the location be chosen so that no objects such as trees or buildings occlude an appreciable portion of the sky as viewed from the CRM. The entire sequence of collecting and recording a data package from power on through the measurements, including the positioning of the instrument to make the measurement of the solar disk, takes about 5 minutes.

Data were collected on 64 days at the Visibility Laboratory and portions of 16 days at San Clemente Island. These data were collected with various types of air masses such as stable or unstable continental tropical (superior in the winter), stable or unstable maritime, and transitional air masses which were changing either from maritime to continental or from stable to unstable. A total of 615 packages were collected on the roof of the Visibility Laboratory. On 33 days at least 10 packages were collected throughout the day so that data recorded at various sun elevations would be available for studies of diurnal variations. Some of the rooftop data were collected with the skies partly cloudy or with thin high broken clouds. The data collected with clouds are not included in the analyses made for this report. However, it is felt that there will be times when a satellite would be able to see through the thin veil of clouds to the surface of the ocean and these data are available for future use.

Several problems arose in the collection of the optical data. Shortly after the CRM was used at San Clemente Island and the data sheets were returned, it was noted that some of the reports seemed spurious. Through telephone conversations with the Island personnel checks were made on whether the CRM was being used according to instructions in the manual. On the day that contact was made the conditions at San Clemente Island were not favorable for data collection. On the next suitable day for data collection, with both CRM models in operation at their respective locations, data were compared and the results again seemed to be too unlike to be accounted for by air mass differences, especially since both locations were under the influence of maritime air. Therefore, a technician packed the CRM Serial No. 1 in use at the Laboratory and went to San Clemente Island in early January for an instrument exchange and personnel retraining. This could not be accomplished earlier because with turnover of personnel at San Clemente Island, holidays, and generally poor weather, it was not feasible. Upon return of the CRM Serial No. 2 to the Visibility Laboratory it was recalibrated and no malfunctions could be noted. The CRM was installed on the roof of the Visibility Laboratory and data were collected for a few days. When these data were used to derive the values for vertical beam transmittance and vertical path radiance, they seemed faulty. The CRM was again taken into the calibration chamber and it was noted that although there was no malfunction of any of the components there was a spider web in the sunshade. When this web was cleaned out the data recorded were once again in the expected region.

Another problem occurred later when the data for the visible range of the spectrum exceeded the limits for vertical beam transmittance. Inspection disclosed that the photopic filter had come apart. A second filter was prepared from the same piece of material as the first and the instrument was recalibrated. Dur- this period the data obtained using the near infrared filter were not in question.

METEOROLOGICAL DATA

When data were collected at the Visibility Laboratory careful observations and notations were made of sky condition, visibility, wind direction and velocity, temperature, relative humidity, and any other pertinent factors that could be determined such as obstructions to visibility in any direction and the indication of whether or not smog was present over the city. While there are frequent occasions when smog is present over downtown San Diego it does not usually affect Point Loma where the data were collected. The temperature and relative humidity were read from a hygrothermograph installed in a thermoscreen on the roof. The wind data were read from dials connected to a wind vane installed 18 feet above the roof in the free airflow.

Radiosonde data were obtained for the ESSA station situated at Montgomery Field which is about 8 miles inland from the ocean and 12 miles NE of the Visibility Laboratory and also for San Nicolas Island

50 miles WNW of San Clemente Island. In some cases data were available from soundings taken at the facilities of the Naval Electronics Laboratory Center on the ocean side of Point Loma. These were for the lower levels only and in the three cases which coincided with data collection on the roof there was more moisture in the lower levels here than at Montgomery Field. Data were collected from about 30 to 1500 feet above sea level.

The air masses were determined according to source region from U. S. Department of Commerce Daily Weather Maps. The stability was determined according to the Showalter Stability Index[15]. These indices were obtained from the ESSA office at Lindbergh Field. The meteorological conditions at Lindbergh Field were compared with those recorded on the rooftop. In many cases it could be seen that the relative humidities were higher on the roof than at Lindbergh Field. This is not surprising as the peninsula of Point Loma is often enveloped in low clouds or fog while the airport and downtown San Diego are only partly cloudy.

At times during late spring and early summer the sun elevation angle was greater than 70 degrees. When the CRM was positioned to measure the sky at $\beta = 90$, the sky telephotometer was recording data at less than 20 degrees above the horizon and it appeared that the sky was being contaminated by surface conditions. In these instances measurements were also taken at $\beta = 80$ and $\beta = 70$. While these measurements were lower, the calculations for vertical path radiance as computed by the equations described earlier were seemingly not affected by the near horizon sky. The plots for path radiance therefore show only values for $\beta = 90$ degrees.

A subcontract was given to Allied Research Associates to prepare a complete cloud climatology for the area off the coast of Southern California. Clear sky amounts versus the probability of achieving that coverage were plotted for each month of the year. The results are contained in the Appendix and include:

(1) Computer listings of the cloud amount and cloud type for San Clemente, San Diego, and San Nicolas stations.

(2) Cumulative probability listings of cloud amount for the three combined stations for a 5 year period of overlap.

(3) Cumulative probability graphs of cloud and cloud-free amount for the three combined stations at midmorning and midafternoon.

(4) Comparisons between satellite-observed and ground-observed cloud cover for the Southern California coastal area.

DATA ANALYSIS

Values for vertical beam transmittance and vertical path radiance were derived from the ground-based measurements through the methods described earlier. The data were separated according to air mass type since previous investigation[16] had shown that relationships existed. The various air masses that occured were:

cTw	stable continental tropical
cTk	unstable continental tropical
mPw	stable maritime polar
mPk	unstable maritime polar
cTw → mPw	stable continental tropical changing to stable maritime polar
mPw → cTw	stable maritime polar changing to stable continental tropical
mPw → mPk	maritime polar changing from stable to unstable
mPk → mPw	maritime polar changing from unstable to stable.

The data were also separated so that the clear-day data were plotted as a function of the sun elevation angle in order to determine the diurnal variation in the atmospheric conditions. Following examination of the daily plots of vertical beam transmittance it was noted that in general the values were lower for higher sun elevation.

The values available from San Clemente were also examined to determine the amount of change between the two locations. The data showed no significant difference.

Following the diurnal analysis the data were plotted seasonally with the periods defined as follows: Fall – September, October, and November; Winter – December, January, and February; Spring – March, April, and May; Summer – June.

Comparisons of the data measured with the photopic filter were made with other data collected in the San Diego area to check for consistency. These comparisons showed that the same relationships existed. No comparisons could be made with data collected with "red" filters because the filters previously used were in the 0.5 to 0.72 micron range while the range of the infrared filter was 0.7 to 1.1 microns.

VERTICAL BEAM TRANSMITTANCE

Derived data for vertical beam transmittance as a function of sun elevation angle and the type of air mass are shown by seasons in Figs. 13 through 16.

DIURNAL VARIATIONS

Usually the values for vertical beam transmittance decrease as sun elevation increases. On some days the decrease is greater than it is on others. This is true of both the continental and maritime types of air mass.

SEASONAL VARIATIONS

Examination of the seasonal data shows there is little variation in the air masses between seasons except that the transitional air masses have lower values during the spring than at other times.

In Fig. 13 the data for the fall indicate higher values for the dry continental air mass than for the maritime air masses that flow over the Visibility Laboratory from the ocean. This is valid at all sun elevation angles. Data were collected for one day with the air mass changing character from continental to maritime and these points are interspersed with the stable and unstable maritime air.

Fall Weather Patterns. September marks the end of the summer season. Stratus clouds form or drift in from seaward during the evenings and dissipate in the forenoon. Storm conditions are rare. October marks the transition between the summer and winter seasons. Outbreaks of polar air from the northwest occur more frequently, preceded by short periods of weak frontal activity and followed by several days of clear skies and fair weather. Santa Ana winds can occur and when they do the air is continental tropical. The clouds are usually associated with weak frontal activity rather than the prevailing morning and evening stratus of the summer season. November is a continuation of the transition between summer and winter. Outbreaks of polar air are more frequent and accompanied by short periods of weak frontal activity. Several days of clear skies and fair weather follow the cloudy skies and rain showers associated with the fronts.

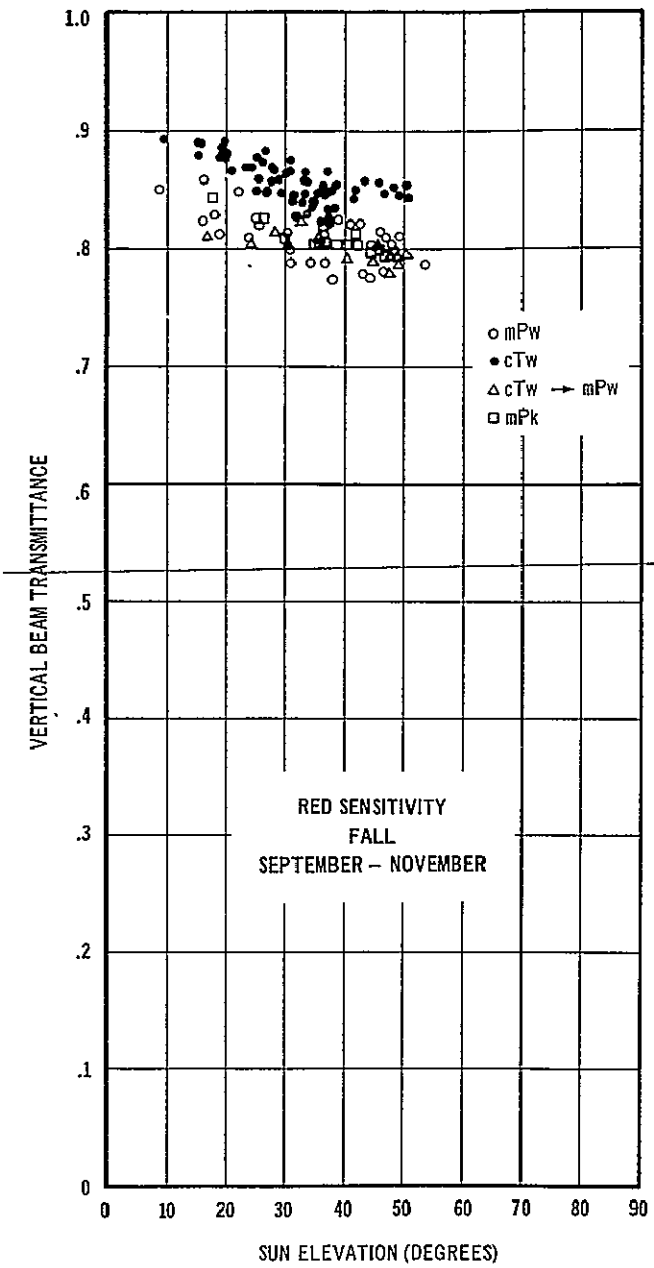
1.0
.9
.8
.7
.6
.5
.4
.3
.2
.1
0
VERTICAL BEAM TRANSMITTANCE
o mPw
• cTw
△ cTw → mPw
□ mPk
RED SENSITIVITY
FALL
SEPTEMBER – NOVEMBER
0 10 20 30 40 50 60 70 80 90
SUN ELEVATION (DEGREES)

Fig. 13

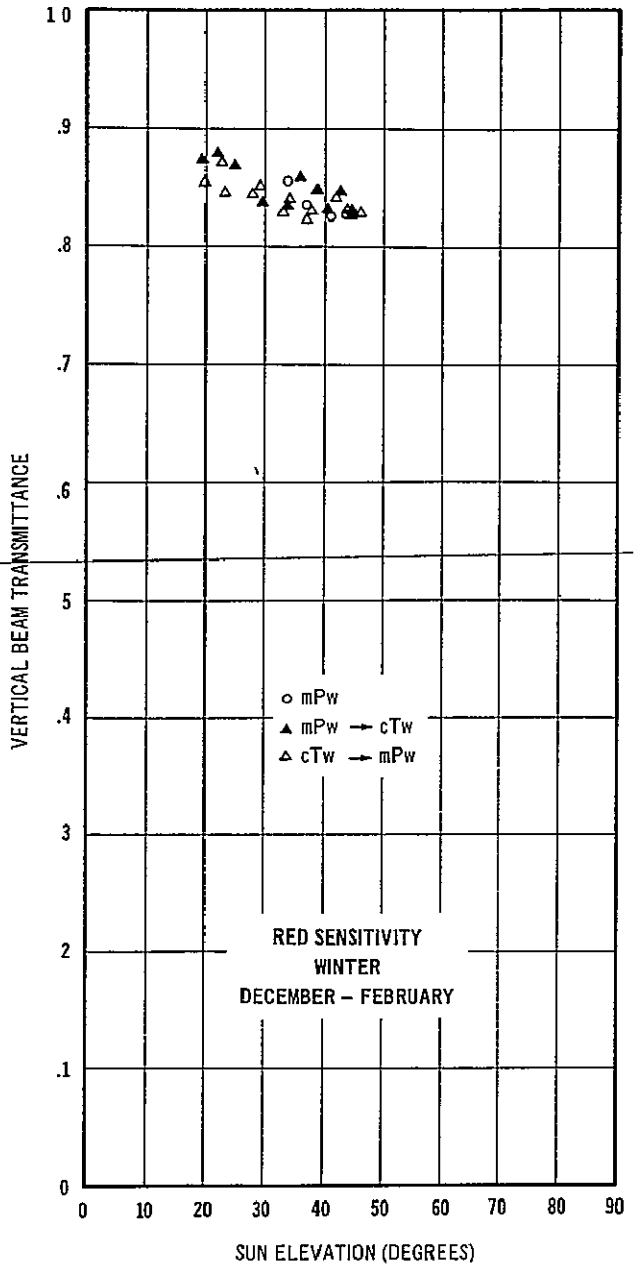
1.0
.9
.8
.7
.6
.5
.4
3
2
.1
0
VERTICAL BEAM TRANSMITTANCE
o mPw
▲ mPw → cTw
△ cTw → mPw
RED SENSITIVITY
WINTER
DECEMBER – FEBRUARY
0 10 20 30 40 50 60 70 80 90
SUN ELEVATION (DEGREES)

Fig. 14

Figure 14 shows the data for the winter season. Unfortunately, because of poorer weather, there are fewer points for comparison. There are also some winter season data available for study taken when high thin clouds were present but they have not been included in this report because it was felt there should be as complete an understanding as possible of the clear day situations before studying the effects with cloud conditions. It is hoped that these data will be utilized since an orbiting spacecraft is often able to achieve a signal of the earth even when there is a thin veil of cirrus. The data all appear higher than for the other seasons but since there are so few for comparison it is not possible to determine the real cause for this departure.

Winter Weather Patterns. December is the beginning of the winter season and is usually characterized by relatively longer periods of good weather. There are occasional periods of fog and stratus and more frequent cold frontal passages. Santa Ana winds are more frequent and bring continental air masses. January and February are quite similar to one another. There are normally frequent frontal passages occurring on an average of every 7 to 10 days. This is the period of the greatest rainfall for the San Diego area.

The data for spring are shown in Fig. 15. Like the data collected in the fall, the spring values are higher for the continental air mass than for the maritime or for the transitional air masses. The transitional air masses again are interspersed with the stable maritime data.

Spring Weather Patterns. March marks the beginning of the transition from winter. Frontal passages decrease and Santa Ana conditions are less frequent. In April frontal passages are almost nonexistent. There is an increase in fog and low stratus conditions along the coast. During May the fog is infrequent but haze is the main obstruction to visibility. Frontal passages are both rare and weak and rainfall is at a minimum. Low stratus clouds are on the increase and sometimes last throughout the day although they usually dissipate shortly after sunrise.

Summer data were collected only during June in 1970. Data had been collected in August of 1969 but those data are not included in the analysis because the period occurred during the construction and checkout of the CRM models and before their final calibrations and twinning.

Summer Patterns. June in this area has the stratus regime well established and there are frequent coastal clouds. Data were collected whenever possible after the stratus had burned off. No data were obtained from San Clemente Island. It is evident from Fig. 16 that all of the data were collected with maritime air masses and that they show little differences.

VERTICAL PATH RADIANCE (See Figs. 17 through 20.)

These data have also been examined by seasons. It is difficult to find a real separation by air mass in the collected data. There were fewer comparisons that could be made with data collected on previous experiments as this kind of data was not always part of the data collection sequence. In order to form better conclusions it is necessary that more data of this type be acquired. One result does seem evident however. During the spring (Fig. 19) the values of vertical path radiance are greater than they are for the fall period (Fig. 17) in both the continental and maritime air mass type. But there is a smaller range of values for the continental air mass because the maritime air was more prevalent.

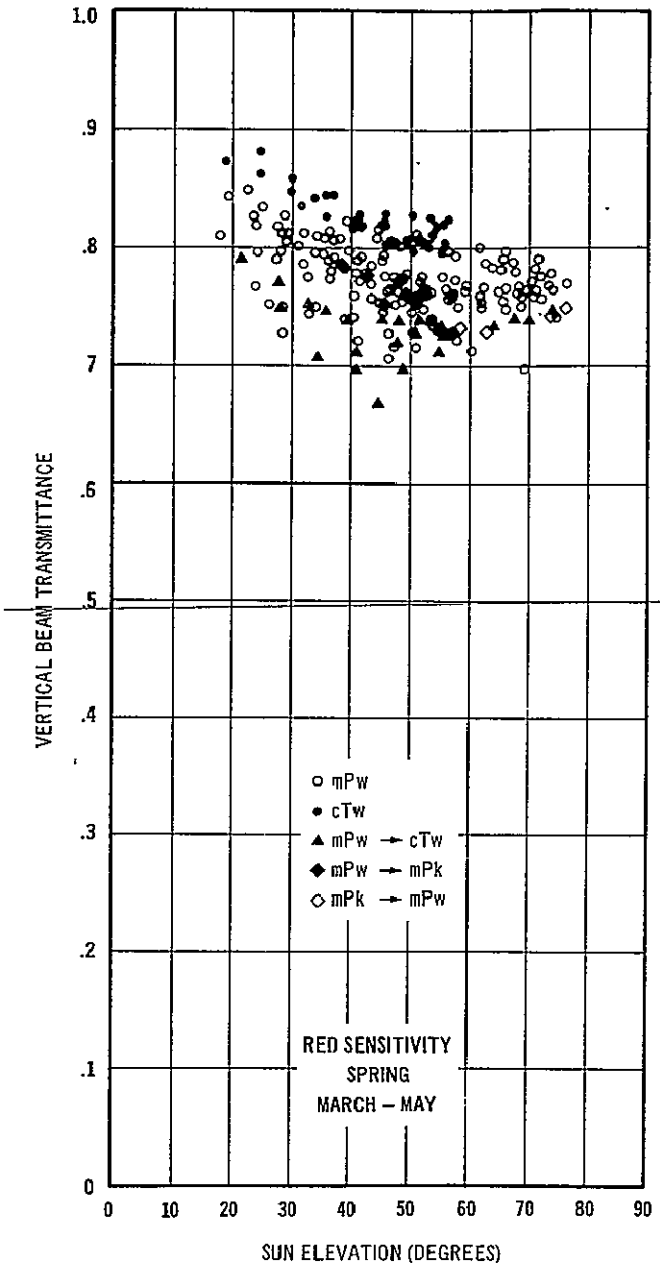
VERTICAL BEAM TRANSMITTANCE
1.0
.9
.8
.7
.6
.5
.4
.3
.2
.1
0
0 10 20 30 40 50 60 70 80 90
SUN ELEVATION (DEGREES)
mPw
cTw
mPw → cTw
mPw → mPk
mPk → mPw
RED SENSITIVITY
SPRING
MARCH – MAY

Fig. 15

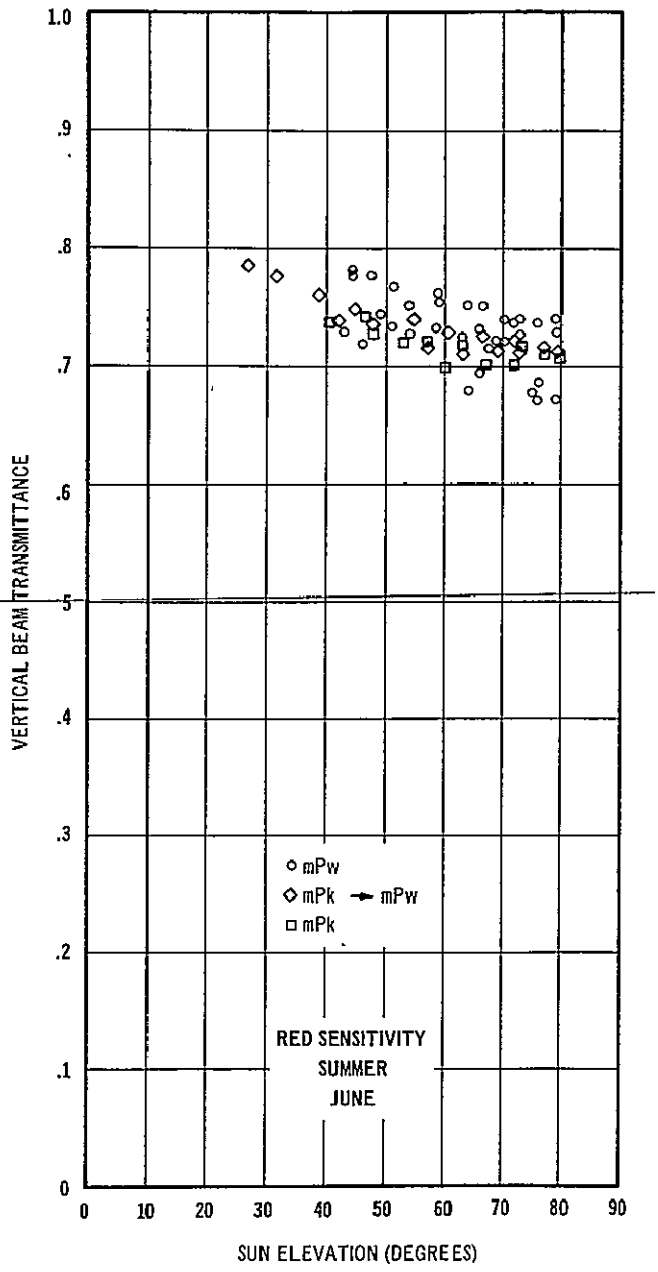
VERTICAL BEAM TRANSMITTANCE
1.0
.9
.8
.7
.6
.5
.4
.3
.2
.1
0
0 10 20 30 40 50 60 70 80 90
SUN ELEVATION (DEGREES)
mPw
mPk → mPw
mPk
RED SENSITIVITY
SUMMER
JUNE

Fig. 16

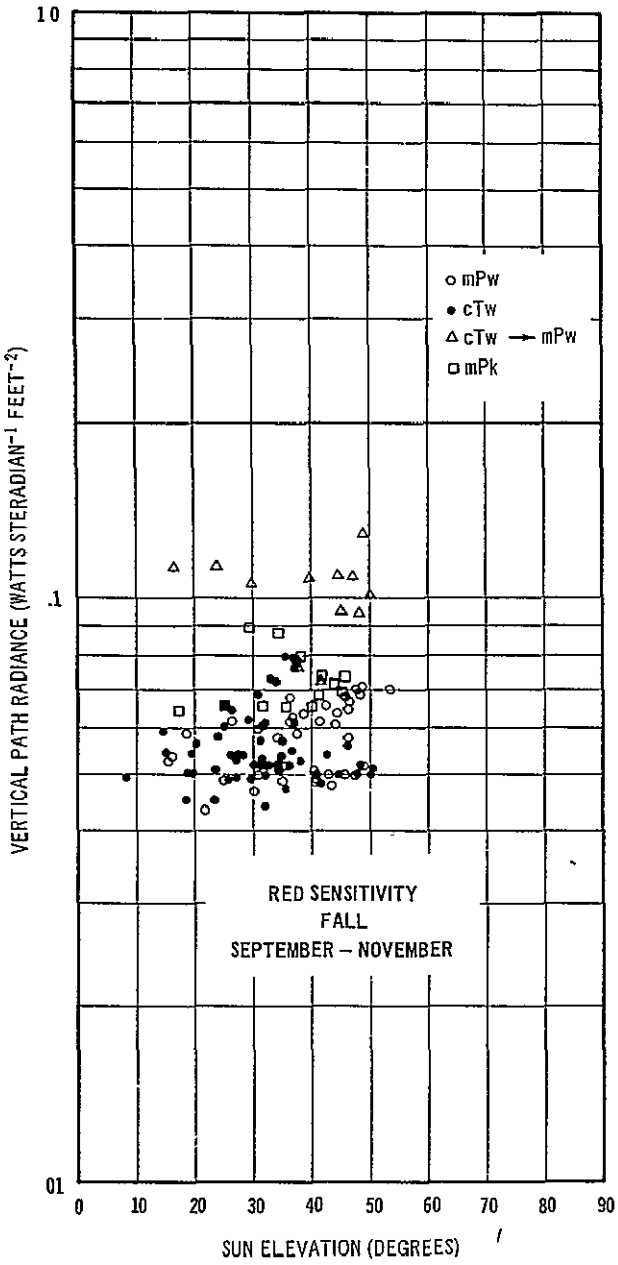
10
.1
01
VERTICAL PATH RADIANCE (WATTS STERADIAN^{-1} FEET^{-2})
o mPw
• cTw
△ cTw → mPw
□ mPk
RED SENSITIVITY
FALL
SEPTEMBER – NOVEMBER
0 10 20 30 40 50 60 70 80 90
SUN ELEVATION (DEGREES)

Fig. 17

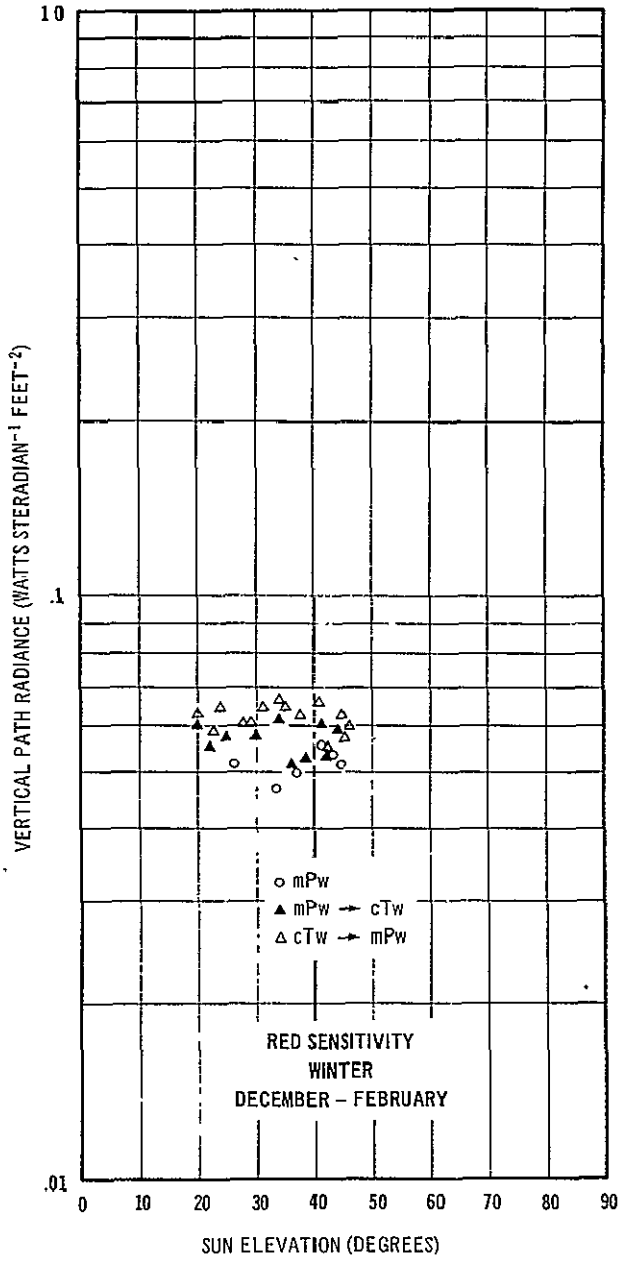
10
.1
.01
VERTICAL PATH RADIANCE (WATTS STERADIAN^{-1} FEET^{-2})
o mPw
▲ mPw → cTw
△ cTw → mPw
RED SENSITIVITY
WINTER
DECEMBER – FEBRUARY
0 10 20 30 40 50 60 70 80 90
SUN ELEVATION (DEGREES)

Fig. 18

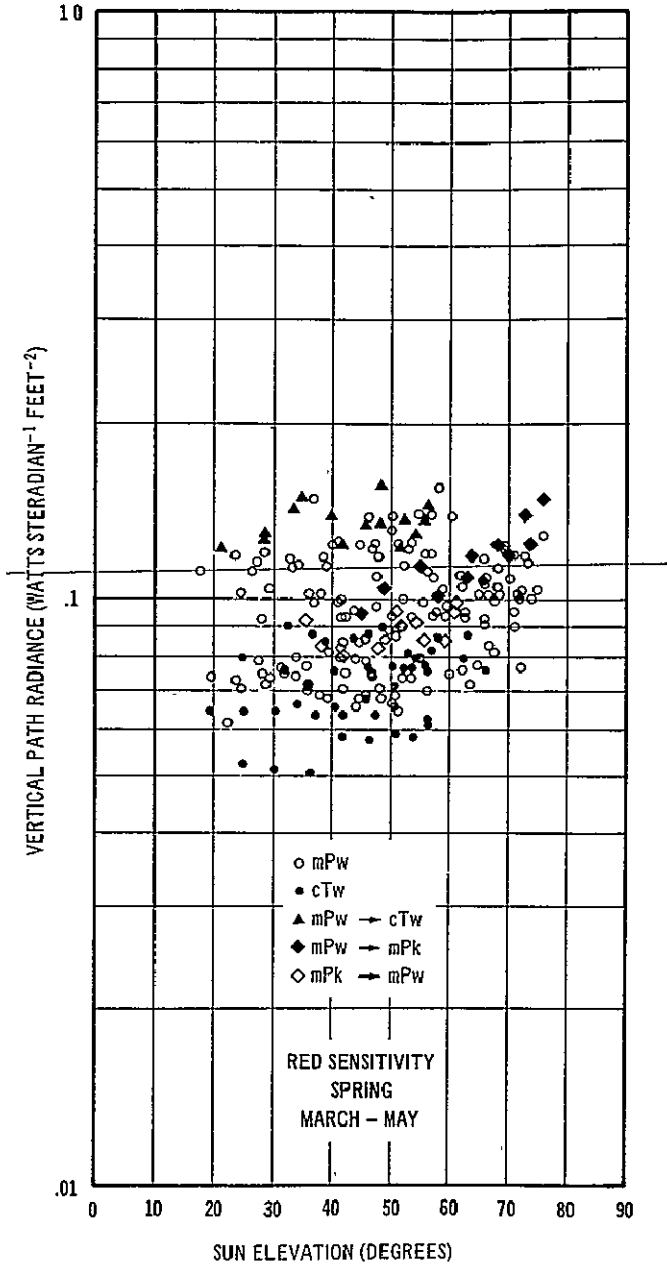
1.0
.1
.01
VERTICAL PATH RADIANCE (WATTS STERADIAN^{-1} FEET^{-2})
0 10 20 30 40 50 60 70 80 90
SUN ELEVATION (DEGREES)
○ mPw
• cTw
▲ mPw → cTw
◆ mPw → mPk
◇ mPk → mPw
RED SENSITIVITY
SPRING
MARCH – MAY

Fig. 19

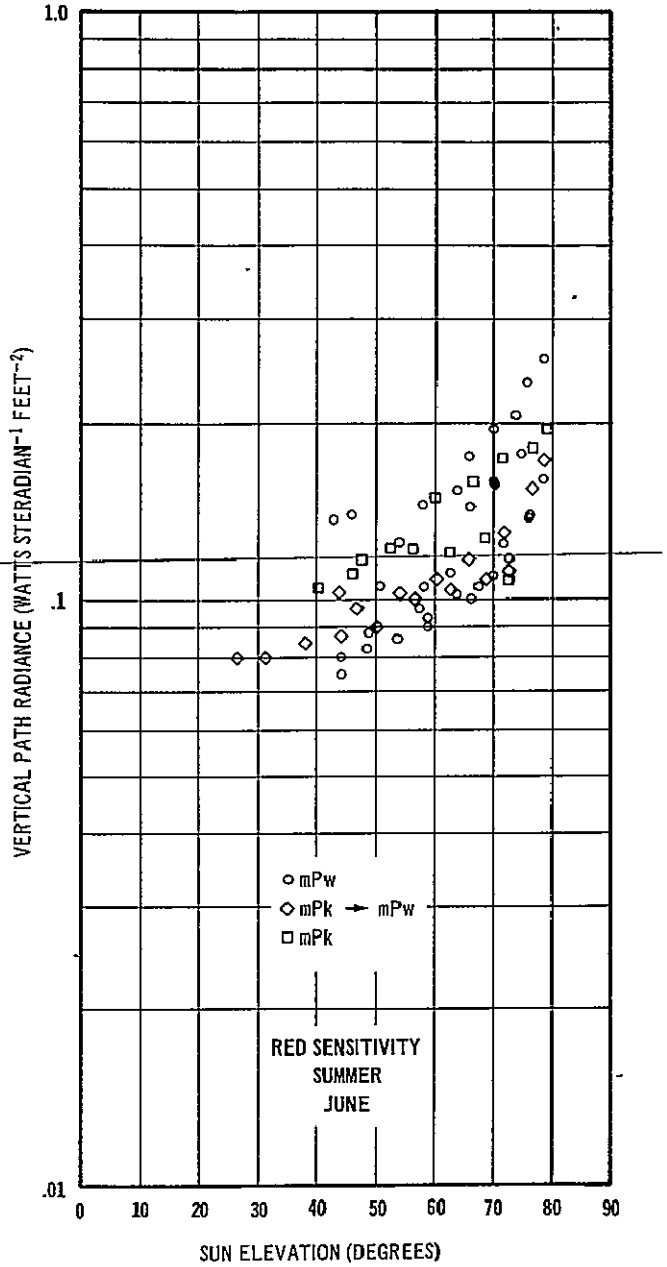
1.0
.1
.01
VERTICAL PATH RADIANCE (WATTS STERADIAN^{-1} FEET^{-2})
0 10 20 30 40 50 60 70 80 90
SUN ELEVATION (DEGREES)
○ mPw
◇ mPk → mPw
□ mPk
RED SENSITIVITY
SUMMER
JUNE

Fig. 20

CONCLUSIONS

The principal effect of the atmosphere upon remote sensing by visible light results from the scattering of the sunlight and the skylight upwards toward the orbiting spacecraft. Path radiance depends upon both the optical state of the atmosphere and upon the nature of the lighting on the path by the sun, the sky, and the ground. It adds to whatever image-forming light from the ground reaches the spacecraft. Thus, it veils the image by reducing its apparent contrast. Knowledge of path radiance is a critical requirement for the design of remote sensors.

Beam transmittance is a property of the atmosphere but not of its lighting. The beam transmittance of the path of sight is that fraction of the image-forming light which reaches the remote sensor without having experienced disruptive scattering. Knowledge of beam transmittance is an important requirement for the design of visible remote sensors.

A remote sensor sees the apparent radiance of the sea which contains the space-averaged radiance of the surface of the sea plus the path radiance due to sunlight and skylight scattered toward the satellite by the atmosphere throughout the path of sight. Another component arises from the daylight which has penetrated into the depths of the sea and has been redirected upward by the scattering processes within the water. Fortunately, this scattered component can be eliminated completely if the satellite makes its observations in the terms of red or infrared light. At these wavelengths the water molecule absorbs very strongly. Thus, the component of the daylight which enters the ocean is absorbed so completely that no appreciable amount of it is scattered upward toward the satellite.

There is very little difference in the data collected at San Clemente Island and San Diego, which indicates that at least this 80-mile portion of the ocean has homogeneous atmospheric characteristics. Further data collection is necessary to determine the area limitations on the air mass distributions. It is difficult to generalize the results concerning vertical path radiance from this sample; more data of this kind are also needed. The analysis of the vertical beam transmittance data does show higher values for the continental air mass throughout all the seasons. In addition there is a diurnal variation in that the values for the vertical beam transmittance are usually lower as the sun elevation increases. This is true for all seasons although at times it is less marked than at others.

SUGGESTIONS

This study was the initial effort in an anticipated long range project. A major portion of the contract period was spent in building and testing the CRM models. This allowed only restricted exploration of some aspects of the atmospheric limitations on remote sensing of sea state roughness from aircraft and orbital spacecraft. Building a data bank requires a great deal more time.

It is suggested that future efforts include the following.

(1) Continue to explore the relationships between the significant optical properties of the atmosphere and measurable meteorological characteristics by means of the same kinds of techniques now employed:

(a) using the same geographic area between San Diego and San Clemente but extending it north and west as understanding of the pertinent properties of the region increases;

(b) using the same near infrared CRM's to continue data collection in the 0.7 to 1.1 micron range but extending the study to include the near ultraviolet and visible spectral regions by building and using two more CRM's adapted to these regions; three of the narrow-band sensitivities in the visible region should match the three sensitivities of the sensors carried by the C-130 research aircraft;

(c) expanding the data base by acquiring a satellite readout receiver so that APT satellite pictures of the research area can be studied in real time.

(2) Initiate a study to determine the areas or regions of the oceans where further investigations like the present one should be made and prepare recommendations for obtaining such information during GARP (when a unique set of meteorological data will be available) by means of CRM's on small islands or on ships (oceanographic, weather, Navy, etc.) if a suitable, inexpensive, reliable CRM for general shipboard use can be designed; because GARP begins in 1973 the development of a shipboard CRM should be initiated in 1970.

(3) Continue to test the fidelity of atmospheric computer models, including reduction and study of C-130 data during the planned combination balloon and aircraft flights at Holloman Air Force Base during the summer of 1970.

REFERENCES

1. Duntley, S. Q., Boileau, A. R., Preisendorfer, R. W., "Image Transmission by the Troposphere," J. Opt. Soc. Am. **47**, 499 (1957).

2. Duntley, S. Q., et al., "Visibility," Applied Optics **3**, 549 (1964).

3. Gordon, J. I., "Model of a Clear Atmosphere," J. Opt. Soc. Am. **59**, 14 (1969).

4. Duntley, S. Q. and Edgerton, C. F., "The Use of Meteorological Satellite Photographs for the Measurement of Sea State," Contract NObs-86012, Lot II, Final Report (June 1966).

5. Gordon, J. I., Harris, J. L., and Duntley, S. Q., "Earth-to-Space Contrast Transmittance Measurements from Ground Stations," SIO Ref. 63-2 (1963).

6. Duntley, S. Q., Johnson, R. W., and Gordon, J. I., "Ground-Based Measurements of Earth-to-Space Beam Transmittance, Path Radiance, and Contrast Transmittance," Technical Documentary Report No. AL-TDR-64-245 (1964).

7. Johnson, F. S., "The Solar Constant," J. Meteor. **11**, 431 (1954).

8. Thekaekara, M. P., Kruger, R., and Duncan, C. H., "Solar Irradiance Measurements from a Research Aircraft," Applied Optics **8**, 1713 (1969).

9. Gordon, J. I. and Church, P. V., "Inherent Radiance of the Center of the Sun, Spectrally and Broadband," Visibility Laboratory Internal Memorandum CV-68-002t.

10. Kasten, F., "A New Table and Approximate Formula for Relative Optical Air Mass," Cold Regions Research and Engineering Laboratory, U. S. Army Materiel Command, Hanover, New Hampshire (1964).

11. Barbrow, L. E., "Memorandum on a Procedure for Obtaining Spectral Radiant Intensity of Tungsten Filament Lamps," J. Opt. Soc. Am. **49**, 1122 (1959).

12. Forsythe, W. E., *Smithsonian Physical Tables*, (Smithsonian Institution, Washington, D. C., 1954), 9th rev. ed.

13. Pivovonsky, M., and Nagel, M. R., *Tables of Blackbody Radiation Functions* (The Macmillan Company, New York, 1961).

14. Optical Society of America, *The Science of Color* (Crowell, New York, 1953).

15. Showalter, A. K., "A Stability Index for Thunderstorm Forecasting," Bull. Amer. Meteor. Soc. *34*, 250 (1953).

16. Edgerton, C. F., "Relationship between Meteorological Conditions and Optical Properties of the Atmosphere," SIO Ref. 67-27 (1967).

THE APPENDIX

The appendix presents the results of a study prepared by Allied Research Associates, Inc. under a subcontract. It includes:

1. Computer listings of cloud amount and cloud type for the San Clemente, San Diego, and San Nicolas Stations. These listings were compiled from the WBAN-10B data tapes using a computer program developed for this purpose by Allied. The record length is 10 years for each station although the specific time intervals are staggered. Cloud amount (in tenths) is presented at 3-hour intervals throughout a 24-hour day for 12 months of the year. For each Local Standard Time (LST) both the actual number of observations (first row of output) and the equivalent percentages (second row of output) are provided.

The cloud-type data for the same stations and the same time periods are presented for the daylight hours only (0700, 1000, 1300, 1600, and 1900 hours LST). The data are stratified into six basic categories including clear skies (no cloud), fog, low, middle and high clouds, and vertical cloud structures. Insofar as the primary goal is to determine the ability of a satellite camera to have a clear line of sight to the surface, the low, middle, and high cloudiness categories are further stratified by their broken or overcast characteristics. Specifically, the 11 "cloud-type" categories are as follows:

Type	Includes
0	Clear skies (no cloud)
1	Fog
2	Nimbostratus (low, thick overcast)
3	Stratus and Fractostratus (low overcast)
4	Stratocumulus and Fractocumulus (low, overcast/broken)
5	Cumulus (low broken)
6	Altostratus (middle overcast)
7	Altocumulus and Altocumulus Castellanus (middle broken)
8	Cirrostratus (high overcast)
9	Cirrus (high broken)
10	Cumulonimbus and Cumulonimbus Mamma (vertical)

Again both the actual number of observations and the percentages are shown. In this case, however, it is the percentage of times that the particular cloud type was observed (at that station, for that month, at that time of day). Because two or more cloud types are often present at one time, the percentages in these tabulations do not total 100.

2. Cumulative probability listings of cloud amount for the three combined stations (San Clemente, San Diego, and San Nicolas) for a 5-year period (January 1961 through December 1965). A shorter time base is used in these compilations because less than 6 years of overlapping data were available for the three stations selected. The cumulative probability listings were derived for the daylight hours only and indicate the probability of observing cloudiness equal to or less than the specified amount. For example, in the month of March at 1600 LST in the afternoon, the probability that the cloud cover is 20 percent or less (equal to the probability that the sky will be 80 percent or more cloud-free) is 37 percent. In all cases, due to a lack of observations, the data base for the 0700 and 1900 listings is 25 and 50 percent less than that for the 1000, 1300, and 1600 listings.

3. Cumulative probability graphs of cloud (and cloud-free) amount for the three combined stations at midmorning (1000) and midafternoon (1600). These graphs were prepared from the cumulative listings described above and are drawn for 12 months of the year. Looking at the graph for March it can be seen that the probability of the skies being 80 percent or more cloud-free increases from 32 percent to 37 percent between 1000 and 1600 LST. The magnitude of this diurnal change increases with the coming of the summer months.

4. Comparisons between satellite-observed and ground-observed cloud cover for the southern California coastal area.

SAN CLEMENTE ISLAND, CALIFORNIA STA93117

JANUARY PERIOD 4/60 THRU 3/69

TOTAL CLOUD AMOUNT (TENTHS)

LST	0	1	2	3	4	5	6	7	8	9	10	TOTAL
1	62	2	11	16	8	3	4	6	7	4	42	165.0
	37.6	1.2	6.7	9.7	4.8	1.8	2.4	3.6	4.2	2.4	25.5	
4	64	9	10	7	6	5	4	8	7	1	46	167.0
	38.3	5.4	6.0	4.2	3.6	3.0	2.4	4.8	4.2	0.6	27.5	
7	62	14	16	14	19	10	13	14	15	10	73	260.0
	23.8	5.4	6.2	5.4	7.3	3.8	5.0	5.4	5.8	3.8	28.1	
10	66	17	12	14	11	12	18	19	12	27	62	270.0
	24.4	6.3	4.4	5.2	4.1	4.4	6.7	7.0	4.4	10.0	23.0	
13	67	17	15	9	11	23	10	11	20	19	58	260.0
	25.8	6.5	5.8	3.5	4.2	8.8	3.8	4.2	7.7	7.3	22.3	
16	66	10	13	13	18	16	17	16	14	22	64	269.0
	24.5	3.7	4.8	4.8	6.7	5.9	6.3	5.9	5.2	8.2	23.8	
19	40	12	7	15	10	11	7	9	14	4	41	170.0
	23.5	7.1	4.1	8.8	5.9	6.5	4.1	5.3	8.2	2.4	24.1	
22	55	11	12	11	9	7	8	3	5	9	39	169.0
	32.5	6.5	7.1	6.5	5.3	4.1	4.7	1.8	3.0	5.3	23.1	

SAN CLEMENTE ISLAND, CALIFORNIA STA93117

JANUARY PERIOD 4/60 THRU 3/69

CLOUD TYPE

	(CLEAR)	(FOG)	(LOW CLOUD)				(MIDDLE CLOUD)		(HIGH CLOUD)		(VERTICAL)
LST	0	1	2	3	4	5	6	7	8	9	10
7	62	26	3	40	70	20	3	28	11	67	0
	23.8	10.0	1.2	15.4	26.9	7.7	1.2	10.8	4.2	25.8	0.0
10	66	22	2	38	80	25	4	34	12	78	1
	24.4	8.1	0.7	14.1	29.6	9.3	1.5	12.6	4.4	25.9	0.4
13	67	12	1	33	83	26	4	27	15	76	1
	25.8	4.6	0.4	12.7	31.9	10.0	1.5	10.4	5.8	29.2	0.4
16	66	18	1	33	72	26	2	34	21	78	1
	24.5	6.7	0.4	12.3	26.8	9.7	0.7	12.6	7.8	29.0	0.4
19	40	14	0	30	41	11	1	18	11	49	0
	23.5	8.2	0.0	17.6	24.1	6.5	0.6	10.6	6.5	28.8	0.0

SAN CLEMENTE ISLAND, CALIFORNIA STA93117

FEBRUARY PERIOD 4/60 THRU 3/69

TOTAL CLOUD AMOUNT (TENTHS)

LST	0	1	2	3	4	5	6	7	8	9	10	TOTAL
1	73	5	8	14	6	5	5	7	8	3	36	170.0
	42.9	2.9	4.7	8.2	3.5	2.9	2.9	4.1	4.7	1.8	21.2	
4	67	6	4	13	8	6	6	11	4	6	39	170.0
	39.4	3.5	2.4	7.6	4.7	3.5	3.5	6.5	2.4	3.5	22.9	
7	52	14	11	10	12	10	14	14	21	19	69	246.0
	21.1	5.7	4.5	4.1	4.9	4.1	5.7	5.7	8.5	7.7	28.0	
10	53	13	11	7	16	17	6	17	19	26	69	254.0
	20.9	5.1	4.3	2.8	6.3	6.7	2.4	6.7	7.5	10.2	27.2	
13	55	11	15	16	7	14	9	17	16	18	68	246.0
	22.4	4.5	6.1	6.5	2.8	5.7	3.7	6.9	6.5	7.3	27.6	
16	61	17	11	12	11	14	9	11	20	23	65	254.0
	24.0	6.7	4.3	4.7	4.3	5.5	3.5	4.3	7.9	9.1	25.6	
19	48	12	6	11	7	12	9	14	15	3	33	170.0
	28.2	7.1	3.5	6.5	4.1	7.1	5.3	8.2	8.8	1.8	19.4	
22	61	12	8	13	11	9	3	13	8	4	28	170.0
	35.9	7.1	4.7	7.6	6.5	5.3	1.8	7.6	4.7	2.4	16.5	

SAN CLEMENTE ISLAND, CALIFORNIA STA93117

FEBRUARY PERIOD 4/60 THRU 3/69

CLOUD TYPE

	(CLEAR)	(FOG)	(LOW CLOUD)				(MIDDLE CLOUD)		(HIGH CLOUD)		(VERTICAL)
LST	0	1	2	3	4	5	6	7	8	9	10
7	52	27	0	41	81	32	2	28	13	56	1
	21.1	11.0	0.0	16.7	32.9	13.0	0.8	11.4	5.3	22.8	0.4
10	53	20	0	37	74	40	3	36	17	66	2
	20.9	7.9	0.0	14.6	29.1	15.7	1.2	14.2	6.7	26.0	0.8
13	55	12	0	36	65	47	2	28	15	73	2
	22.4	4.9	0.0	14.6	26.4	19.1	0.8	11.4	6.1	29.7	0.8
16	61	19	0	30	59	42	3	36	13	78	3
	24.0	7.5	0.0	11.8	23.2	16.5	1.2	14.2	5.1	30.7	1.2
19	48	13	0	26	40	10	2	26	8	51	1
	28.2	7.6	0.0	15.3	23.5	5.9	1.2	15.3	4.7	30.0	0.6

SAN CLEMENTE ISLAND, CALIFORNIA STA93117

MARCH PERIOD 4/60 THRU 3/69

TOTAL CLOUD AMOUNT (TENTHS)

LST	0	1	2	3	4	5	6	7	8	9	10	TOTAL
1	63	4	12	8	7	7	4	10	12	5	54	186.0
	33.9	2.2	6.5	4.3	3.8	3.8	2.2	5.4	6.5	2.7	29.0	
4	59	4	7	11	5	9	5	10	9	11	56	186.0
	31.7	2.2	3.8	5.9	2.7	4.8	2.7	5.4	4.8	5.9	30.1	
7	40	12	13	19	10	11	15	25	21	19	85	270.0
	14.8	4.4	4.8	7.0	3.7	4.1	5.6	9.3	7.8	7.0	31.5	
10	42	20	13	17	10	10	12	23	24	29	79	279.0
	15.1	7.2	4.7	6.1	3.6	3.6	4.3	8.2	8.6	10.4	28.3	
13	54	20	17	8	14	14	22	21	20	16	65	271.0
	19.9	7.4	6.3	3.0	5.2	5.2	8.1	7.7	7.4	5.9	24.0	
16	59	12	14	16	16	21	7	15	28	27	64	279.0
	21.1	4.3	5.0	5.7	5.7	7.5	2.5	5.4	10.0	9.7	22.9	
19	41	13	9	13	6	13	8	15	24	11	45	198.0
	20.7	6.6	4.5	6.6	3.0	6.6	4.0	7.6	12.1	5.6	22.7	
22	64	8	14	12	5	8	9	11	18	5	44	198.0
	32.3	4.0	7.1	6.1	2.5	4.0	4.5	5.6	9.1	2.5	22.2	

SAN CLEMENTE ISLAND, CALIFORNIA STA93117

MARCH PERIOD 4/60 THRU 3/69

CLOUD TYPE

	(CLEAR)	(FOG)	(LOW CLOUD)				(MIDDLE CLOUD)		(HIGH CLOUD)		(VERTICAL)
LST	0	1	2	3	4	5	6	7	8	9	10
7	40	14	3	53	104	53	3	32	7	72	0
	14.8	5.2	1.1	19.6	38.5	19.6	1.1	11.9	2.6	26.7	0.0
10	42	11	0	49	104	66	3	34	15	61	1
	15.1	3.9	0.0	17.6	37.3	23.7	1.1	12.2	5.4	21.9	0.4
13	54	9	0	33	90	69	5	24	13	70	1
	19.9	3.3	0.0	12.2	33.2	25.5	1.8	8.9	4.8	25.8	0.4
16	59	11	0	34	77	54	6	24	16	78	2
	21.1	3.9	0.0	12.2	27.6	19.4	2.2	8.6	5.7	28.0	0.7
19	41	7	0	36	58	30	3	28	9	58	0
	20.7	3.5	0.0	18.2	29.3	15.2	1.5	14.1	4.5	29.3	0.0

SAN CLEMENTE ISLAND, CALIFORNIA STA93117

APRIL PERIOD 4/60 THRU 3/69

TOTAL CLOUD AMOUNT (TENTHS)

LST	0	1	2	3	4	5	6	7	8	9	10	TOTAL
1	59	6	7	10	4	7	3	5	10	9	54	174.0
	33.9	3.4	4.0	5.7	2.3	4.6	1.7	2.9	5.7	5.2	31.0	
4	47	7	9	8	10	9	5	7	7	7	58	174.0
	27.0	4.0	5.2	4.6	5.7	5.2	2.9	4.0	4.0	4.0	33.3	
7	46	13	11	14	12	8	12	17	19	28	80	260.0
	17.7	5.0	4.2	5.4	4.6	3.1	4.6	6.5	7.3	10.8	30.8	
10	53	14	15	14	11	8	14	25	25	17	74	270.0
	19.6	5.2	5.6	5.2	4.1	3.0	5.2	9.3	9.3	6.3	27.4	
13	67	19	17	14	9	12	15	19	16	17	55	260.0
	25.8	7.3	6.5	5.4	3.5	4.6	5.8	7.3	6.2	6.5	21.2	
16	73	22	14	16	15	9	8	15	16	21	59	268.0
	27.2	8.2	5.2	6.0	5.6	3.4	3.0	5.6	6.0	7.8	22.0	
19	46	14	11	10	10	4	6	6	16	9	48	180.0
	25.6	7.8	6.1	5.6	5.6	2.2	3.3	3.3	8.9	5.0	26.7	
22	69	11	5	15	5	7	5	10	6	3	45	181.0
	38.1	6.1	2.8	8.3	2.8	3.9	2.8	5.5	3.3	1.7	24.9	

SAN CLEMENTE ISLAND, CALIFORNIA STA93117

APRIL PERIOD 4/60 THRU 3/69

CLOUD TYPE

	(CLEAR)	(FOG)	(LOW CLOUD)				(MIDDLE CLOUD)		(HIGH CLOUD)		(VERTICAL)
LST	0	1	2	3	4	5	6	7	8	9	10
7	46	22	0	49	106	53	2	21	9	37	2
	17.7	8.5	0.0	18.8	40.8	20.4	0.8	8.1	3.5	14.2	0.8
10	53	16	0	40	106	63	5	29	8	49	2
	19.6	5.9	0.0	14.8	39.3	23.3	1.9	10.7	3.0	18.1	0.7
13	67	14	0	43	86	55	2	21	11	57	3
	25.8	5.4	0.0	16.5	33.1	21.2	0.8	8.1	4.2	21.9	1.2
16	73	14	0	46	82	51	3	22	10	53	2
	27.2	5.2	0.0	17.2	30.6	19.0	1.1	8.2	3.7	19.8	0.7
19	46	5	0	29	55	31	3	12	6	39	2
	25.6	2.8	0.0	16.1	30.6	17.2	1.7	6.7	3.3	21.7	1.1

SAN CLEMENTE ISLAND, CALIFORNIA STA93117

MAY PERIOD 4/60 THRU 3/69

TOTAL CLOUD AMOUNT (TENTHS)

LST	0	1	2	3	4	5	6	7	8	9	10	TOTAL
1	30	3	3	8	10	9	4	5	11	4	99	186.0
	16.1	1.6	1.6	4.3	5.4	4.8	2.2	2.7	5.9	2.2	53.2	
4	25	2	7	9	7	4	7	4	10	7	104	186.0
	13.4	1.1	3.8	4.8	3.8	2.2	3.8	2.2	5.4	3.8	55.9	
7	36	8	10	8	11	11	7	13	17	15	135	271.0
	13.3	3.0	3.7	3.0	4.1	4.1	2.6	4.8	6.3	5.5	49.8	
10	35	16	13	16	5	16	11	13	18	21	107	271.0
	12.9	5.9	4.8	5.9	1.8	5.9	4.1	4.8	6.6	7.7	39.5	
13	51	12	12	16	11	17	11	18	27	18	78	271.0
	18.8	4.4	4.4	5.9	4.1	6.3	4.1	6.6	10.0	6.6	28.8	
16	48	9	7	6	6	12	14	12	13	18	72	217.0
	22.1	4.1	3.2	2.8	2.8	5.5	6.5	5.5	6.0	8.3	33.2	
19	29	8	9	7	5	8	9	8	11	11	81	186.0
	15.6	4.3	4.8	3.8	2.7	4.3	4.8	4.3	5.9	5.9	43.5	
22	35	1	6	6	12	7	4	9	13	3	90	186.0
	18.8	0.5	3.2	3.2	6.5	3.8	2.2	4.8	7.0	1.6	48.4	

SAN CLEMENTE ISLAND, CALIFORNIA STA93117

MAY PERIOD 4/60 THRU 3/69

CLOUD TYPE

	(CLEAR)	(FOG)		(LOW CLOUD)			(MIDDLE CLOUD)		(HIGH CLOUD)		(VERTICAL)
LST	0	1	2	3	4	5	6	7	8	9	10
7	36	11	0	88	132	26	0	16	7	19	0
	13.3	4.1	0.0	32.5	48.7	9.6	0.0	5.9	2.6	7.0	0.0
10	35	8	0	76	144	34	1	16	12	18	0
	12.9	3.0	0.0	28.0	53.1	12.5	0.4	5.9	4.4	6.6	0.0
13	51	5	0	68	130	34	0	14	10	36	1
	18.8	1.8	0.0	25.1	48.0	12.5	0.0	5.2	3.7	13.3	0.4
16	48	2	0	54	101	24	3	11	9	34	0
	22.1	0.9	0.0	24.9	46.5	11.1	1.4	5.1	4.1	15.7	0.0
19	29	7	0	51	90	14	1	13	3	31	1
	15.6	3.8	0.0	27.4	48.4	7.5	0.5	7.0	1.6	16.7	0.5

SAN CLEMENTE ISLAND, CALIFORNIA STA93117

JUNE PERIOD 4/60 THRU 3/69

TOTAL CLOUD AMOUNT (TENTHS)

LST	0	1	2	3	4	5	6	7	8	9	10	TOTAL
1	21	1	3	11	1	1	4	7	9	3	119	180.0
	11.7	0.6	1.7	6.1	0.6	0.6	2.2	3.9	5.0	1.7	66.1	
4	11	6	4	1	2	2	5	7	9	8	125	180.0
	6.1	3.3	2.2	0.6	1.1	1.1	2.8	3.9	5.0	4.4	69.4	
7	13	4	3	5	1	2	6	5	15	14	194	262.0
	5.0	1.5	1.1	1.9	0.4	0.8	2.3	1.9	5.7	5.3	74.0	
10	23	3	7	3	4	15	7	15	13	11	162	263.0
	8.7	1.1	2.7	1.1	1.5	5.7	2.7	5.7	4.9	4.2	61.6	
13	33	10	6	11	9	9	11	16	28	20	109	262.0
	12.6	3.8	2.3	4.2	3.4	3.4	4.2	6.1	10.7	7.6	41.6	
16	34	8	8	4	3	6	8	17	20	24	79	211.0
	16.1	3.8	3.8	1.9	1.4	2.8	3.8	8.1	9.5	11.4	37.4	
19	19	10	10	1	9	4	8	7	10	14	88	180.0
	10.6	5.6	5.6	0.6	5.0	2.2	4.4	3.9	5.6	7.8	48.9	
22	22	7	5	6	4	5	5	9	10	6	101	180.0
	12.2	3.9	2.8	3.3	2.2	2.8	2.8	5.0	5.6	3.3	56.1	

SAN CLEMENTE ISLAND, CALIFORNIA STA93117

JUNE PERIOD 4/60 THRU 3/69

CLOUD TYPE

	(CLEAR)	(EGG)		(LOW CLOUD)			(MIDDLE CLOUD)		(HIGH CLOUD)		(VERTICAL)
LST	0	1	2	3	4	5	6	7	8	9	10
7	13	31	0	109	133	9	0	4	0	4	0
	5.0	11.8	0.0	41.6	50.8	3.4	0.0	1.5	0.0	1.5	0.0
10	23	17	0	108	146	15	0	5	0	6	0
	8.7	6.5	0.0	41.1	55.5	5.7	0.0	1.9	0.0	2.3	0.0
13	33	10	0	87	152	19	1	5	2	13	0
	12.6	3.8	0.0	33.2	58.0	7.3	0.4	1.9	0.8	5.0	0.0
16	34	3	0	86	101	14	0	2	1	9	0
	16.1	1.4	0.0	40.8	47.9	6.6	0.0	0.9	0.5	4.3	0.0
19	19	7	0	92	72	12	0	7	2	6	0
	10.6	3.9	0.0	51.1	40.0	6.7	0.0	3.9	1.1	3.3	0.0

SAN CLEMENTE ISLAND, CALIFORNIA STA93117

JULY PERIOD 4/60 THRU 3/69

TOTAL CLOUD AMOUNT (TENTHS)

LST	0	1	2	3	4	5	6	7	8	9	10	TOTAL
1	16	5	6	4	8	2	9	9	9	11	107	186.0
	8.6	2.7	3.2	2.2	4.3	1.1	4.8	4.8	4.8	5.9	57.5	
4	7	3	2	3	4	4	4	5	18	9	127	186.0
	3.8	1.6	1.1	1.6	2.2	2.2	2.2	2.7	9.7	4.8	68.3	
7	12	1	4	4	2	7	4	6	16	24	189	269.0
	4.5	0.4	1.5	1.5	0.7	2.6	1.5	2.2	5.9	8.9	70.3	
10	17	6	4	10	14	18	8	18	29	36	115	275.0
	6.2	2.2	1.5	3.6	5.1	6.5	2.9	6.5	10.5	13.1	41.8	
13	32	11	16	10	20	26	15	28	34	21	56	269.0
	11.9	4.1	5.9	3.7	7.4	9.7	5.6	10.4	12.6	7.8	20.8	
16	30	8	1	11	9	20	9	24	26	26	59	223.0
	13.5	3.6	0.4	4.9	4.0	9.0	4.0	10.8	11.7	11.7	26.5	
19	18	4	1	6	0	12	5	9	21	18	92	186.(
	9.7	2.2	0.5	3.2	0.0	6.5	2.7	4.8	11.3	9.7	49.5	
22	22	5	6	9	9	7	3	3	17	18	87	186.(
	11.8	2.7	3.2	4.8	4.8	3.8	1.6	1.6	9.1	9.7	46.8	

SAN CLEMENTE ISLAND, CALIFORNIA STA93117

JULY PERIOD 4/60 THRU 3/69

CLOUD TYPE

	(CLEAR)	(FOG)	(LOW CLOUD)				(MIDDLE CLOUD)		(HIGH CLOUD)		(VERTICAL)
LST	0	1	2	3	4	5	6	7	8	9	10
7	12	27	0	156	90	3	1	22	1	11	0
	4.5	10.0	0.0	58.0	33.5	1.1	0.4	8.2	0.4	4.1	0.0
10	17	12	0	148	111	0	0	26	1	22	0
	6.2	4.4	0.0	53.8	40.4	0.0	0.0	9.5	0.4	8.0	0.0
13	32	7	0	132	96	1	0	21	6	28	2
	11.9	2.6	0.0	49.1	35.7	0.4	0.0	7.8	2.2	10.4	0.7
16	30	3	0	134	57	0	0	18	4	23	0
	13.5	1.3	0.0	60.1	25.6	0.0	0.0	8.1	1.8	10.3	0.0
19	18	9	0	133	29	0	1	14	2	14	0
	9.7	4.8	0.0	71.5	15.6	0.0	0.5	7.5	1.1	7.5	0.0

SAN CLEMENTE ISLAND, CALIFORNIA STA93117

AUGUST PERIOD 4/60 THRU 3/69

TOTAL CLOUD AMOUNT (TENTHS)

LST	0	1	2	3	4	5	6	7	8	9	10	TOTAL
1	21	4	6	5	6	8	2	9	13	9	103	186.0
	11.3	2.2	3.2	2.7	3.2	4.3	1.1	4.8	7.0	4.8	55.4	
4	15	2	10	4	5	2	8	4	14	8	114	186.0
	8.1	1.1	5.4	2.2	2.7	1.1	4.3	2.2	7.5	4.3	61.3	
7	17	7	4	4	5	3	5	14	17	34	161	271.0
	6.3	2.6	1.5	1.5	1.8	1.1	1.8	5.2	6.3	12.5	59.4	
10	15	6	15	17	15	9	15	15	25	33	105	270.0
	5.6	2.2	5.6	6.3	5.6	3.3	5.6	5.6	9.3	12.2	38.9	
13	37	21	12	16	31	18	20	30	22	22	42	271.0
	13.7	7.7	4.4	5.9	11.4	6.6	7.4	11.1	8.1	8.1	15.5	
16	25	13	14	8	10	15	15	24	23	21	49	217.0
	11.5	6.0	6.5	3.7	4.6	6.9	6.9	11.1	10.6	9.7	22.6	
19	18	5	12	10	8	7	9	7	16	11	83	186.0
	9.7	2.7	6.5	5.4	4.3	3.8	4.8	3.8	8.6	5.9	44.6	
22	22	3	9	10	9	5	4	9	18	12	85	186.0
	11.8	1.6	4.8	5.4	4.8	2.7	2.2	4.8	9.7	6.5	45.7	

SAN CLEMENTE ISLAND, CALIFORNIA STA93117

AUGUST PERIOD 4/60 THRU 3/69

CLOUD TYPE

	(CLEAR)	(FOG)	(LOW CLOUD)				(MIDDLE CLOUD)		(HIGH CLOUD)		(VERTICAL)
LST	0	1	2	3	4	5	6	7	8	9	10
7	17	26	0	158	81	0	0	25	0	12	0
	6.3	9.6	0.0	58.3	29.9	0.0	0.0	9.2	0.0	4.4	0.0
10	15	10	0	159	99	1	0	32	1	16	0
	5.6	3.7	0.0	58.9	36.7	0.4	0.0	11.9	0.4	5.9	0.0
13	37	5	0	143	80	9	0	26	1	27	0
	13.7	1.8	0.0	52.8	29.5	3.3	0.0	9.6	0.4	10.0	0.0
16	25	1	0	136	49	5	0	21	0	15	1
	11.5	0.5	0.0	62.7	22.6	2.3	0.0	9.7	0.0	6.9	0.5
19	18	7	0	119	36	3	0	20	0	11	0
	9.7	3.8	0.0	64.0	19.4	1.6	0.0	10.8	0.0	5.9	0.0

SAN CLEMENTE ISLAND, CALIFORNIA STA93117

SEPTEMBER PERIOD 4/60 THRU 3/69

TOTAL CLOUD AMOUNT (TENTHS)

LST	0	1	2	3	4	5	6	7	8	9	10	TOTAL
1	50	5	6	11	4	1	1	9	12	6	75	180.0
	27.8	2.8	3.3	6.1	2.2	0.6	0.6	5.0	6.7	3.3	41.7	
4	49	1	5	4	6	3	8	7	9	7	82	181.0
	27.1	0.6	2.8	2.2	3.3	1.7	4.4	3.9	5.0	3.9	45.3	
7	38	12	5	9	4	5	12	8	29	13	130	265.0
	14.3	4.5	1.9	3.4	1.5	1.9	4.5	3.0	10.9	4.9	49.1	
10	45	9	14	16	8	9	10	15	26	17	98	267.0
	16.9	3.4	5.2	6.0	3.0	3.4	3.7	5.6	9.7	6.4	36.7	
13	65	17	13	16	18	15	8	21	17	16	54	260.0
	25.0	6.5	5.0	6.2	6.9	5.8	3.1	8.1	6.5	6.2	20.8	
16	58	19	13	10	8	5	12	10	19	14	50	218.0
	26.6	8.7	6.0	4.6	3.7	2.3	5.5	4.6	8.7	6.4	22.9	
19	45	6	10	8	9	10	4	8	10	12	58	180.0
	25.0	3.3	5.6	4.4	5.0	5.6	2.2	4.4	5.6	6.7	32.2	
22	55	5	5	7	9	6	1	8	10	11	63	180.0
	30.6	2.8	2.8	3.9	5.0	3.3	0.6	4.4	5.6	6.1	35.0	

SAN CLEMENTE ISLAND, CALIFORNIA STA93117

SEPTEMBER PERIOD 4/60 THRU 3/69

CLOUD TYPE

	(CLEAR)	(FOG)	(LOW CLOUD)				(MIDDLE CLOUD)		(HIGH CLOUD)		(VERTICAL)
LST	0	1	2	3	4	5	6	7	8	9	10
7	38	12	1	118	96	14	0	17	0	15	0
	14.3	4.5	0.4	44.5	36.2	5.3	0.0	6.4	0.0	5.7	0.0
10	45	10	1	96	114	19	1	24	1	17	0
	16.9	3.7	0.4	36.0	42.7	7.1	0.4	9.0	0.4	6.4	0.0
13	65	2	0	79	101	29	0	17	2	25	1
	25.0	0.8	0.0	30.4	38.8	11.2	0.0	6.5	0.8	9.6	0.4
16	58	1	0	84	63	16	0	16	1	24	2
	26.6	0.5	0.0	38.5	28.9	7.3	0.0	7.3	0.5	11.0	0.9
19	45	3	0	79	49	7	0	11	0	16	1
	25.0	1.7	0.0	43.9	27.2	3.9	0.0	6.1	0.0	8.9	0.6

SAN CLEMENTE ISLAND, CALIFORNIA STA93117

OCTOBER PERIOD 4/60 THRU 3/69

TOTAL CLOUD AMOUNT (TENTHS)

LST	0	1	2	3	4	5	6	7	8	9	10	TOTAL
1	66 35.5	0 0.0	15 8.1	9 4.8	10 5.4	8 4.3	3 1.6	7 3.8	15 8.1	3 1.6	50 26.9	186.0
4	61 32.8	4 2.2	7 3.8	3 1.6	7 3.8	9 4.8	5 2.7	10 5.4	13 7.0	4 2.2	63 33.9	186.0
7	57 21.1	15 5.6	6 2.2	13 4.8	9 3.3	6 2.2	6 2.2	21 7.8	14 5.2	18 6.7	105 38.9	270.0
10	65 24.1	14 5.2	10 3.7	14 5.2	11 4.1	16 5.9	13 4.8	18 6.7	11 4.1	20 7.4	78 28.9	270.0
13	71 26.3	20 7.4	13 4.8	16 5.9	20 7.4	13 4.8	9 3.3	16 5.9	19 7.0	13 4.8	60 22.2	270.0
16	74 30.3	17 7.0	14 5.7	13 5.3	17 7.0	11 4.5	7 2.9	9 3.7	19 7.8	13 5.3	50 20.5	244.0
19	52 28.0	5 2.7	11 5.9	16 8.6	15 8.1	11 5.9	11 5.9	10 5.4	8 4.3	6 3.2	41 22.0	186.0
22	59 31.7	7 3.8	13 7.0	8 4.3	18 9.7	6 3.2	7 3.8	5 2.7	9 4.8	11 5.9	43 23.1	186.0

SAN CLEMENTE ISLAND, CALIFORNIA STA93117

OCTOBER PERIOD 4/60 THRU 3/69

CLOUD TYPE

	(CLEAR)	(FOG)	(LOW CLOUD)				(MIDDLE CLOUD)		(HIGH CLOUD)		(VERTICAL)
LST	0	1	2	3	4	5	6	7	8	9	10
7	57 21.1	27 10.0	0 0.0	85 31.5	97 35.9	10 3.7	0 0.0	20 7.4	1 0.4	37 13.7	1 0.4
10	65 24.1	22 8.1	0 0.0	73 27.0	105 38.9	12 4.4	0 0.0	17 6.3	1 0.4	48 17.8	2 0.7
13	71 26.3	15 5.6	0 0.0	61 22.6	104 38.5	14 5.2	0 0.0	19 7.0	3 1.1	61 22.6	2 0.7
16	74 30.3	11 4.5	0 0.0	56 23.0	64 26.2	15 6.1	1 0.4	19 7.8	6 2.5	57 23.4	0 0.0
19	52 28.0	9 4.8	0 0.0	57 30.6	40 21.5	9 4.8	0 0.0	10 5.4	3 1.6	40 21.5	1 0.5

SAN CLEMENTE ISLAND, CALIFORNIA STA93117

NOVEMBER PERIOD 4/60 THRU 3/69

TOTAL CLOUD AMOUNT (TENTHS)

LST	0	1	2	3	4	5	6	7	8	9	10	TOTAL
1	65	5	7	14	5	7	5	5	15	7	45	180.0
	36.1	2.8	3.9	7.8	2.8	3.9	2.8	2.8	8.3	3.9	25.0	
4	58	9	10	7	15	7	6	8	10	4	46	180.0
	32.2	5.0	5.6	3.9	8.3	3.9	3.3	4.4	5.6	2.2	25.6	
7	47	11	16	12	19	10	9	17	30	26	77	268.0
	17.5	4.1	6.0	4.5	7.1	3.7	3.4	6.3	11.2	7.5	28.7	
10	55	11	11	15	8	13	20	21	17	20	76	267.0
	20.6	4.1	4.1	5.6	3.0	4.9	7.5	7.9	6.4	7.5	28.5	
13	53	11	15	16	14	12	11	22	21	18	74	267.0
	19.9	4.1	5.6	6.0	5.2	4.5	4.1	8.2	7.9	6.7	27.7	
16	52	9	22	13	19	15	11	16	23	16	71	267.0
	19.5	3.4	8.2	4.9	7.1	5.6	4.1	6.0	8.6	6.0	26.6	
19	45	8	12	10	11	13	8	11	11	5	46	180.0
	25.0	4.4	6.7	5.6	6.1	7.2	4.4	6.1	6.1	2.8	25.6	
22	58	11	10	6	10	8	8	6	9	9	45	180.0
	32.2	6.1	5.6	3.3	5.6	4.4	4.4	3.3	5.0	5.0	25.0	

SAN CLEMENTE ISLAND, CALIFORNIA STA93117

NOVEMBER PERIOD 4/60 THRU 3/69

CLOUD TYPE

	(CLEAR)	(FOG)	(LOW CLOUD)				(MIDDLE CLOUD)		(HIGH CLOUD)		(VERTICAL)
LST	0	1	2	3	4	5	6	7	8	9	10
7	47	16	5	62	96	35	3	29	7	71	4
	17.5	6.0	1.9	23.1	35.8	13.1	1.1	10.8	2.6	26.5	1.5
10	55	13	5	41	103	47	0	34	11	73	3
	20.6	4.9	1.9	15.4	38.6	17.6	0.0	12.7	4.1	27.3	1.1
13	53	12	2	36	97	50	1	36	8	82	3
	19.9	4.5	0.7	13.5	36.3	18.7	0.4	13.5	3.0	30.7	1.1
16	52	17	3	33	99	45	3	34	15	83	2
	19.5	6.4	1.1	12.4	37.1	16.9	1.1	12.7	5.6	31.1	0.7
19	45	11	5	33	51	21	3	19	12	38	1
	25.0	6.1	2.8	18.3	28.3	11.7	1.7	10.6	6.7	21.1	0.6

SAN CLEMENTE ISLAND, CALIFORNIA STA93117

DECEMBER PERIOD 4/60 THRU 3/69

TOTAL CLOUD AMOUNT (TENTHS)

LST	0	1	2	3	4	5	6	7	8	9	10	TOTAL
1	68	6	5	8	8	5	5	5	6	1	29	146.0
	46.6	4.1	3.4	5.5	5.5	3.4	3.4	3.4	4.1	0.7	19.9	
4	84	5	9	7	9	6	3	6	4	1	22	156.0
	53.8	3.2	5.8	4.5	5.8	3.8	1.9	3.8	2.6	0.6	14.1	
7	58	11	12	26	17	13	8	17	28	12	62	264.0
	22.0	4.2	4.5	9.8	6.4	4.9	3.0	6.4	10.6	4.5	23.5	
10	58	14	7	26	22	14	14	26	18	12	56	267.0
	21.7	5.2	2.6	9.7	8.2	5.2	5.2	9.7	6.7	4.5	21.0	
13	52	16	17	13	15	15	14	19	20	20	63	264.0
	19.7	6.1	6.4	4.9	5.7	5.7	5.3	7.2	7.6	7.6	23.9	
16	57	18	14	12	11	12	13	16	18	18	64	253.0
	22.5	7.1	5.5	4.7	4.3	4.7	5.1	6.3	7.1	7.1	25.3	
19	50	7	16	10	4	7	5	7	12	4	25	147.0
	34.0	4.8	10.9	6.8	2.7	4.8	3.4	4.8	8.2	2.7	17.0	
22	65	10	5	10	6	7	4	6	4	2	27	146.0
	44.5	6.8	3.4	6.8	4.1	4.8	2.7	4.1	2.7	1.4	18.5	

SAN CLEMENTE ISLAND, CALIFORNIA STA93117

DECEMBER PERIOD 4/60 THRU 3/69

CLOUD TYPE

	(CLEAR)	(FOG)	(LOW CLOUD)				(MIDDLE CLOUD)		(HIGH CLOUD)		(VERTICAL)
LST	0	1	2	3	4	5	6	7	8	9	10
7	58	33	2	34	77	35	5	31	6	77	3
	22.0	12.5	0.8	12.9	29.2	13.3	1.9	11.7	2.3	29.2	1.1
10	58	23	0	32	81	47	2	32	5	92	1
	21.7	8.6	0.0	12.0	30.3	17.6	0.7	12.0	1.9	34.5	0.4
13	52	29	1	31	68	51	4	29	4	93	2
	19.7	11.0	0.4	11.7	25.8	19.3	1.5	11.0	1.5	35.2	0.8
16	57	23	1	25	64	37	1	26	4	83	2
	22.5	9.1	0.4	9.9	25.3	14.6	0.4	10.3	1.6	32.8	0.8
19	50	7	2	26	29	11	1	8	3	41	1
	34.0	4.8	1.4	17.7	19.7	7.5	0.7	5.4	2.0	27.9	0.7

SAN DIEGO, CALIFORNIA STA93112

JANUARY PERIOD 1/59 THRU 12/68

TOTAL CLOUD AMOUNT (TENTHS)

LST	0	1	2	3	4	5	6	7	8	9	10	TOTAL
1	126	6	11	14	9	12	6	13	13	18	82	310.0
	40.6	1.9	3.5	4.5	2.9	3.9	1.9	4.2	4.2	5.8	26.5	
4	130	11	15	11	5	5	13	15	14	12	79	310.0
	41.9	3.5	4.8	3.5	1.6	1.6	4.2	4.8	4.5	3.9	25.5	
7	78	20	20	17	11	19	7	20	24	15	79	310.0
	25.2	6.5	6.5	5.5	3.5	6.1	2.3	6.5	7.7	4.8	25.5	
10	92	29	11	22	10	15	17	13	24	25	52	310.0
	29.7	9.4	3.5	7.1	3.2	4.8	5.5	4.2	7.7	8.1	16.8	
13	83	26	23	17	25	7	19	18	27	16	49	310.0
	26.8	8.4	7.4	5.5	8.1	2.3	6.1	5.8	8.7	5.2	15.8	
16	79	25	23	23	16	26	9	17	19	19	54	310.0
	25.5	8.1	7.4	7.4	5.2	8.4	2.9	5.5	6.1	6.1	17.4	
19	117	19	24	24	15	10	11	13	17	12	48	310.0
	37.7	6.1	7.7	7.7	4.8	3.2	3.5	4.2	5.5	3.9	15.5	
22	121	14	13	14	18	12	11	20	9	7	71	310.0
	39.0	4.5	4.2	4.5	5.8	3.9	3.5	6.5	2.9	2.3	22.9	

SAN DIEGO, CALIFORNIA STA93112

JANUARY PERIOD 1/59 THRU 12/68

CLOUD TYPE

	(CLEAR)	(FOG)	(LOW CLOUD)				(MIDDLE CLOUD)		(HIGH CLOUD)		(VERTICAL)
LST	0	1	2	3	4	5	6	7	8	9	10
7	78	27	1	29	70	27	19	45	38	82	1
	25.2	8.7	0.3	9.4	22.6	8.7	6.1	14.5	12.3	26.5	0.3
10	92	16	2	27	60	37	13	48	45	87	3
	29.7	5.2	0.6	8.7	19.4	11.9	4.2	15.5	14.5	28.1	1.0
13	83	3	3	17	54	54	10	41	48	104	1
	26.8	1.0	1.0	5.5	17.4	17.4	3.2	13.2	15.5	33.5	0.3
16	79	5	3	21	48	48	15	44	44	100	1
	25.5	1.6	1.0	6.8	15.5	15.5	4.8	14.2	14.2	32.3	0.3
19	117	13	0	29	66	28	4	26	29	57	0
	37.7	4.2	0.0	9.4	21.3	9.0	1.3	8.4	9.4	18.4	0.0

SAN DIEGO, CALIFORNIA STA93112

FEBRUARY PERIOD 1/59 THRU 12/68

TOTAL CLOUD AMOUNT (TENTHS)

LST	0	1	2	3	4	5	6	7	8	9	10	TOTAL
1	112 39.7	4 1.4	8 2.8	10 3.5	9 3.2	14 5.0	10 3.5	11 3.9	16 5.7	19 6.7	69 24.5	282.0
4	121 42.9	6 2.1	6 2.1	10 3.5	3 1.1	7 2.5	8 2.8	11 3.9	16 5.7	9 3.2	85 30.1	282.0
7	71 25.2	19 6.7	12 4.3	12 4.3	17 6.0	13 4.6	10 3.5	12 4.3	23 8.2	22 7.8	71 25.2	282.0
10	72 25.5	21 7.4	19 6.7	13 4.6	10 3.5	15 5.3	13 4.6	14 5.0	16 5.7	28 9.9	61 21.6	282.0
13	82 29.1	15 5.3	13 4.6	19 6.7	12 4.3	12 4.3	16 5.7	24 8.5	27 9.6	20 7.1	42 14.9	282.0
16	74 26.2	17 6.0	19 6.7	20 7.1	21 7.4	9 3.2	6 2.1	21 7.4	22 7.8	23 8.2	5 17.7	282.0
19	86 30.4	2 7.1	24 8.5	14 4.9	15 5.3	13 4.6	10 3.5	17 6.0	16 5.7	19 6.7	49 17.3	283.0
22	113 39.9	9 3.2	13 4.6	19 6.7	12 4.2	8 2.8	9 3.2	13 4.6	14 4.9	16 5.7	57 2 .1	283.0

SAN DIEGO, CALIFORNIA STA93112

FEBRUARY PERIOD 1/59 THRU 12/68

CLOUD TYPE

	(CLEAR)	(FOG)	(LOW CLOUD)				(MIDDLE CLOUD)		(HIGH CLOUD)		(VERTICAL)
LST	0	1	2	3	4	5	6	7	8	9	10
7	71 25.2	39 13.8	1 0.4	54 19.1	65 23.0	43 15.2	6 2.1	36 12.8	20 7.1	74 26.2	1 0.4
10	72 25.5	15 5.3	2 0.7	39 13.8	71 25.2	49 17.4	12 4.3	34 12.6	20 7.1	93 33.0	3 1.1
13	82 29.1	6 2.1	1 0.4	18 6.4	61 21.6	72 25.5	12 4.3	35 12.4	29 10.3	91 32.3	3 1.1
16	74 26.2	9 3.2	1 0.4	20 7.1	63 22.3	72 25.5	10 3.5	38 13.5	34 12.1	86 30.5	4 1.4
19	86 30.4	7 2.5	2 0.7	38 13.4	62 21.9	48 17.0	10 3.5	38 13.4	27 9.5	64 22.6	1 0.4

SAN DIEGO, CALIFORNIA

STA93112

MARCH

PERIOD 1/59 THRU 12/68

TOTAL CLOUD AMOUNT (TENTHS)

LST	0	1	2	3	4	5	6	7	8	9	10	TOTAL
1	76 24.5	16 5.2	18 5.8	18 5.8	8 2.6	7 2.3	12 3.9	17 5.5	23 7.4	17 5.5	98 31.6	310.0
4	77 24.8	18 5.8	12 3.9	12 3.9	10 3.2	6 1.9	16 5.2	10 3.2	12 3.9	23 7.4	114 36.8	310.0
7	49 15.8	25 8.1	13 4.2	11 3.5	10 3.2	12 3.9	11 3.5	17 5.5	27 8.7	36 11.6	99 31.9	310.0
10	52 16.8	20 6.5	20 6.5	19 6.1	17 5.5	17 5.5	16 5.2	22 7.1	23 7.4	30 9.7	74 23.9	310.0
13	63 20.3	29 9.4	21 6.8	15 4.8	8 2.6	22 7.1	21 6.8	26 8.4	31 10.0	23 7.4	51 16.5	310.0
16	55 17.7	22 7.1	30 9.7	23 7.4	14 4.5	13 4.2	21 6.8	25 8.1	18 5.8	20 6.5	69 22.3	310.0
19	59 19.0	21 6.8	24 7.7	21 6.8	19 6.1	15 4.8	17 5.5	22 7.1	24 7.7	17 5.5	71 22.9	310.0
22	71 22.9	20 6.5	21 6.8	19 6.1	8 2.6	17 5.5	13 4.2	12 3.9	19 6.1	22 7.1	88 28.4	310.0

SAN DIEGO, CALIFORNIA

STA93112

MARCH

PERIOD 1/59 THRU 12/68

CLOUD TYPE

	(CLEAR)	(FOG)	(LOW CLOUD)				(MIDDLE CLOUD)		(HIGH CLOUD)		(VERTICAL)
LST	0	1	2	3	4	5	6	7	8	9	10
7	49 15.8	38 12.3	1 0.3	57 18.4	123 39.7	62 20.0	11 3.5	39 12.6	18 5.8	72 23.2	3 1.0
10	52 16.8	6 1.9	0 0.0	35 11.3	111 35.8	95 30.6	12 3.9	33 10.6	32 10.3	82 26.5	2 0.6
13	63 20.3	5 1.6	1 0.3	31 10.0	84 27.1	96 31.0	6 1.9	38 12.3	35 11.3	93 30.0	2 0.6
16	55 17.7	7 2.3	1 0.3	30 9.7	98 31.6	95 30.6	4 1.3	40 12.9	48 15.5	90 29.0	1 0.3
19	59 19.0	9 2.9	2 0.6	49 15.8	102 32.9	63 20.3	5 1.6	35 11.3	39 12.6	66 21.3	2 0.6

SAN DIEGO, CALIFORNIA STA93112

APRIL PERIOD 1/59 THRU 12/68

TOTAL CLOUD AMOUNT (TENTHS)

LST	0	1	2	3	4	5	6	7	8	9	10	TOTAL
1	72 24.0	16 5.3	15 5.0	12 4.0	14 4.7	11 3.7	15 5.0	10 3.3	15 5.0	13 4.3	107 35.7	300.0
4	55 18.3	14 4.7	9 3.0	17 5.7	13 4.3	7 2.3	9 3.0	16 5.3	13 4.3	15 5.0	132 44.0	300.0
7	45 15.0	18 6.0	12 4.0	10 3.3	8 2.7	15 5.0	6 2.0	17 5.7	24 8.0	25 8.3	120 40.0	300.0
10	66 22.0	20 6.7	13 4.3	20 6.7	20 6.7	21 7.0	18 6.0	16 5.3	24 8.0	21 7.0	61 20.3	300.0
13	82 27.3	23 7.7	16 5.3	19 6.3	15 5.0	27 9.0	14 4.7	22 7.3	21 7.0	26 8.7	35 11.7	300.0
16	72 24.0	22 7.3	20 6.7	24 8.0	15 5.0	19 6.3	18 6.0	21 7.0	26 8.7	21 7.0	42 14.0	300.0
19	68 22.7	22 7.3	20 6.7	14 4.7	18 6.0	21 7.0	20 6.7	21 7.0	22 7.3	16 5.3	58 19.3	300.0
22	85 28.3	11 3.7	20 6.7	11 3.7	12 4.0	10 3.3	18 6.0	17 5.7	15 5.0	9 3.0	92 30.7	300.0

SAN DIEGO, CALIFORNIA STA93112

APRIL PERIOD 1/59 THRU 12/68

CLOUD TYPE

	(CLEAR)	(FOG)	(LOW CLOUD)				(MIDDLE CLOUD)		(HIGH CLOUD)		(VERTICAL)
LST	0	1	2	3	4	5	6	7	8	9	10
7	45 15.0	28 9.3	0 0.0	64 21.3	138 46.0	66 22.0	4 1.3	29 9.7	14 4.7	30 10.0	0 0.0
10	66 22.0	8 2.7	1 0.3	39 13.0	125 41.7	84 28.0	3 1.0	25 8.3	21 7.0	55 18.3	1 0.3
13	82 27.3	3 1.0	1 0.3	27 9.0	104 34.7	78 26.0	1 0.3	26 8.7	22 7.3	60 20.0	1 0.3
16	72 24.0	7 2.3	0 0.0	34 11.3	106 35.3	71 23.7	4 1.3	27 9.0	21 7.0	76 25.3	0 0.0
19	68 22.7	7 2.3	0 0.0	42 14.0	119 39.7	52 17.3	6 2.0	25 8.3	19 6.3	70 23.3	0 0.0

SAN DIEGO, CALIFORNIA STA93112

MAY PERIOD 1/59 THRU 12/68

TOTAL CLOUD AMOUNT (TENTHS)

LST	0	1	2	3	4	5	6	7	8	9	10	TOTAL
1	49	6	11	13	11	8	7	10	26	14	155	310.0
	15.8	1.9	3.5	4.2	3.5	2.6	2.3	3.2	8.4	4.5	50.0	
4	29	3	5	11	9	7	10	15	22	8	191	310.0
	9.4	1.0	1.6	3.5	2.9	2.3	3.2	4.8	7.1	2.6	61.6	
7	21	10	12	5	8	11	6	11	14	25	187	310.0
	6.8	3.2	3.9	1.6	2.6	3.5	1.9	3.5	4.5	8.1	60.3	
10	58	20	15	8	14	13	19	22	16	26	99	310.0
	18.7	6.5	4.8	2.6	4.5	4.2	6.1	7.1	5.2	8.4	31.9	
13	86	30	17	28	20	14	14	23	18	21	39	310.0
	27.7	9.7	5.5	9.0	6.5	4.5	4.5	7.4	5.8	6.8	12.6	
16	70	31	24	18	17	14	16	23	22	22	53	310.0
	22.6	10.0	7.7	5.8	5.5	4.5	5.2	7.4	7.1	7.1	17.1	
19	37	24	27	17	18	14	16	21	21	21	94	310.0
	11.9	7.7	8.7	5.5	5.8	4.5	5.2	6.8	6.8	6.8	30.3	
22	55	17	16	15	11	9	13	21	12	10	131	310.0
	17.7	5.5	5.2	4.8	3.5	2.9	4.2	6.8	3.9	3.2	42.3	

SAN DIEGO, CALIFORNIA STA93112

MAY PERIOD 1/59 THRU 12/68

CLOUD TYPE

	(CLEAR)	(FOG)	(LOW CLOUD)				(MIDDLE CLOUD)		(HIGH CLOUD)		(VERTICAL)
LST	0	1	2	3	4	5	6	7	8	9	10
7	21	17	0	79	215	52	1	14	5	21	6
	6.8	5.5	0.0	25.5	69.4	16.8	0.3	4.5	1.6	6.8	0.0
10	58	5	0	51	185	59	2	16	10	33	0
	18.7	1.6	0.0	16.5	59.7	19.0	0.6	5.2	3.2	10.6	0.0
13	86	3	0	34	142	67	0	19	14	40	1
	27.7	1.0	0.0	11.0	45.8	21.6	0.0	6.1	4.5	12.9	0.3
16	70	3	0	42	156	55	3	18	22	51	2
	22.6	1.0	0.0	13.5	50.3	17.7	1.0	5.8	7.1	16.5	0.6
19	37	1	0	58	188	44	3	21	11	62	0
	11.9	0.3	0.0	18.7	60.6	14.2	1.0	6.8	3.5	20.0	0.0

SAN DIEGO, CALIFORNIA STA93112

JUNE PERIOD 1/59 THRU 12/68

TOTAL CLOUD AMOUNT (TENTHS)

LST	0	1	2	3	4	5	6	7	8	9	10	TOTAL
1	18	4	2	10	4	2	4	6	15	8	227	300.0
	6.0	1.3	0.7	3.3	1.3	0.7	1.3	2.0	5.0	2.7	75.7	
4	12	1	4	4	3	6	4	4	4	3	255	300.0
	4.0	0.3	1.3	1.3	1.0	2.0	1.3	1.3	1.3	1.0	85.0	
7	8	3	2	2	7	3	2	5	6	15	247	300.0
	2.7	1.0	0.7	0.7	2.3	1.0	0.7	1.7	2.0	5.0	82.3	
10	60	19	17	10	8	14	5	13	10	10	134	300.0
	20.0	6.3	5.7	3.3	2.7	4.7	1.7	4.3	3.3	3.3	44.7	
13	99	25	15	15	11	9	16	16	12	8	74	300.0
	33.0	8.3	5.0	5.0	3.7	3.0	5.3	5.3	4.0	2.7	24.7	
16	86	30	13	18	10	14	15	16	15	17	66	300.0
	28.7	10.0	4.3	6.0	3.3	4.7	5.0	5.3	5.0	5.7	22.0	
19	45	25	14	17	13	16	12	17	15	14	112	300.0
	15.0	8.3	4.7	5.7	4.3	5.3	4.0	5.7	5.0	4.7	37.3	
22	30	15	12	16	7	4	11	7	12	13	173	300.0
	10.0	5.0	4.0	5.3	2.3	1.3	3.7	2.3	4.0	4.3	57.7	

SAN DIEGO, CALIFORNIA STA93112

JUNE PERIOD 1/59 THRU 12/68

CLOUD TYPE

	(CLEAR)	(FOG)		(LOW CLOUD)			(MIDDLE CLOUD)		(HIGH CLOUD)		(VERTICAL)
LST	0	1	2	3	4	5	6	7	8	9	10
7	8	28	0	154	155	28	0	10	0	5	0
	2.7	9.3	0.0	51.3	51.7	9.3	0.0	3.3	0.0	1.7	0.0
10	60	7	0	121	142	33	0	7	2	13	0
	20.0	2.3	0.0	40.3	47.3	11.0	0.0	2.3	0.7	4.3	0.0
13	99	4	0	86	115	37	1	10	11	22	0
	33.0	1.3	0.0	28.7	38.3	12.3	0.3	3.3	3.7	7.3	0.0
16	86	3	0	90	133	32	0	10	9	17	1
	28.7	1.0	0.0	30.0	44.3	10.7	0.0	3.3	3.0	5.7	0.3
19	45	3	0	123	144	24	0	17	4	24	0
	15.0	1.0	0.0	41.0	48.0	8.0	0.0	5.7	1.3	8.0	0.0

SAN DIEGO, CALIFORNIA STA93112

JULY PERIOD 1/59 THRU 12/68

TOTAL CLOUD AMOUNT (TENTHS)

LST	0	1	2	3	4	5	6	7	8	9	10	TOTAL
1	35 11.3	9 2.9	8 2.6	16 5.2	11 3.5	5 1.6	11 3.5	11 3.5	16 5.2	13 4.2	175 56.5	310.0
4	16 5.2	8 2.6	7 2.3	5 1.6	9 2.9	4 1.3	3 1.0	9 2.9	11 3.5	11 3.5	227 73.2	310.0
7	11 3.5	3 1.0	8 2.6	8 2.6	6 1.9	5 1.6	9 2.9	8 2.6	17 5.5	15 4.8	220 71.0	310.0
10	83 26.8	30 9.7	30 9.7	16 5.2	14 4.5	16 5.2	14 4.5	10 3.2	17 5.5	12 3.9	68 21.9	310.0
13	118 38.1	37 11.9	29 9.4	22 7.1	19 6.1	13 4.2	12 3.9	16 5.2	11 3.5	9 2.9	24 7.7	310.0
16	111 35.8	40 12.9	34 11.0	14 4.5	23 7.4	11 3.5	16 5.2	14 4.5	16 5.2	11 3.5	20 6.5	310.0
19	62 20.0	52 16.8	30 9.7	25 8.1	13 4.2	12 3.9	17 5.5	24 7.7	20 6.5	15 4.8	40 12.9	310.0
22	56 18.1	23 7.4	29 9.4	22 7.1	12 3.9	11 3.5	11 3.5	16 5.2	18 5.8	15 4.8	97 31.3	310.0

SAN DIEGO, CALIFORNIA STA93112

JULY PERIOD 1/59 THRU 12/68

CLOUD TYPE

	(CLEAR)	(FOG)	(LOW CLOUD)				(MIDDLE CLOUD)		(HIGH CLOUD)		(VERTICAL)
LST	0	1	2	3	4	5	6	7	8	9	10
7	11 3.5	23 7.4	0 0.0	226 72.9	49 15.8	1 0.3	1 0.3	34 11.0	1 0.3	21 6.8	0 0.0
10	83 26.8	9 2.9	0 0.0	151 48.7	43 13.9	7 2.3	2 0.6	50 16.1	7 2.3	40 12.9	1 0.3
13	118 38.1	3 1.0	0 0.0	88 28.4	40 12.9	31 10.0	4 1.3	55 17.7	12 3.9	66 21.3	20 6.5
16	111 35.8	0 0.0	0 0.0	99 31.9	50 16.1	31 10.0	3 1.0	67 21.6	14 4.5	57 18.4	18 5.8
19	62 20.0	0 0.0	0 0.0	151 48.7	59 19.0	7 2.3	7 2.3	65 21.0	10 3.2	68 21.9	4 1.3

SAN DIEGO, CALIFORNIA STA93112

AUGUST PERIOD 1/59 THRU 12/68

TOTAL CLOUD AMOUNT (TENTHS)

LST	0	1	2	3	4	5	6	7	8	9	10	TOTAL
1	47	13	9	13	5	3	11	6	11	11	181	310.0
	15.2	4.2	2.9	4.2	1.6	1.0	3.5	1.9	3.5	3.5	58.4	
4	31	2	4	6	9	5	12	11	11	12	207	310.0
	10.0	0.6	1.3	1.9	2.9	1.6	3.9	3.5	3.5	3.9	66.8	
7	16	7	8	8	5	2	12	13	27	27	185	310.0
	5.2	2.3	2.6	2.6	1.6	0.6	3.9	4.2	8.7	8.7	59.7	
10	107	27	28	17	16	14	8	18	13	8	54	310.0
	34.5	8.7	9.0	5.5	5.2	4.5	2.6	5.8	4.2	2.6	17.4	
13	140	33	27	18	18	13	8	12	13	6	22	310.0
	45.2	10.6	8.7	5.8	5.8	4.2	2.6	3.9	4.2	1.9	7.1	
16	97	47	33	35	18	14	11	13	15	11	16	310.0
	31.3	15.2	10.6	11.3	5.8	4.5	3.5	4.2	4.8	3.5	5.2	
19	71	37	37	21	24	22	19	19	15	12	33	310.0
	22.9	11.9	11.9	6.8	7.7	7.1	6.1	6.1	4.8	3.9	10.6	
22	67	23	18	24	14	10	15	16	21	11	91	310.0
	21.6	7.4	5.8	7.7	4.5	3.2	4.8	5.2	6.8	3.5	29.4	

SAN DIEGO, CALIFORNIA STA93112

AUGUST PERIOD 1/59 THRU 12/68

CLOUD TYPE

	(CLEAR)	(FOG)	(LOW CLOUD)				(MIDDLE CLOUD)		(HIGH CLOUD)		(VERTICAL)
LST	0	1	2	3	4	5	6	7	8	9	10
7	16	14	0	217	58	5	0	41	1	19	0
	5.2	4.5	0.0	70.0	18.7	1.6	0.0	13.2	0.3	6.1	0.0
10	107	8	0	126	46	20	1	43	4	35	1
	34.5	2.6	0.0	40.6	14.8	6.5	0.3	13.9	1.3	11.3	0.3
13	140	4	0	78	37	39	3	53	6	60	27
	45.2	1.3	0.0	25.2	11.9	12.6	1.0	17.1	1.9	19.4	8.7
16	97	3	0	120	41	46	4	62	6	64	32
	31.3	1.0	0.0	38.7	13.2	14.8	1.3	20.0	1.9	20.6	10.3
19	71	2	0	159	54	7	5	46	8	56	4
	22.9	0.6	0.0	51.3	17.4	2.3	1.6	14.8	2.6	18.1	1.3

SAN DIEGO, CALIFORNIA STA93112

SEPTEMBER PERIOD 1/59 THRU 12/68

TOTAL CLOUD AMOUNT (TENTHS)

LST	0	1	2	3	4	5	6	7	8	9	10	TOTAL
1	64 21.3	9 3.0	6 2.0	5 1.7	8 2.7	5 1.7	9 3.0	10 3.3	11 3.7	4 1.3	169 56.3	300.0
4	56 18.7	7 2.3	8 2.7	3 1.0	6 2.0	5 1.7	4 1.3	5 1.7	9 3.0	7 2.3	190 63.3	300.0
7	45 15.0	7 2.3	13 4.3	6 2.0	8 2.7	6 2.0	6 2.0	7 2.3	13 4.3	17 5.7	172 57.3	300.0
10	103 34.3	31 10.3	12 4.0	19 6.3	11 3.7	13 4.3	3 1.0	12 4.0	10 3.3	20 6.7	66 22.0	300.0
13	135 45.0	27 9.0	22 7.3	18 6.0	11 3.7	17 5.7	6 2.0	10 3.3	14 4.7	9 3.0	31 10.3	300.0
16	126 42.0	39 13.0	20 6.7	11 3.7	14 4.7	11 3.7	10 3.3	10 3.3	12 4.0	13 4.3	34 11.3	300.0
19	93 31.0	25 8.3	26 8.7	20 6.7	14 4.7	15 5.0	8 2.7	12 4.0	15 5.0	20 6.7	52 17.3	300.0
22	72 24.0	15 5.0	14 4.7	17 5.7	12 4.0	6 2.0	14 4.7	9 3.0	17 5.7	7 2.3	117 39.0	300.0

SAN DIEGO, CALIFORNIA STA93112

SEPTEMBER PERIOD 1/59 THRU 12/68

CLOUD TYPE

	(CLEAR)	(FOG)	(LOW CLOUD)				(MIDDLE CLOUD)		(HIGH CLOUD)		(VERTICAL)
LST	0	1	2	3	4	5	6	7	8	9	10
7	45 15.0	32 11.0	0 0.0	138 46.0	91 30.3	14 4.7	3 1.0	31 10.3	1 0.3	16 5.3	0 0.0
10	103 34.3	7 2.3	0 0.0	93 31.0	86 28.7	34 11.3	3 1.0	38 12.7	4 1.3	20 6.7	0 0.0
13	135 45.0	1 0.3	0 0.0	55 18.3	82 27.3	41 13.7	4 1.3	33 11.0	5 1.7	33 11.0	8 2.7
16	126 42.0	3 1.0	0 0.0	56 18.7	89 29.7	25 8.3	5 1.7	39 13.0	10 3.3	27 9.0	15 5.0
19	93 31.0	2 0.7	0 0.0	105 35.0	85 28.3	8 2.7	5 1.7	29 9.7	7 2.3	26 8.7	3 1.0

SAN DIEGO, CALIFORNIA STA93112

OCTOBER PERIOD 1/59 THRU 12/68

TOTAL CLOUD AMOUNT (TENTHS)

LST	0	1	2	3	4	5	6	7	8	9	10	TOTAL
1	93	7	13	9	9	8	7	7	13	8	136	310.0
	30.0	2.3	4.2	2.9	2.9	2.6	2.3	2.3	4.2	2.6	43.9	
4	96	6	9	5	9	6	8	4	12	13	142	310.0
	31.0	1.9	2.9	1.6	2.9	1.9	2.6	1.3	3.9	4.2	45.8	
7	67	19	10	8	11	7	9	7	20	23	129	310.0
	21.6	6.1	3.2	2.6	3.5	2.3	2.9	2.3	6.5	7.4	41.6	
10	93	22	22	21	17	8	16	11	22	15	63	310.0
	30.0	7.1	7.1	6.8	5.5	2.6	5.2	3.5	7.1	4.8	20.3	
13	125	29	19	22	13	11	19	14	16	22	20	310.0
	40.3	9.4	6.1	7.1	4.2	3.5	6.1	4.5	5.2	7.1	6.5	
16	106	31	16	28	11	18	15	15	20	20	30	310.0
	34.2	10.0	5.2	9.0	3.5	5.8	4.8	4.8	6.5	6.5	9.7	
19	116	19	14	16	21	9	12	21	18	12	52	310.0
	37.4	6.1	4.5	5.2	6.8	2.9	3.9	6.8	5.8	3.9	16.8	
22	106	9	22	15	9	5	10	10	8	12	104	310.0
	34.2	2.9	7.1	4.8	2.9	1.6	3.2	3.2	2.6	3.9	33.5	

SAN DIEGO, CALIFORNIA STA93112

OCTOBER PERIOD 1/59 THRU 12/68

CLOUD TYPE

	(CLEAR)	(FOG)	(LOW CLOUD)				(MIDDLE CLOUD)		(HIGH CLOUD)		(VERTICAL)
LST	0	1	2	3	4	5	6	7	8	9	10
7	67	61	0	97	72	19	5	34	9	35	2
	21.6	19.7	0.0	31.3	23.2	6.1	1.6	11.0	2.9	11.3	0.6
10	93	15	0	72	74	34	7	29	15	47	1
	30.0	4.8	0.0	23.2	23.9	11.0	2.3	9.4	4.8	15.2	0.3
13	125	4	0	38	53	43	5	35	20	68	3
	40.3	1.3	0.0	12.3	17.1	13.9	1.6	11.3	6.5	21.9	1.0
16	106	7	0	51	53	33	9	35	21	63	5
	34.2	2.3	0.0	16.5	17.1	10.6	2.9	11.3	6.8	20.3	1.6
19	116	13	0	69	75	10	5	25	11	37	1
	37.4	4.2	0.0	22.3	24.2	3.2	1.6	8.1	3.5	11.9	0.3

SAN DIEGO, CALIFORNIA

STA93112

NOVEMBER

PERIOD 1/59 THRU 12/68

TOTAL CLOUD AMOUNT (TENTHS)

LST	0	1	2	3	4	5	6	7	8	9	10	TOTAL
1	92 30.7	10 3.3	12 4.0	10 3.3	14 4.7	7 2.3	11 3.7	11 3.7	18 6.0	13 4.3	102 34.0	300.0
4	105 35.0	9 3.0	13 4.3	7 2.3	7 2.3	7 2.3	13 4.3	14 4.7	10 3.3	14 4.7	101 33.7	300.0
7	74 24.7	12 4.0	16 5.3	13 4.3	9 3.0	8 2.7	9 3.0	13 4.3	26 8.7	29 9.7	91 30.3	300.0
10	78 26.0	13 4.3	20 6.7	19 6.3	12 4.0	19 6.3	12 4.0	19 6.3	21 7.0	29 9.7	58 19.3	300.0
13	76 25.3	27 9.0	22 7.3	18 6.0	13 4.3	14 4.7	8 2.7	28 9.3	19 6.3	20 6.7	55 18.3	300.0
16	66 22.0	33 11.0	24 8.0	18 6.0	17 5.7	12 4.0	13 4.3	20 6.7	28 9.3	18 6.0	51 17.0	300.0
19	88 29.3	21 7.0	26 8.7	12 4.0	17 5.7	10 3.3	10 3.3	15 5.0	25 8.3	7 2.3	69 23.0	300.0
22	95 31.7	20 6.7	17 5.7	13 4.3	15 5.0	5 1.7	9 3.0	9 3.0	17 5.7	13 4.3	87 29.0	300.0

SAN DIEGO, CALIFORNIA

STA93112

NOVEMBER

PERIOD 1/59 THRU 12/68

CLOUD TYPE

	(CLEAR)	(FOG)	(LOW CLOUD)				(MIDDLE CLOUD)		(HIGH CLOUD)		(VERTICAL)
LST	0	1	2	3	4	5	6	7	8	9	10
7	74 24.7	41 13.7	0 0.0	62 20.7	86 28.7	40 13.3	13 4.3	47 15.7	18 6.0	60 20.0	2 0.7
10	78 26.0	12 4.0	0 0.0	36 12.0	79 26.3	57 19.0	8 2.7	52 17.3	29 9.7	81 27.0	4 1.3
13	76 25.3	5 1.7	1 0.3	20 6.7	73 24.3	70 23.3	4 1.3	56 18.7	36 12.0	98 32.7	2 0.7
16	66 22.0	13 4.3	2 0.7	41 13.7	72 24.0	63 21.0	5 1.7	47 15.7	36 12.0	97 32.3	2 0.7
19	88 29.3	22 7.3	1 0.3	54 18.0	80 26.7	30 10.0	3 1.0	23 7.7	21 7.0	53 17.7	2 0.7

SAN DIEGO, CALIFORNIA STA93112

DECEMBER PERIOD 1/59 THRU 12/68

TOTAL CLOUD AMOUNT (TENTHS)

LST	0	1	2	3	4	5	6	7	8	9	10	TOTAL
1	116	15	10	14	12	6	14	9	13	12	89	310.0
	37.4	4.8	3.2	4.5	3.9	1.9	4.5	2.9	4.2	3.9	28.7	
4	122	12	14	11	5	8	11	10	13	12	92	310.0
	39.4	3.9	4.5	3.5	1.6	2.6	3.5	3.2	4.2	3.9	29.7	
7	73	32	15	15	13	13	15	19	17	21	77	310.0
	23.5	10.3	4.8	4.8	4.2	4.2	4.8	6.1	5.5	6.8	24.8	
10	85	26	10	22	14	15	8	12	27	25	66	310.0
	27.4	8.4	3.2	7.1	4.5	4.8	2.6	3.9	8.7	8.1	21.3	
13	86	16	20	15	19	11	19	22	30	21	51	310.0
	27.7	5.2	6.5	4.8	6.1	3.5	6.1	7.1	9.7	6.8	16.5	
16	81	19	13	20	18	16	20	12	28	26	57	310.0
	26.1	6.1	4.2	6.5	5.8	5.2	6.5	3.9	9.0	8.4	18.4	
19	96	25	20	22	13	12	16	15	12	15	64	310.0
	31.0	8.1	6.5	7.1	4.2	3.9	5.2	4.8	3.9	4.8	20.6	
22	110	17	15	11	12	11	8	13	13	8	92	310.0
	35.5	5.5	4.8	3.5	3.9	3.5	2.6	4.2	4.2	2.6	29.7	

SAN DIEGO, CALIFORNIA STA93112

DECEMBER PERIOD 1/59 THRU 12/68

CLOUD TYPE

	(CLEAR)	(FOG)	(LOW CLOUD)				(MIDDLE CLOUD)		(HIGH CLOUD)		(VERTICAL)
LST	0	1	2	3	4	5	6	7	8	9	10
7	73	35	2	40	86	26	16	53	14	89	2
	23.5	11.3	0.6	12.9	27.7	8.4	5.2	17.1	4.5	28.7	0.6
10	85	20	2	38	71	50	12	45	32	92	1
	27.4	6.5	0.6	12.3	22.9	16.1	3.9	14.5	10.3	29.7	0.3
13	86	11	3	24	63	64	15	44	31	97	2
	27.7	3.5	1.0	7.7	20.3	20.6	4.8	14.2	10.0	31.3	0.6
16	81	12	1	31	66	54	10	52	31	101	3
	26.1	3.9	0.3	10.0	21.3	17.4	3.2	16.8	10.0	32.6	1.0
19	96	27	2	35	63	30	5	37	23	56	1
	31.0	8.7	0.6	11.3	20.3	9.7	1.6	11.9	7.4	18.1	0.3

SAN NICHOLAS ISLAND, CALIFORNIA STA93116

JANUARY PERIOD 1/5? THRU 12/59

TOTAL CLOUD AMOUNT (TENTHS)

LST	0	1	2	3	4	5	6	7	8	9	10	TOTAL
1	0 0.0	0 0.0	0 0.0	0 0.0	0 0.0	0 0.0	0 0.0	0 0.0	0 0.0	0 0.0	0 0.0	0.0
4	0 0.0	0 0.0	0 0.0	0 0.0	0 0.0	0 0.0	0 0.0	0 0.0	0 0.0	0 0.0	0 0.0	0.0
7	47 16.5	17 6.0	20 7.0	21 7.4	15 5.3	19 6.7	8 2.8	22 7.7	25 8.8	18 6.3	73 25.6	285.0
10	64 20.6	18 5.8	21 6.8	21 6.8	13 4.2	14 4.5	13 4.2	16 5.2	32 10.3	16 5.2	82 26.5	310.0
13	55 19.1	15 5.2	12 4.2	21 7.3	11 3.8	14 4.9	11 3.8	19 6.6	30 10.4	17 5.9	83 28.8	288.0
16	55 18.9	20 6.9	19 6.5	16 5.5	15 5.2	12 4.1	13 4.5	19 6.5	27 9.3	19 6.5	76 26.1	291.0
19	0 0.0	0 0.0	0 0.0	0 0.0	0 0.0	0 0.0	0 0.0	0 0.0	0 0.0	0 0.0	0 0.0	0.0
22	0 0.0	0 0.0	0 0.0	0 0.0	0 0.0	0 0.0	0 0.0	0 0.0	0 0.0	0 0.0	0 0.0	0.0

SAN NICHOLAS ISLAND, CALIFORNIA STA93116

JANUARY PERIOD 1/5? THRU 12/59

CLOUD TYPE

	(CLEAR)	(FOG)	(LOW CLOUD)				(MIDDLE CLOUD)		(HIGH CLOUD)		(VERTICAL)
LST	0	1	2	3	4	5	6	7	8	9	10
7	47 16.5	44 15.4	0 0.0	55 19.3	80 28.1	20 7.0	16 5.6	41 14.4	19 6.7	67 23.5	1 0.4
10	64 20.6	32 10.3	2 0.6	62 20.0	79 25.5	30 9.7	14 4.5	35 11.3	26 8.4	72 23.2	0 0.0
13	55 19.1	31 10.8	0 0.0	49 17.0	66 22.9	30 10.4	16 5.6	32 11.1	32 11.1	69 24.0	1 0.3
16	55 18.9	30 10.3	0 0.0	41 14.1	61 21.0	30 10.3	16 5.5	28 9.6	39 13.4	85 29.2	0 0.0
19	0 0.0	0 0.0	0 0.0	0 0.0	0 0.0	0 0.0	0 0.0	0 0.0	0 0.0	0 0.0	0 0.0

SAN NICHOLAS ISLAND, CALIFORNIA STA93114

FEBRUARY PERIOD 1/50 THRU 12/59

TOTAL CLOUD AMOUNT (TENTHS)

LST	0	1	2	3	4	5	6	7	8	9	10	TOTAL
1	0	0	0	0	0	0	0	0	0	0	0	0.0
	0.0	0.0	0.0	0.0	0.0	0.0	0.0	0.0	0.0	0.0	0.0	
4	0	0	0	0	0	0	0	0	0	0	0	0.0
	0.0	0.0	0.0	0.0	0.0	0.0	0.0	0.0	0.0	0.0	0.0	
7	77	14	11	9	11	11	5	14	18	9	79	258.0
	29.8	5.4	4.3	3.5	4.3	4.3	1.9	5.4	7.0	3.5	30.6	
10	87	13	7	11	8	10	11	13	19	11	91	281.0
	31.0	4.6	2.5	3.9	2.8	3.6	3.9	4.6	6.8	3.9	32.4	
13	82	15	14	13	9	5	13	16	15	10	72	264.0
	31.1	5.7	5.3	4.9	3.4	1.9	4.9	6.1	5.7	3.8	27.3	
16	86	16	9	14	11	12	13	11	15	13	63	263.0
	32.7	6.1	3.4	5.3	4.2	4.6	4.9	4.2	5.7	4.9	24.0	
19	0	0	0	1	0	0	0	0	0	1	0	2.0
	0.0	0.0	0.0	50.0	0.0	0.0	0.0	0.0	0.0	50.0	0.0	
22	0	0	0	0	0	0	0	1	0	0	0	1.0
	0.0	0.0	0.0	0.0	0.0	0.0	0.0	100.0	0.0	0.0	0.0	

SAN NICHOLAS ISLAND, CALIFORNIA STA93116

FEBRUARY PERIOD 1/50 THRU 12/59

CLOUD TYPE

	(CLEAR)	(FOG)	(LOW CLOUD)				(MIDDLE CLOUD)		(HIGH CLOUD)		(VERTICAL)
LST	0	1	2	3	4	5	6	7	8	9	10
7	77	35	0	34	60	17	11	25	13	45	0
	29.8	13.6	0.0	13.2	23.3	6.6	4.3	9.7	5.0	17.4	0.0
10	87	33	1	39	61	22	14	30	16	53	1
	31.1	11.8	0.4	13.9	21.8	7.9	5.0	10.7	5.7	18.9	0.4
13	82	21	0	31	67	21	14	29	24	45	0
	31.1	8.0	0.0	11.7	25.4	8.0	5.3	11.0	9.1	17.0	0.0
16	86	19	0	35	58	15	12	24	33	41	1
	32.7	7.2	0.0	13.3	22.1	5.7	4.6	9.1	12.5	15.6	0.4
19	0	1	0	1	1	0	0	0	0	0	0
	0.0	50.0	0.0	50.0	50.0	0.0	0.0	0.0	0.0	0.0	0.0

SAN NICHOLAS ISLAND, CALIFORNIA STA93116

MARCH PERIOD 1/50 THRU 12/59

TOTAL CLOUD AMOUNT (TENTHS)

LST	0	1	2	3	4	5	6	7	8	9	10	TOTAL
1	0 0.0	0 0.0	0 0.0	0 0.0	0 0.0	0 0.0	0 0.0	0 0.0	0 0.0	0 0.0	0 0.0	0.0
4	0 0.0	0 0.0	0 0.0	0 0.0	0 0.0	0 0.0	0 0.0	0 0.0	0 0.0	0 0.0	0 0.0	0.0
7	67 23.7	14 4.9	20 7.1	8 2.8	7 2.5	6 2.1	13 4.6	18 6.4	19 6.7	16 5.7	95 33.6	283.0
10	79 25.5	17 5.5	13 4.2	16 5.2	8 2.6	22 7.1	16 5.2	22 7.1	25 8.1	17 5.5	75 24.2	310.0
13	76 26.0	20 6.8	16 5.5	19 6.5	10 3.4	13 4.5	19 6.5	19 6.5	28 9.6	16 5.5	56 19.2	292.0
16	94 31.5	13 4.4	23 7.7	17 5.7	15 5.0	12 4.0	13 4.4	11 3.7	26 8.7	10 3.4	64 21.5	298.0
19	0 0.0	0 0.0	0 0.0	0 0.0	0 0.0	0 0.0	0 0.0	0 0.0	0 0.0	0 0.0	0 0.0	0.0
22	0 0.0	0 0.0	0 0.0	0 0.0	0 0.0	0 0.0	0 0.0	0 0.0	0 0.0	0 0.0	0 0.0	0.0

SAN NICHOLAS ISLAND, CALIFORNIA STA93116

MARCH PERIOD 1/50 THRU 12/59

CLOUD TYPE

	(CLEAR)	(FOG)	(LOW CLOUD)				(MIDDLE CLOUD)		(HIGH CLOUD)		(VERTICAL)
LST	0	1	2	3	4	5	6	7	8	9	10
7	67 23.7	33 11.7	0 0.0	66 23.3	79 27.9	36 12.7	18 6.4	33 11.7	20 7.1	49 17.3	1 0.4
10	79 25.5	16 5.2	0 0.0	53 17.1	91 29.4	41 13.2	15 4.8	38 12.3	29 9.4	64 20.6	1 0.3
13	76 26.0	14 4.8	0 0.0	31 10.6	80 27.4	42 14.4	17 5.8	34 11.6	35 12.0	71 24.3	1 0.3
16	94 31.6	14 4.7	3 1.0	26 8.8	68 22.9	32 10.8	17 5.7	26 8.8	34 11.4	66 22.2	2 0.7
19	0 0.0	0 0.0	0 0.0	0 0.0	0 0.0	0 0.0	0 0.0	0 0.0	0 0.0	0 0.0	0 0.0

SAN NICHOLAS ISLAND, CALIFORNIA STA93116

APRIL PERIOD 1/50 THRU 12/59

TOTAL CLOUD AMOUNT (TENTHS)

LST	0	1	2	3	4	5	6	7	8	9	10	TOTAL
1	0 0.0	0 0.0	0 0.0	0 0.0	0 0.0	0 0.0	0 0.0	0 0.0	0 0.0	0 0.0	0 0.0	0.0
4	0 0.0	0 0.0	0 0.0	0 0.0	0 0.0	0 0.0	0 0.0	0 0.0	0 0.0	0 0.0	0 0.0	0.0
7	50 18.2	7 2.6	12 4.4	12 4.4	8 2.9	6 2.2	4 1.5	9 3.3	24 8.8	15 5.5	127 46.4	274.0
10	63 21.0	5 1.7	19 6.3	11 3.7	17 5.7	17 5.7	12 4.0	9 3.0	23 7.7	20 6.7	104 34.7	300.0
13	72 25.4	14 4.9	18 6.4	15 5.3	14 4.9	12 4.2	17 6.0	10 3.5	21 7.4	15 5.3	75 26.5	283.0
16	76 28.5	9 3.4	18 6.7	16 6.0	12 4.5	10 3.7	12 4.5	17 6.4	25 9.4	13 4.9	59 22.1	267.0
19	0 0.0	0 0.0	0 0.0	0 0.0	0 0.0	0 0.0	0 0.0	0 0.0	0 0.0	0 0.0	0 0.0	0.0
22	0 0.0	0 0.0	0 0.0	0 0.0	0 0.0	0 0.0	0 0.0	0 0.0	0 0.0	0 0.0	0 0.0	0.0

SAN NICHOLAS ISLAND, CALIFORNIA STA93116

APRIL PERIOD 1/50 THRU 12/59

CLOUD TYPE

	(CLEAR)	(FOG)	(LOW CLOUD)				(MIDDLE CLOUD)		(HIGH CLOUD)		(VERTICAL)
LST	0	1	2	3	4	5	6	7	8	9	10
7	50 18.2	52 19.0	0 0.0	54 19.7	104 38.0	28 10.2	12 4.4	25 9.1	11 4.0	23 8.4	0 0.0
10	63 21.0	30 10.0	0 0.0	52 17.3	139 46.3	30 10.0	13 4.3	23 7.7	16 5.3	39 13.0	0 0.0
13	72 25.4	13 4.6	0 0.0	34 12.0	132 46.6	37 13.1	12 4.2	23 8.1	20 7.1	35 12.4	0 0.0
16	76 28.5	13 4.9	0 0.0	46 17.2	94 35.2	31 11.6	9 3.4	16 6.0	20 7.5	43 16.1	0 0.0
19	0 0.0	0 0.0	0 0.0	0 0.0	0 0.0	0 0.0	0 0.0	0 0.0	0 0.0	0 0.0	0 0.0

SAN NICHOLAS ISLAND, CALIFORNIA STA93116

MAY PERIOD 1/50 THRU 12/59

TOTAL CLOUD AMOUNT (TENTHS)

LST	0	1	2	3	4	5	6	7	8	9	10	TOTAL
1	0 0.0	0 0.0	0 0.0	0 0.0	0 0.0	0 0.0	0 0.0	0 0.0	0 0.0	0 0.0	0 0.0	0.0
4	0 0.0	0 0.0	0 0.0	0 0.0	0 0.0	0 0.0	0 0.0	0 0.0	0 0.0	0 0.0	0 0.0	0.0
7	53 17.1	12 3.9	11 3.5	13 4.2	10 3.2	8 2.6	7 2.3	13 4.2	19 6.1	13 4.2	151 48.7	310.0
10	62 20.0	15 4.8	18 5.8	17 5.5	14 4.5	12 3.9	12 3.9	16 5.2	25 8.1	12 3.9	107 34.5	310.0
13	87 28.1	19 6.1	17 5.5	22 7.1	12 3.9	13 4.2	11 3.5	22 7.1	25 8.1	15 4.8	67 21.6	310.0
16	60 32.1	16 8.6	9 4.8	15 8.0	10 5.3	8 4.3	3 1.6	9 4.8	15 8.0	7 3.7	35 18.7	187.0
19	0 0.0	0 0.0	0 0.0	0 0.0	0 0.0	0 0.0	0 0.0	0 0.0	0 0.0	0 0.0	0 0.0	0.0
22	0 0.0	0 0.0	0 0.0	0 0.0	0 0.0	0 0.0	0 0.0	0 0.0	0 0.0	0 0.0	0 0.0	0.0

SAN NICHOLAS ISLAND, CALIFORNIA STA93116

MAY PERIOD 1/50 THRU 12/59

CLOUD TYPE

	(CLEAR)	(FOG)	(LOW CLOUD)				(MIDDLE CLOUD)		(HIGH CLOUD)		(VERTICAL)
LST	0	1	2	3	4	5	6	7	8	9	10
7	53 17.1	57 18.4	0 0.0	94 30.3	107 34.5	21 6.8	5 1.6	14 4.5	7 2.3	36 11.6	0 0.0
10	62 20.0	38 12.3	0 0.0	92 29.7	120 38.7	31 10.0	4 1.3	19 6.1	13 4.2	42 13.5	1 0.3
13	87 28.1	14 4.5	0 0.0	89 28.7	98 31.6	32 10.3	8 2.6	20 6.5	15 4.8	44 14.2	2 0.6
16	60 32.4	10 5.4	0 0.0	46 24.9	46 24.9	15 8.1	5 2.7	11 5.9	8 4.3	33 17.8	0 0.0
19	0 0.0	0 0.0	0 0.0	0 0.0	0 0.0	0 0.0	0 0.0	0 0.0	0 0.0	0 0.0	0 0.0

SAN NICHOLAS ISLAND, CALIFORNIA STA93116

JUNE PERIOD 1/50 THRU 12/59

TOTAL CLOUD AMOUNT (TENTHS)

LST	0	1	2	3	4	5	6	7	8	9	10	TOTAL
1	0	0	0	0	0	0	0	0	0	0	0	0.0
	0.0	0.0	0.0	0.0	0.0	0.0	0.0	0.0	0.0	0.0	0.0	
4	0	0	0	0	0	0	0	0	0	0	0	0.0
	0.0	0.0	0.0	0.0	0.0	0.0	0.0	0.0	0.0	0.0	0.0	
7	70	9	7	11	3	9	5	15	8	10	153	300.0
	23.3	3.0	2.3	3.7	1.0	3.0	1.7	5.0	2.7	3.3	51.0	
10	86	20	11	11	8	10	9	13	14	16	102	300.0
	28.7	6.7	3.7	3.7	2.7	3.3	3.0	4.3	4.7	5.3	34.0	
13	115	18	22	14	10	9	12	14	18	13	55	300.0
	38.3	6.0	7.3	4.7	3.3	3.0	4.0	4.7	6.0	4.3	18.3	
16	95	15	29	9	5	8	11	9	5	6	28	211.0
	45.0	7.1	9.5	4.3	2.4	3.8	5.2	4.3	2.4	2.8	13.3	
19	0	0	0	0	0	0	0	0	0	0	1	1.0
	0.0	0.0	0.0	0.0	0.0	0.0	0.0	0.0	0.0	0.0	100.0	
22	0	0	0	0	0	0	0	0	0	0	0	0.0
	0.0	0.0	0.0	0.0	0.0	0.0	0.0	0.0	0.0	0.0	0.0	

SAN NICHOLAS ISLAND, CALIFORNIA STA93116

JUNE PERIOD 1/50 THRU 12/59

CLOUD TYPE

	(CLEAR)	(FOG)	(LOW CLOUD)				(MIDDLE CLOUD)		(HIGH CLOUD)		(VERTICAL)
LST	0	1	2	3	4	5	6	7	8	9	10
7	70	77	0	105	83	13	1	3	6	16	0
	23.3	25.7	0.0	35.0	27.7	4.3	0.3	1.0	2.0	5.3	0.0
10	86	29	0	108	92	19	2	13	5	20	0
	28.7	9.7	0.0	36.0	30.7	6.3	0.7	4.3	1.7	6.7	0.0
13	115	12	0	88	80	21	4	13	8	16	0
	38.3	4.0	0.0	29.3	26.7	7.0	1.3	4.3	2.7	5.3	0.0
16	95	7	0	47	46	12	4	10	6	18	0
	45.0	3.3	0.0	22.3	21.8	5.7	1.9	4.7	2.8	8.5	0.0
19	0	0	0	1	0	0	0	0	0	0	0
	0.0	0.0	0.0	100.0	0.0	0.0	0.0	0.0	0.0	0.0	0.0

SAN NICHOLAS ISLAND, CALIFORNIA STA93116

JULY PERIOD 1/50 THRU 12/59

TOTAL CLOUD AMOUNT (TENTHS)

LST	0	1	2	3	4	5	6	7	8	9	10	TOTAL
1	0 0.0	0 0.0	0 0.0	0 0.0	0 0.0	0 0.0	0 0.0	0 0.0	0 0.0	0 0.0	0 0.0	0.0
4	0 0.0	0 0.0	0 0.0	0 0.0	0 0.0	0 0.0	0 0.0	0 0.0	0 0.0	0 0.0	1 100.0	1.0
7	46 14.8	4 1.3	6 1.9	8 2.6	6 1.9	3 1.0	7 2.3	4 1.3	6 1.9	13 4.2	207 66.8	310.0
10	66 21.3	17 5.5	22 7.1	23 7.4	7 2.3	9 2.9	5 1.6	11 3.5	17 5.5	12 3.9	121 39.0	310.0
13	102 32.9	25 8.1	33 10.6	22 7.1	13 4.2	12 3.9	8 2.6	16 5.2	22 7.1	15 4.8	42 13.5	310.0
16	101 45.3	13 5.8	28 12.6	12 5.4	6 2.7	5 2.2	5 2.2	13 5.8	11 4.9	9 4.0	20 9.0	223.0
19	4 17.4	2 8.7	2 8.7	0 0.0	1 4.3	1 4.3	2 8.7	3 13.0	1 4.3	0 0.0	7 30.4	23.0
22	0 0.0	0 0.0	0 0.0	0 0.0	0 0.0	0 0.0	0 0.0	0 0.0	0 0.0	0 0.0	0 0.0	0.0

SAN NICHOLAS ISLAND, CALIFORNIA STA93116

JULY PERIOD 1/50 THRU 12/59

CLOUD TYPE

	(CLEAR)	(FOG)	(LOW CLOUD)				(MIDDLE CLOUD)		(HIGH CLOUD)		(VERTICAL)
LST	0	1	2	3	4	5	6	7	8	9	10
7	46 14.9	120 38.8	0 0.0	150 48.5	29 9.4	4 1.3	0 0.0	21 6.8	4 1.3	9 2.9	0 0.0
10	66 21.3	54 17.4	0 0.0	164 52.9	52 16.8	5 1.6	0 0.0	29 9.4	4 1.3	21 6.8	0 0.0
13	102 32.9	25 8.1	0 0.0	125 40.3	56 18.1	9 2.9	4 1.3	28 9.0	4 1.3	29 9.4	0 0.0
16	101 45.3	20 9.0	0 0.0	71 31.8	27 12.1	6 2.7	3 1.3	21 9.4	4 1.8	19 8.5	0 0.0
19	4 17.4	3 13.0	0 0.0	11 47.8	0 0.0	0 0.0	1 4.3	2 8.7	1 4.3	5 21.7	0 0.0

SAN NICHOLAS ISLAND, CALIFORNIA STA93116

AUGUST PERIOD 1/50 THRU 12/59

TOTAL CLOUD AMOUNT (TENTHS)

LST	0	1	2	3	4	5	6	7	8	9	10	TOTAL
1	1 50.0	0 0.0	0 0.0	0 0.0	0 0.0	0 0.0	0 0.0	1 50.0	0 0.0	0 0.0	0 0.0	2.0
4	1 50.0	0 0.0	0 0.0	0 0.0	0 0.0	0 0.0	0 0.0	0 0.0	1 50.0	0 0.0	0 0.0	2.0
7	29 9.4	5 1.6	7 2.3	11 3.5	6 1.9	2 0.6	5 1.6	6 1.9	17 5.5	7 2.3	215 69.4	310.0
10	52 16.8	20 6.5	20 6.5	26 8.4	10 3.2	6 1.9	12 3.9	15 4.8	20 6.5	13 4.2	116 37.4	310.0
13	83 26.8	35 11.3	27 8.7	31 10.0	12 3.9	23 7.4	13 4.2	19 6.1	21 6.8	13 4.2	33 10.6	310.0
16	81 35.1	27 11.7	24 10.4	14 6.1	13 5.6	4 1.7	12 5.2	10 4.3	14 6.1	6 2.6	26 11.3	231.0
19	2 8.3	5 20.8	2 8.3	1 4.2	2 8.3	0 0.0	1 4.2	0 0.0	0 0.0	0 0.0	11 45.8	24.0
22	1 50.0	0 0.0	0 0.0	0 0.0	0 0.0	0 0.0	0 0.0	0 0.0	0 0.0	0 0.0	1 50.0	2.0

SAN NICHOLAS ISLAND, CALIFORNIA STA93116

AUGUST PERIOD 1/50 THRU 12/59

CLOUD TYPE

	(CLEAR)	(FOG)	(LOW CLOUD)				(MIDDLE CLOUD)		(HIGH CLOUD)		(VERTICAL)
LST	0	1	2	3	4	5	6	7	8	9	10
7	29 9.4	115 37.1	0 0.0	165 53.2	50 16.1	7 2.3	3 1.0	26 8.4	5 1.6	8 2.6	0 0.0
10	52 16.8	37 11.9	0 0.0	176 56.8	52 16.8	10 3.2	3 1.0	33 10.6	9 2.9	17 5.5	0 0.0
13	83 26.8	17 5.5	0 0.0	146 47.1	58 18.7	13 4.2	3 1.0	28 9.0	10 3.2	27 8.7	0 0.0
16	81 35.1	7 3.0	0 0.0	90 39.0	37 16.0	9 3.9	3 1.3	23 10.0	11 4.8	20 8.7	0 0.0
19	2 8.3	6 25.0	0 0.0	11 45.8	1 4.2	1 4.2	0 0.0	4 16.7	0 0.0	2 8.3	0 0.0

SAN NICHOLAS ISLAND, CALIFORNIA STA93116

SEPTEMBER PERIOD 1/50 THRU 12/59

TOTAL CLOUD AMOUNT (TENTHS)

LST	0	1	2	3	4	5	6	7	8	9	10	TOTAL
1	0 0.0	0 0.0	0 0.0	0 0.0	0 0.0	0 0.0	0 0.0	0 0.0	0 0.0	0 0.0	0 0.0	0.0
4	0 0.0	0 0.0	0 0.0	0 0.0	0 0.0	0 0.0	0 0.0	0 0.0	0 0.0	0 0.0	0 0.0	0.0
7	78 26.4	11 3.7	12 4.1	9 3.1	5 1.7	4 1.4	8 2.7	11 3.7	9 3.1	10 3.4	138 46.8	295.0
1	95 31.8	24 8.0	18 6.0	16 5.4	9 3.0	10 3.3	12 4.0	5 1.7	17 5.7	13 4.3	80 26.8	299.0
13	140 47.0	26 8.7	18 6.0	15 5.0	10 3.4	8 2.7	9 3.0	16 5.4	11 3.7	10 3.4	35 11.7	298.0
16	123 54.4	15 6.6	12 5.3	12 5.3	4 1.8	8 3.5	5 2.2	9 4.0	10 4.4	4 1.8	24 10.6	226.0
19	0 0.0	0 0.0	0 0.0	0 0.0	0 0.0	0 0.0	0 0.0	0 0.0	0 0.0	0 0.0	0 0.0	0.0
22	0 0.0	0 0.0	0 0.0	0 0.0	0 0.0	0 0.0	0 0.0	0 0.0	0 0.0	0 0.0	0 0.0	0.0

SAN NICHOLAS ISLAND, CALIFORNIA STA93116

SEPTEMBER PERIOD 1/50 THRU 12/59

CLOUD TYPE

	(CLEAR)	(FOG)	(LOW CLOUD)				(MIDDLE CLOUD)		(HIGH CLOUD)		(VERTICAL)
LST	0	1	2	3	4	5	6	7	8	9	10
7	78 26.4	75 25.4	0 0.0	101 34.2	54 18.3	7 2.4	4 1.4	30 10.2	2 0.7	9 3.1	0 0.0
10	95 31.8	26 8.7	0 0.0	97 32.4	75 25.1	9 3.0	8 2.7	29 9.7	5 1.7	11 3.7	0 0.0
13	140 47.0	15 5.0	0 0.0	67 22.5	62 20.8	9 3.0	3 1.0	25 8.4	8 2.7	11 3.7	1 0.3
16	123 54.4	10 4.4	0 0.0	52 23.0	32 14.2	4 1.8	5 2.2	20 8.8	5 2.2	9 4.0	1 0.4
19	0 0.0	0 0.0	0 0.0	0 0.0	0 0.0	0 0.0	0 0.0	0 0.0	0 0.0	0 0.0	0 0.0

SAN NICHOLAS ISLAND, CALIFORNIA STA93116

OCTOBER PERIOD 1/50 THRU 12/59

TOTAL CLOUD AMOUNT (TENTHS)

LST	0	1	2	3	4	5	6	7	8	9	10	TOTAL
1	0	0	0	0	0	0	0	0	0	0	0	0.0
	0.0	0.0	0.0	0.0	0.0	0.0	0.0	0.0	0.0	0.0	0.0	
4	0	0	0	0	0	0	0	0	0	0	0	0.0
	0.0	0.0	0.0	0.0	0.0	0.0	0.0	0.0	0.0	0.0	0.0	
7	81	6	11	9	4	7	8	9	18	14	115	282.0
	28.7	2.1	3.9	3.2	1.4	2.5	2.8	3.2	6.4	5.0	40.8	
10	113	17	8	16	7	15	9	17	21	11	76	310.0
	36.5	5.5	2.6	5.2	2.3	4.8	2.9	5.5	6.8	3.5	24.5	
13	124	16	23	9	12	10	17	13	18	12	47	301.0
	41.2	5.3	7.6	3.0	4.0	3.3	5.6	4.3	6.0	4.0	15.6	
16	136	13	22	12	14	9	5	7	16	13	51	298.0
	45.6	4.4	7.4	4.0	4.7	3.0	1.7	2.3	5.4	4.4	17.1	
19	0	0	0	0	0	0	0	0	0	0	0	0.0
	0.0	0.0	0.0	0.0	0.0	0.0	0.0	0.0	0.0	0.0	0.0	
22	0	0	0	0	0	0	0	0	0	0	0	0.0
	0.0	0.0	0.0	0.0	0.0	0.0	0.0	0.0	0.0	0.0	0.0	

SAN NICHOLAS ISLAND, CALIFORNIA STA93116

OCTOBER PERIOD 1/50 THRU 12/59

CLOUD TYPE

	(CLEAR)	(FOG)	(LOW CLOUD)				(MIDDLE CLOUD)		(HIGH CLOUD)		(VERTICAL)
LST	0	1	2	3	4	5	6	7	8	9	10
7	81	78	0	69	55	7	4	24	8	21	0
	28.7	27.7	0.0	24.5	19.5	2.5	1.4	8.5	2.8	7.4	0.0
10	113	34	0	84	64	8	6	26	14	28	0
	36.5	11.0	0.0	27.1	20.6	2.6	1.9	8.4	4.5	9.0	0.0
13	124	15	0	61	58	15	11	23	21	32	0
	41.2	5.0	0.0	20.3	19.3	5.0	3.7	7.6	7.0	10.6	0.0
16	136	22	0	65	49	9	10	28	16	37	0
	45.6	7.4	0.0	21.8	16.4	3.0	3.4	9.4	5.4	12.1	0.0
19	0	0	0	0	0	0	0	0	0	0	0
	0.0	0.0	0.0	0.0	0.0	0.0	0.0	0.0	0.0	0.0	0.0

SAN NICHOLAS ISLAND, CALIFORNIA STA93116

NOVEMBER PERIOD 1/50 THRU 12/59

TOTAL CLOUD AMOUNT (TENTHS)

LST	0	1	2	3	4	5	6	7	8	9	10	TOTAL
1	0	0	0	0	0	0	0	0	0	0	0	0.0
	0.0	0.0	0.0	0.0	0.0	0.0	0.0	0.0	0.0	0.0	0.0	
4	0	0	0	0	0	0	0	0	0	0	0	0.0
	0.0	0.0	0.0	0.0	0.0	0.0	0.0	0.0	0.0	0.0	0.0	
7	106	17	11	16	8	10	12	11	15	9	65	280.0
	37.9	6.1	3.9	5.7	2.9	3.6	4.3	3.9	5.4	3.2	23.2	
10	114	24	13	20	10	11	15	9	23	16	45	300.0
	38.0	8.0	4.3	6.7	3.3	3.7	5.0	3.0	7.7	5.3	15.0	
13	120	28	23	12	13	6	11	12	24	10	31	290.0
	41.4	9.7	7.9	4.1	4.5	2.1	3.8	4.1	8.3	3.4	10.7	
16	127	28	17	13	10	8	11	8	17	9	41	289.0
	43.9	9.7	5.9	4.5	3.5	2.8	3.8	2.8	5.9	3.1	14.2	
19	0	0	0	0	0	0	0	0	0	0	1	1.0
	0.0	0.0	0.0	0.0	0.0	0.0	0.0	0.0	0.0	0.0	100.0	
22	0	0	0	0	0	0	0	0	0	0	0	0.0
	0.0	0.0	0.0	0.0	0.0	0.0	0.0	0.0	0.0	0.0	0.0	

SAN NICHOLAS ISLAND, CALIFORNIA STA93116

NOVEMBER PERIOD 1/50 THRU 12/59

CLOUD TYPE

	(CLEAR)	(FOG)	(LOW CLOUD)				(MIDDLE CLOUD)		(HIGH CLOUD)		(VERTICAL)
LST	0	1	2	3	4	5	6	7	8	9	10
7	106	44	1	64	40	9	19	32	9	50	0
	37.9	15.7	0.4	22.9	14.3	3.2	6.8	11.4	3.2	17.9	0.0
10	114	18	0	65	44	13	15	39	12	63	0
	38.1	6.0	0.0	21.7	14.7	4.3	5.0	13.0	4.0	21.1	0.0
13	120	10	0	43	44	16	15	38	16	56	0
	41.4	3.4	0.0	14.8	15.2	5.5	5.2	13.1	5.5	19.3	0.0
16	127	9	0	50	33	7	15	37	17	57	1
	43.9	3.1	0.0	17.3	11.4	2.4	5.2	12.8	5.9	19.7	0.3
19	0	0	0	1	0	0	0	0	0	0	0
	0.0	0.0	0.0	100.0	0.0	0.0	0.0	0.0	0.0	0.0	0.0

SAN NICHOLAS ISLAND, CALIFORNIA STA93116

DECEMBER PERIOD 1/50 THRU 12/59

TOTAL CLOUD AMOUNT (TENTHS)

LST	0	1	2	3	4	5	6	7	8	9	10	TOTAL
1	0 0.0	0 0.0	0 0.0	0 0.0	0 0.0	0 0.0	0 0.0	0 0.0	0 0.0	0 0.0	0 0.0	0.0
4	1 100.0	0 0.0	0 0.0	0 0.0	0 0.0	0 0.0	0 0.0	0 0.0	0 0.0	0 0.0	0 0.0	1.0
7	87 29.9	12 4.1	15 5.2	20 6.9	13 4.5	13 4.5	7 2.4	19 6.5	18 6.2	16 5.5	71 24.4	291.0
10	95 30.6	14 4.5	20 6.5	10 3.2	18 5.8	14 4.5	9 2.9	17 5.5	22 7.1	19 6.1	72 23.2	310.0
13	94 31.3	17 5.7	19 6.3	21 7.0	10 3.3	12 4.0	10 3.3	15 5.0	21 7.0	16 5.3	65 21.7	300.0
16	104 34.9	21 7.0	17 5.7	10 3.4	11 3.7	7 2.3	6 2.0	15 5.0	11 3.7	20 6.7	76 25.5	298.0
19	0 0.0	0 0.0	0 0.0	0 0.0	0 0.0	0 0.0	0 0.0	0 0.0	0 0.0	0 0.0	0 0.0	0.0
22	0 0.0	0 0.0	0 0.0	0 0.0	0 0.0	0 0.0	0 0.0	0 0.0	0 0.0	0 0.0	0 0.0	0.0

SAN NICHOLAS ISLAND, CALIFORNIA STA93116

DECEMBER PERIOD 1/50 THRU 12/59

CLOUD TYPE

	(CLEAR)	(FOG)		(LOW CLOUD)			(MIDDLE CLOUD)		(HIGH CLOUD)		(VERTICAL)
LST	0	1	2	3	4	5	6	7	8	9	10
7	87 29.9	45 15.5	0 0.0	68 23.4	46 15.8	6 2.1	18 6.2	41 14.1	23 7.9	56 19.2	0 0.0
10	95 30.6	39 12.6	0 0.0	73 23.5	52 16.8	14 4.5	18 5.8	36 11.6	28 9.0	67 21.6	0 0.0
13	94 31.3	27 9.0	0 0.0	56 18.7	55 18.3	19 6.3	19 6.3	35 11.7	25 8.3	75 25.0	0 0.0
16	104 34.9	31 10.4	1 0.3	51 17.1	46 15.4	5 1.7	21 7.0	28 9.4	25 8.4	76 25.5	0 0.0
19	0 0.0	0 0.0	0 0.0	0 0.0	0 0.0	0 0.0	0 0.0	0 0.0	0 0.0	0 0.0	0 0.0

CUMULATIVE PROBABILITY LISTINGS

Composite of: San Clemente
San Diego
San Nicholas

(5-Year Record)

JANUARY

Local Standard Time	Cloud Amount										
	0	1	2	3	4	5	6	7	8	9	10
0700	29	36	43	47	52	55	59	64	72	77	100
1000	32	37	41	46	48	53	59	64	71	80	100
1300	34	39	43	48	53	58	64	70	76	83	100
1600	32	39	45	50	55	60	65	70	77	84	100
1900	39	46	53	61	68	71	74	77	83	87	100

FEBRUARY

Local Standard Time	Cloud Amount										
	0	1	2	3	4	5	6	7	8	9	10
0700	30	36	41	46	50	52	57	60	68	74	100
1000	27	33	38	41	45	53	56	61	66	75	100
1300	30	36	41	47	51	54	59	66	73	81	100
1600	30	36	43	47	53	58	61	66	74	80	100
1900	38	45	51	55	59	65	69	75	78	82	100

MARCH

Local Standard Time	Cloud Amount										
	0	1	2	3	4	5	6	7	8	9	10
0700	20	27	33	38	43	46	52	58	67	74	100
1000	18	26	32	38	43	46	52	60	69	79	100
1300	20	30	37	43	48	53	62	70	77	83	100
1600	21	30	37	43	49	53	58	67	75	82	100
1900	20	27	35	41	45	50	56	65	77	83	100

APRIL

Local Standard Time	Cloud Amount										
	0	1	2	3	4	5	6	7	8	9	10
0700	19	24	27	33	36	41	44	50	57	67	100
1000	23	30	34	41	45	49	55	63	71	78	100
1300	28	36	41	47	52	57	62	69	76	83	100
1600	28	34	42	47	53	58	63	67	73	83	100
1900	24	33	39	43	46	52	57	64	71	75	100

MAY

Local Standard Time	Cloud Amount										
	0	1	2	3	4	5	6	7	8	9	10
0700	11	14	18	20	23	26	30	35	41	49	100
1000	15	23	27	30	34	39	46	51	58	67	100
1300	24	33	38	44	49	53	58	64	72	81	100
1600	25	32	39	44	51	56	62	68	74	80	100
1900	10	21	29	32	38	43	47	53	59	66	100

JUNE

Local Standard Time	Cloud Amount										
	0	1	2	3	4	5	6	7	8	9	10
0700	4	6	7	8	10	12	14	17	20	26	100
1000	12	17	21	24	25	29	31	36	41	46	100
1300	20	26	31	35	40	45	49	55	61	65	100
1600	21	32	38	44	48	51	55	62	68	73	100
1900	11	19	25	29	33	37	41	45	49	56	100

JULY

Local Standard Time	Cloud Amount										
	0	1	2	3	4	5	6	7	8	9	10
0700	6	7	8	10	11	12	14	15	23	30	100
1000	16	21	26	31	35	39	43	47	54	63	100
1300	26	37	45	51	58	65	70	76	82	87	100
1600	32	41	51	55	61	67	72	76	83	90	100
1900	16	27	34	40	43	48	53	57	66	73	100

AUGUST

Local Standard Time	Cloud Amount										
	0	1	2	3	4	5	6	7	8	9	10
0700	7	10	12	14	16	18	20	24	29	39	100
1000	18	25	31	38	43	47	52	56	63	69	100
1300	30	40	51	58	63	69	73	78	83	88	100
1600	33	44	52	61	64	69	73	79	85	90	100
1900	17	25	35	41	46	53	58	66	72	77	100

SEPTEMBER

Local Standard Time	Cloud Amount										
	0	1	2	3	4	5	6	7	8	9	10
0700	16	21	24	27	29	31	35	38	44	49	100
1000	24	33	37	44	49	52	55	59	65	71	100
1300	35	47	54	59	64	68	70	75	80	86	100
1600	43	58	63	67	70	72	76	79	84	88	100
1900	33	39	49	55	61	65	70	74	78	82	100

OCTOBER

Local Standard Time	Cloud Amount										
	0	1	2	3	4	5	6	7	8	9	10
0700	23	30	33	36	39	42	46	49	54	61	100
1000	27	33	37	43	47	50	55	60	68	74	100
1300	31	39	44	52	57	60	65	71	77	86	100
1600	34	42	49	55	59	64	66	70	77	83	100
1900	37	42	47	52	59	63	68	72	78	80	100

NOVEMBER

Local Standard Time	Cloud Amount										
	0	1	2	3	4	5	6	7	8	9	10
0700	21	28	34	40	45	49	52	55	63	71	100
1000	22	28	36	41	44	50	54	61	66	74	100
1300	23	30	37	42	47	52	56	61	68	75	100
1600	24	31	39	43	49	54	58	62	69	78	100
1900	34	39	47	51	57	61	65	69	73	75	100

DECEMBER

Local Standard Time	Cloud Amount										
	0	1	2	3	4	5	6	7	8	9	10
0700	19	26	31	39	45	48	52	58	65	69	100
1000	21	27	32	41	45	49	52	57	65	75	100
1300	19	25	32	37	44	49	54	60	69	79	100
1600	21	26	31	38	43	48	53	58	66	76	100
1900	26	37	45	50	55	59	64	69	74	78	100

MORNING AND AFTERNOON

CUMULATIVE PROBABILITY GRAPHS

Composite of: San Clemente
San Diego
San Nicholas

(5-Year Record)

Prepared for

Scripps Institute of Oceanography

by

Allied Research Associates, Inc.

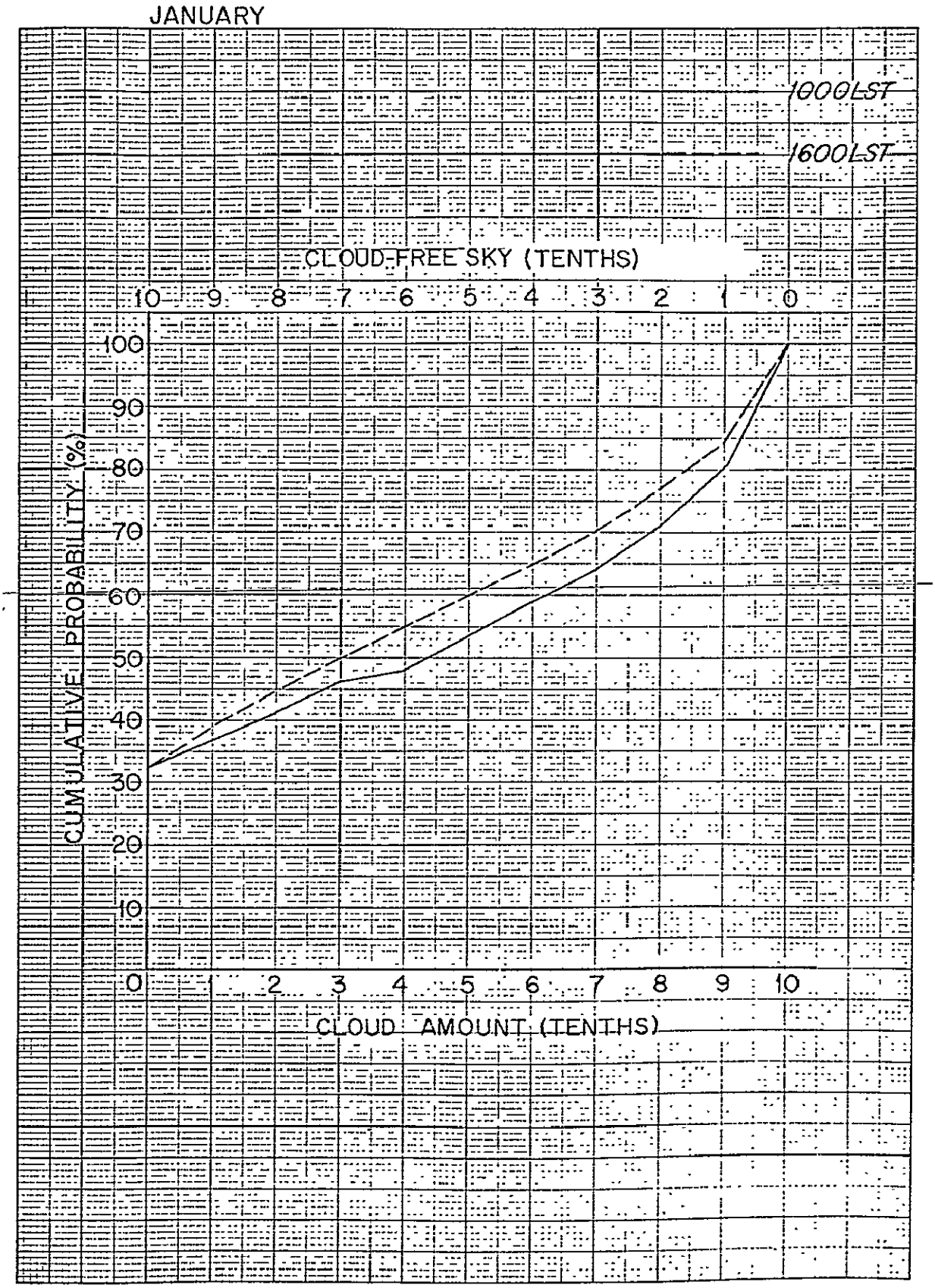
JANUARY
1000LST
1600LST
CLOUD-FREE SKY (TENTHS)
10 9 8 7 6 5 4 3 2 1 0
100
90
80
70
60
50
40
30
20
10
0
CUMULATIVE PROBABILITY (%)
1 2 3 4 5 6 7 8 9 10
CLOUD AMOUNT (TENTHS)

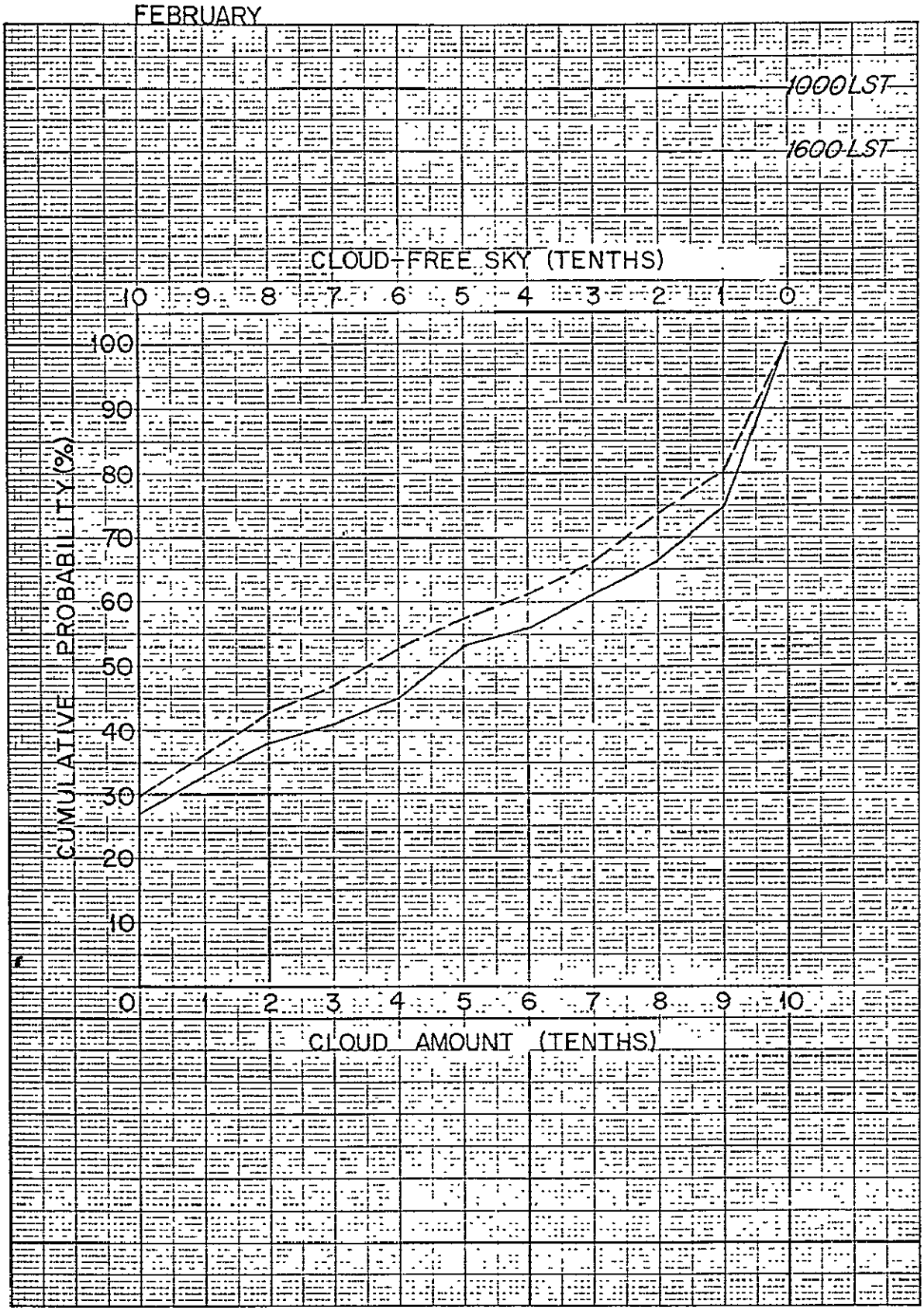
FEBRUARY
1000 LST
1600 LST
CLOUD-FREE SKY (TENTHS)
10 9 8 7 6 5 4 3 2 1 0
CUMULATIVE PROBABILITY (%)
100
90
80
70
60
50
40
30
20
10
0
0 1 2 3 4 5 6 7 8 9 10
CLOUD AMOUNT (TENTHS)

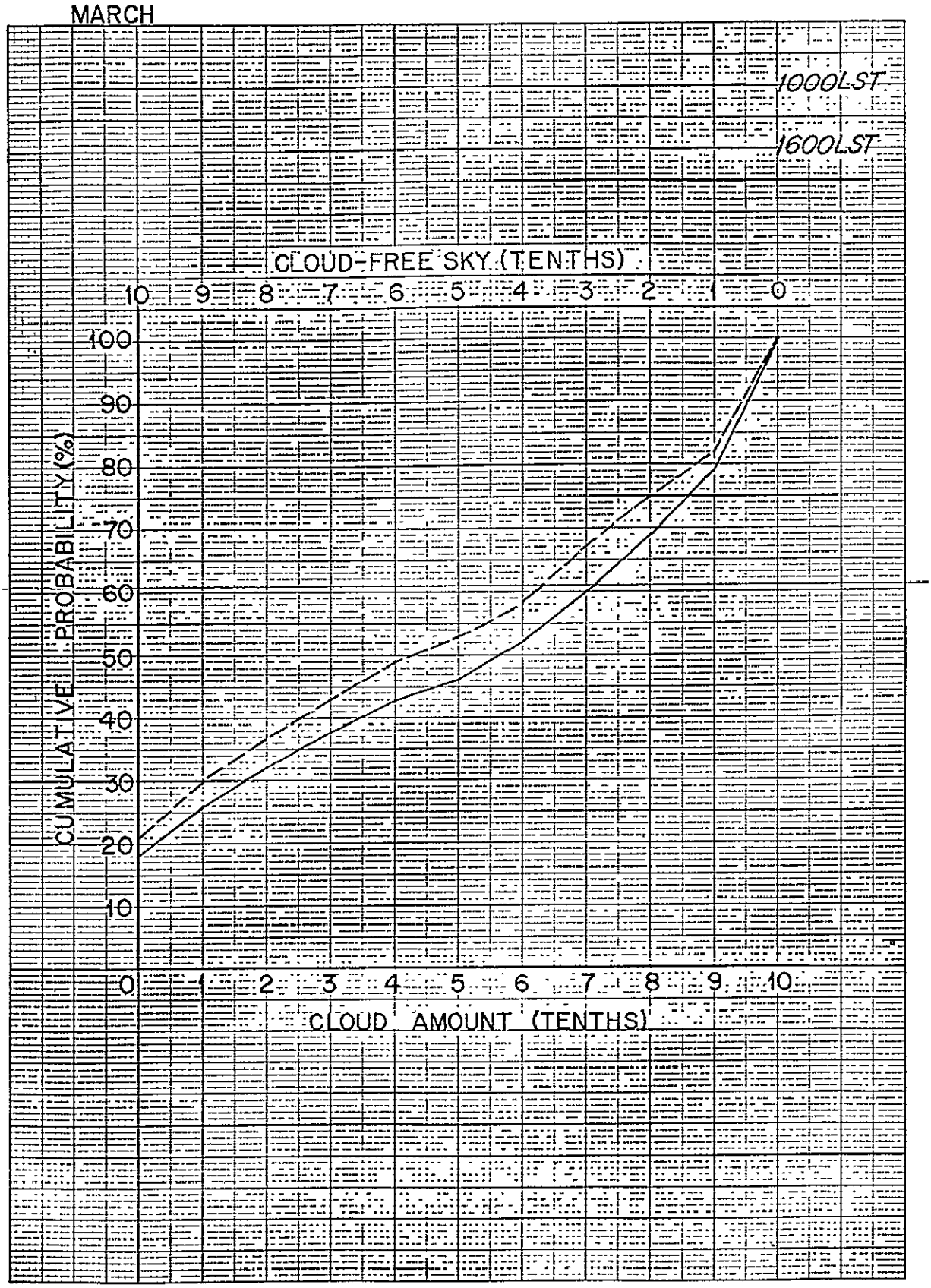
MARCH
1000LST
1600LST
CLOUD-FREE SKY (TENTHS)
10 9 8 7 6 5 4 3 2 1 0
CUMULATIVE PROBABILITY (%)
100
90
80
70
60
50
40
30
20
10
0
1 2 3 4 5 6 7 8 9 10
CLOUD AMOUNT (TENTHS)

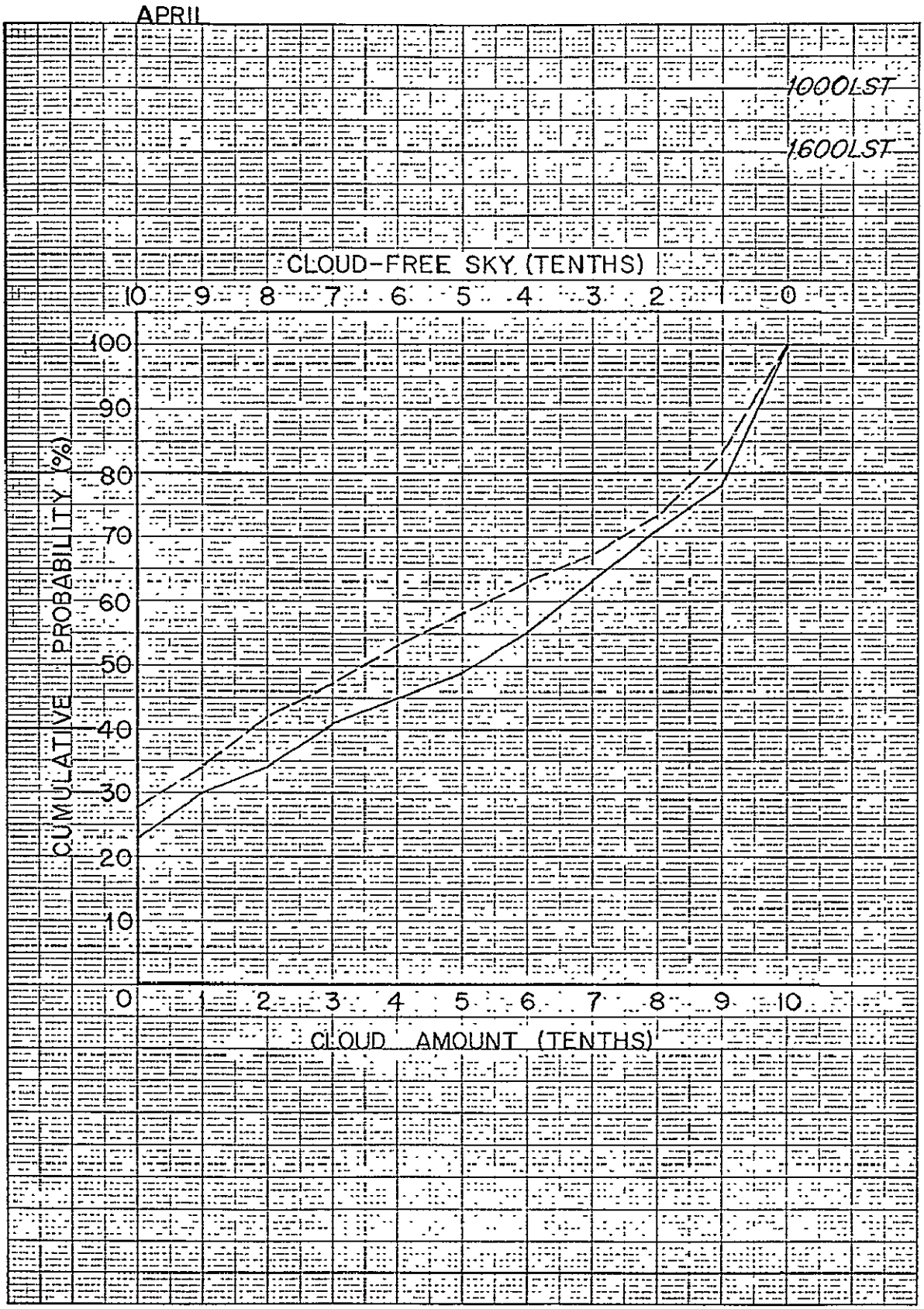
APRIL
1000LST
1600LST
CLOUD-FREE SKY (TENTHS)
10 9 8 7 6 5 4 3 2 1 0
100
90
80
70
60
50
40
30
20
10
0
CUMULATIVE PROBABILITY (%)
1 2 3 4 5 6 7 8 9 10
CLOUD AMOUNT (TENTHS)

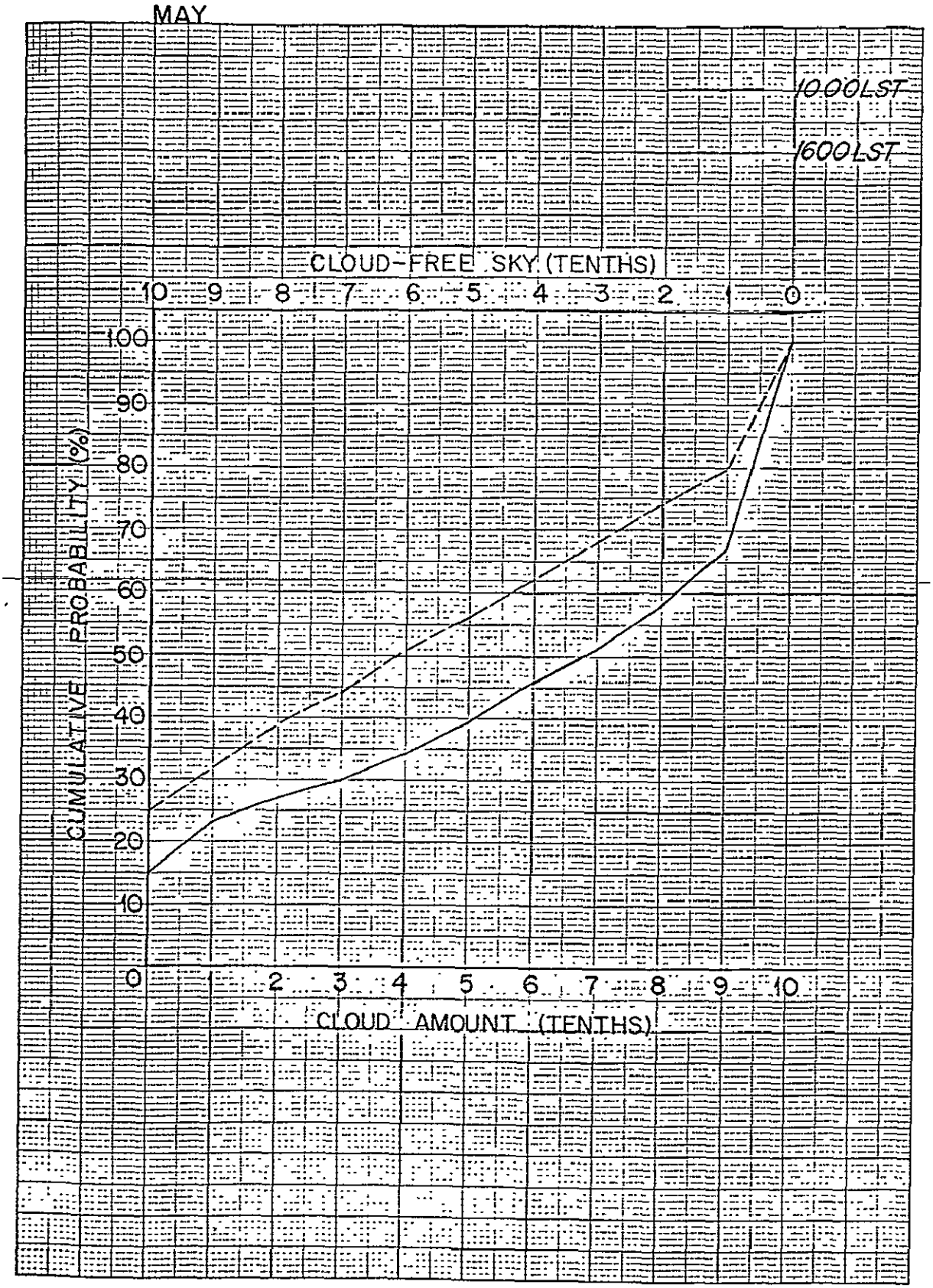
MAY
1000LST
1600LST
CLOUD-FREE SKY (TENTHS)
10 9 8 7 6 5 4 3 2 1 0
100
90
80
70
60
50
40
30
20
10
0
CUMULATIVE PROBABILITY (%)
2 3 4 5 6 7 8 9 10
CLOUD AMOUNT (TENTHS)

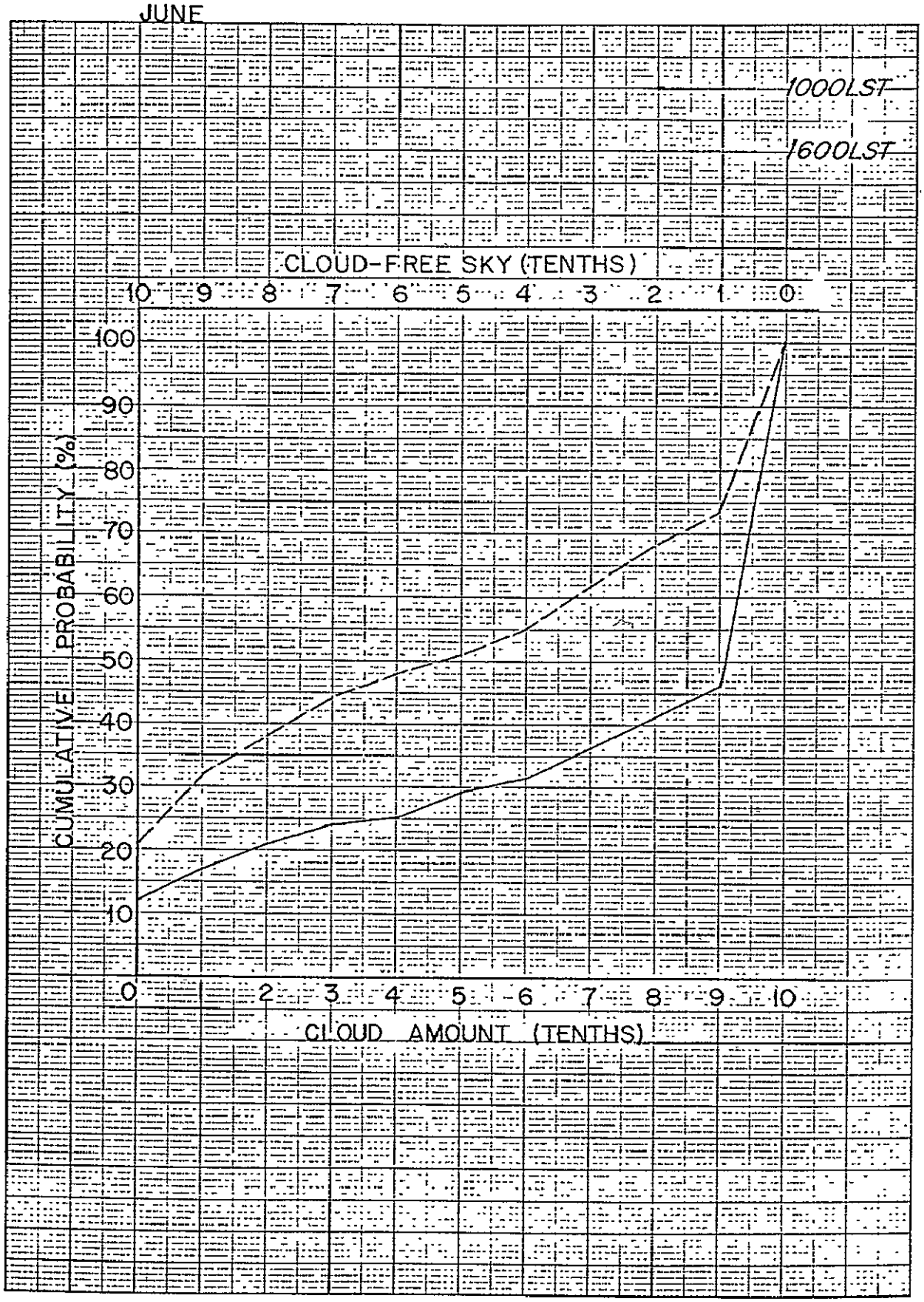
JUNE
1000LST
1600LST
CLOUD-FREE SKY (TENTHS)
10 9 8 7 6 5 4 3 2 1 0
100
90
80
70
60
50
40
30
20
10
0
CUMULATIVE PROBABILITY (%)
0 2 3 4 5 6 7 8 9 10
CLOUD AMOUNT (TENTHS)

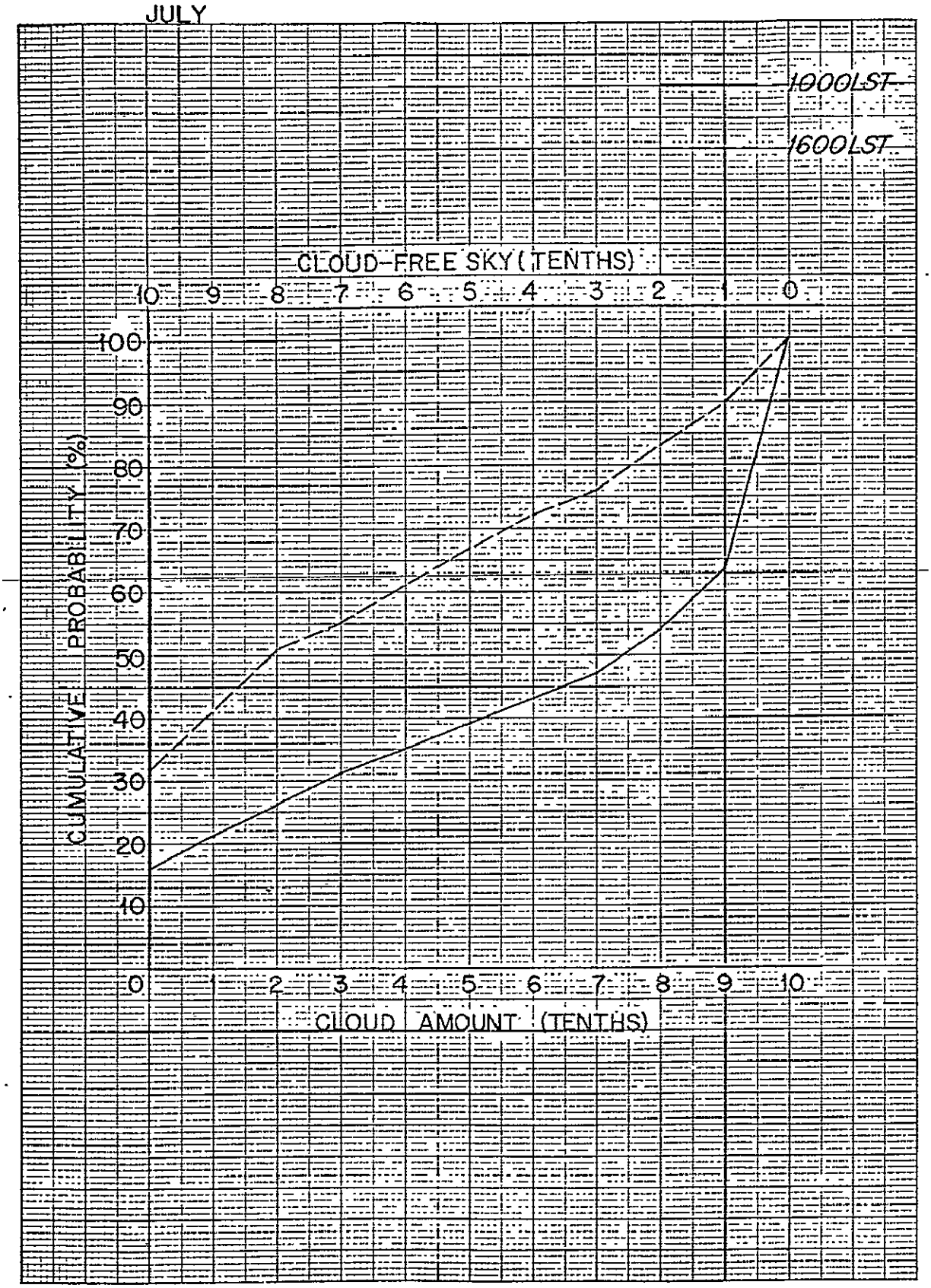
JULY
1000LST
1600LST
CLOUD-FREE SKY (TENTHS)
10 9 8 7 6 5 4 3 2 1 0
CUMULATIVE PROBABILITY (%)
100
90
80
70
60
50
40
30
20
10
0
0 1 2 3 4 5 6 7 8 9 10
CLOUD AMOUNT (TENTHS)

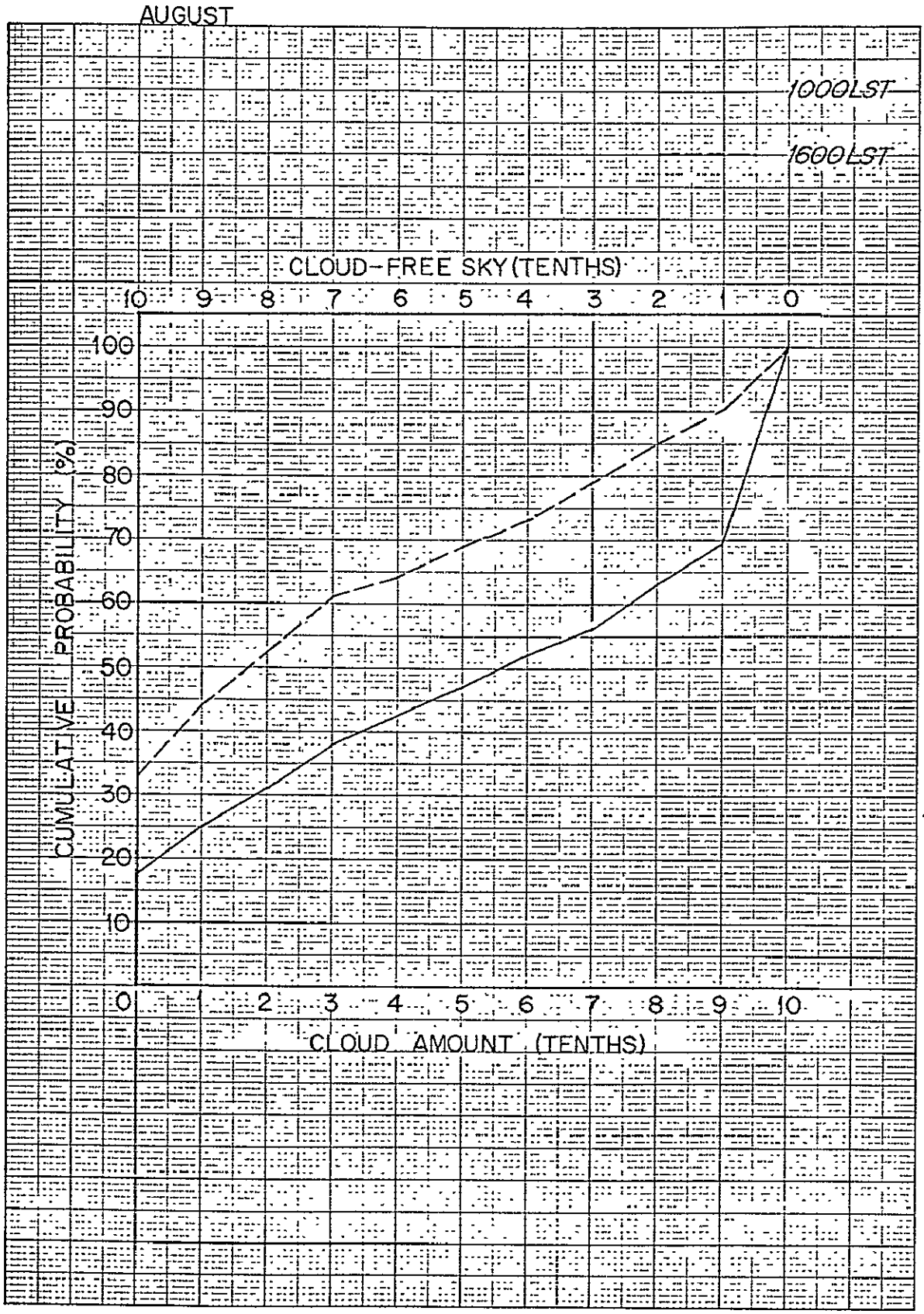
AUGUST
1000LST
1600LST
CLOUD-FREE SKY (TENTHS)
10 9 8 7 6 5 4 3 2 1 0
CUMULATIVE PROBABILITY (%)
100
90
80
70
60
50
40
30
20
10
0
1 2 3 4 5 6 7 8 9 10
CLOUD AMOUNT (TENTHS)

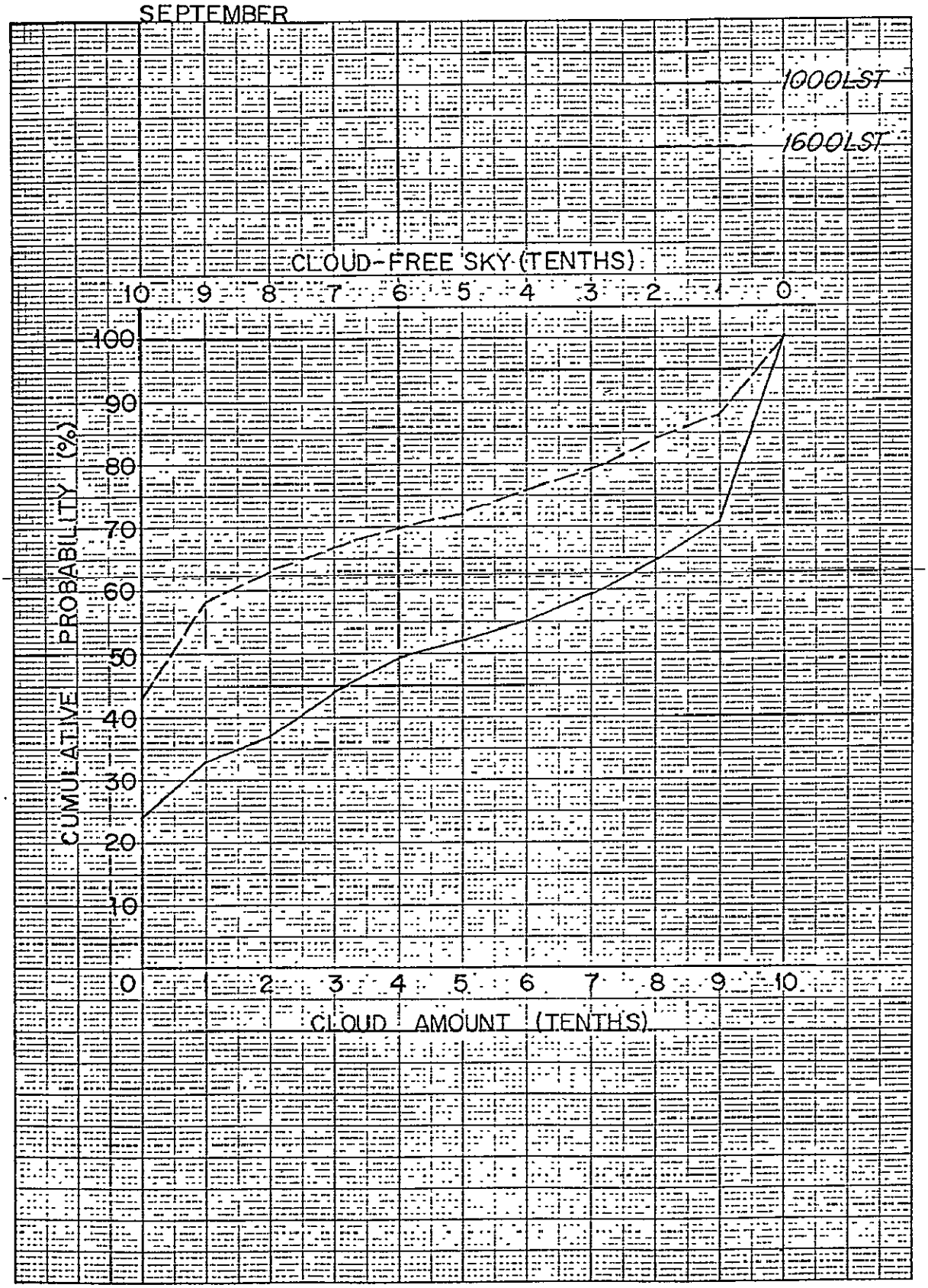
SEPTEMBER
1000LST
1600LST
CLOUD-FREE SKY (TENTHS)
10 9 8 7 6 5 4 3 2 1 0
CUMULATIVE PROBABILITY (%)
100
90
80
70
60
50
40
30
20
10
0
0 1 2 3 4 5 6 7 8 9 10
CLOUD AMOUNT (TENTHS)

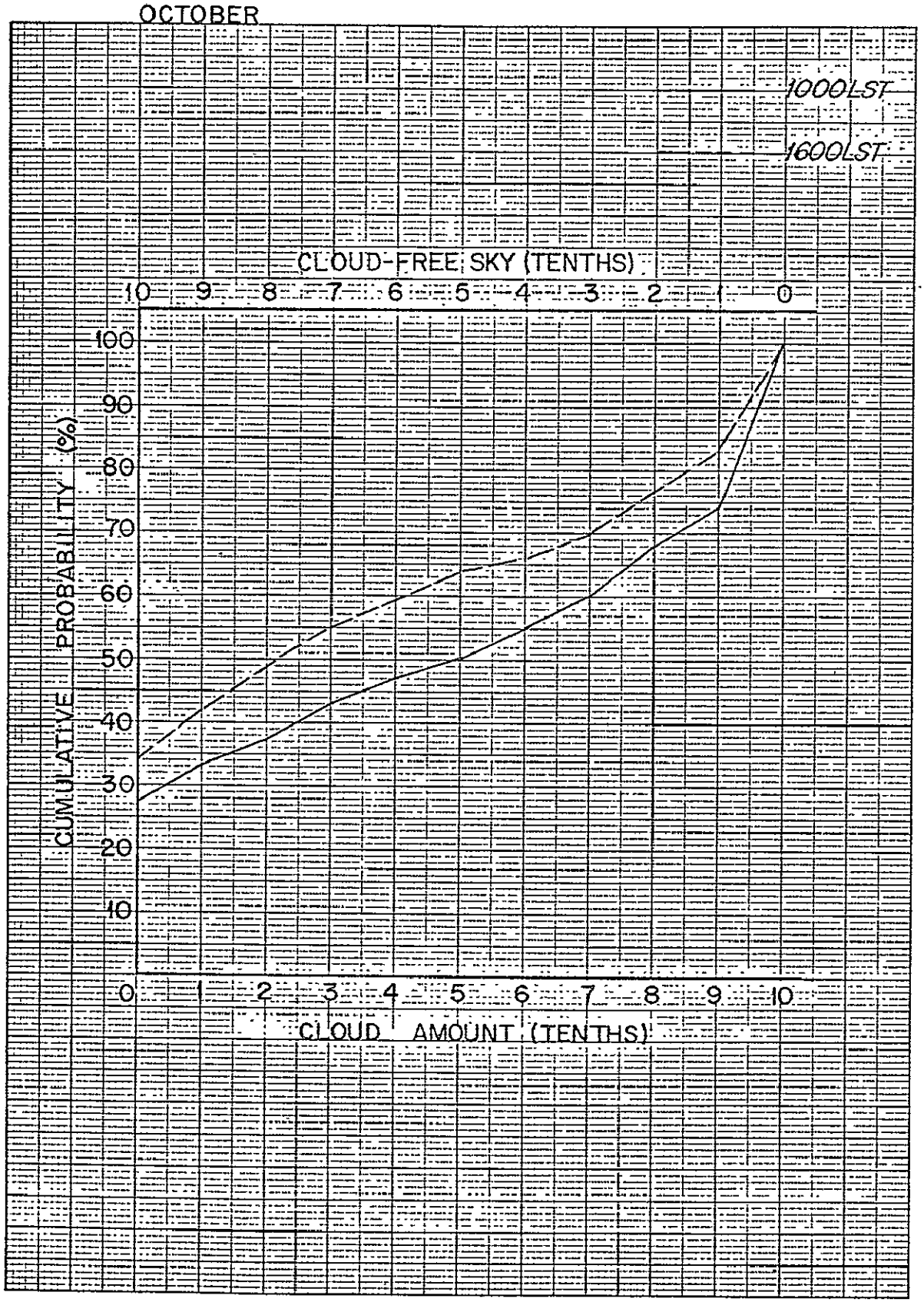
OCTOBER
1000LST
1600LST
CLOUD-FREE SKY (TENTHS)
10 9 8 7 6 5 4 3 2 1 0
CUMULATIVE PROBABILITY (%)
100
90
80
70
60
50
40
30
20
10
0
1 2 3 4 5 6 7 8 9 10
CLOUD AMOUNT (TENTHS)

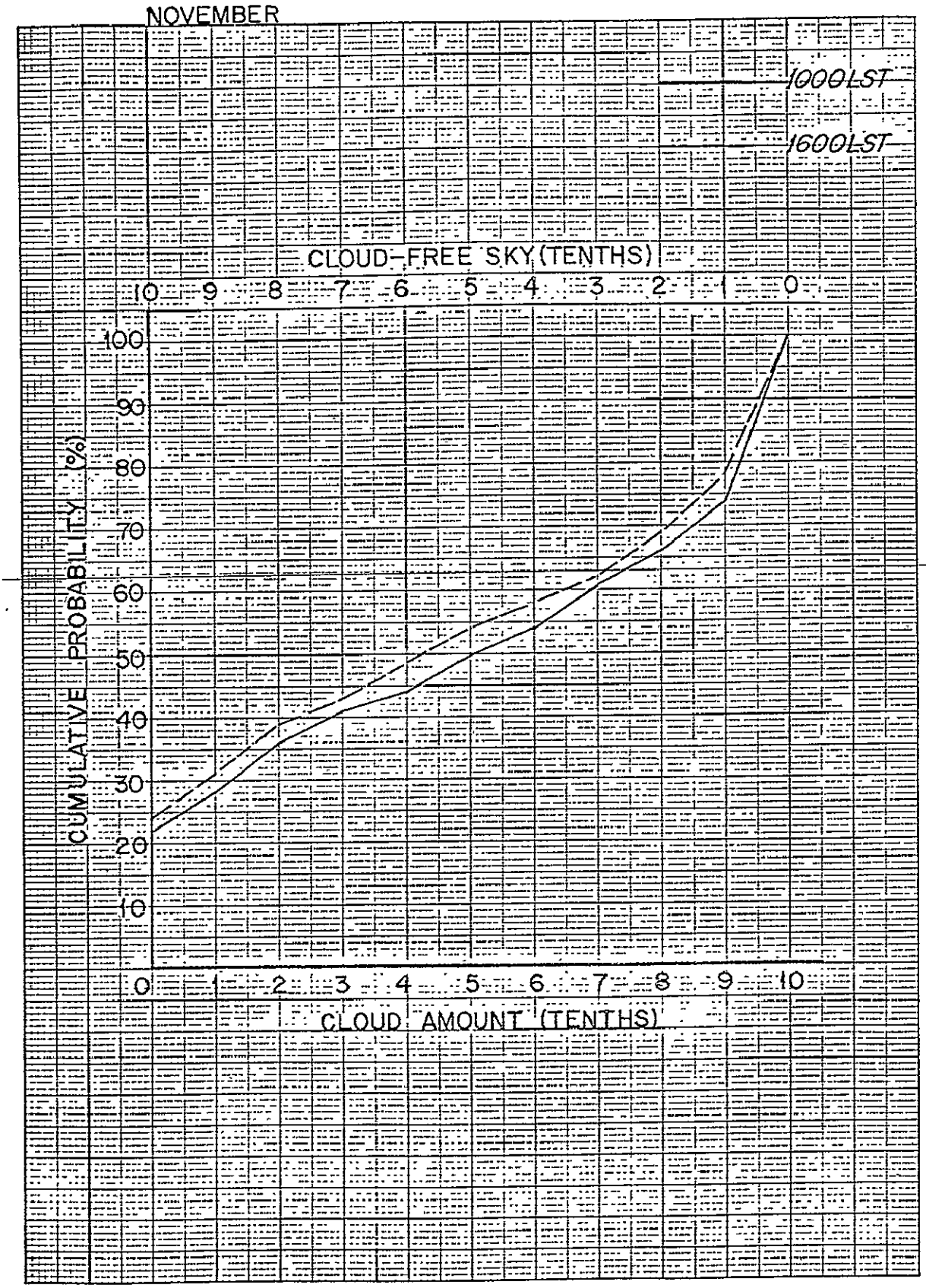
NOVEMBER
1000LST
1600LST
CLOUD-FREE SKY (TENTHS)
10 9 8 7 6 5 4 3 2 1 0
CUMULATIVE PROBABILITY (%)
100
90
80
70
60
50
40
30
20
10
0 1 2 3 4 5 6 7 8 9 10
CLOUD AMOUNT (TENTHS)

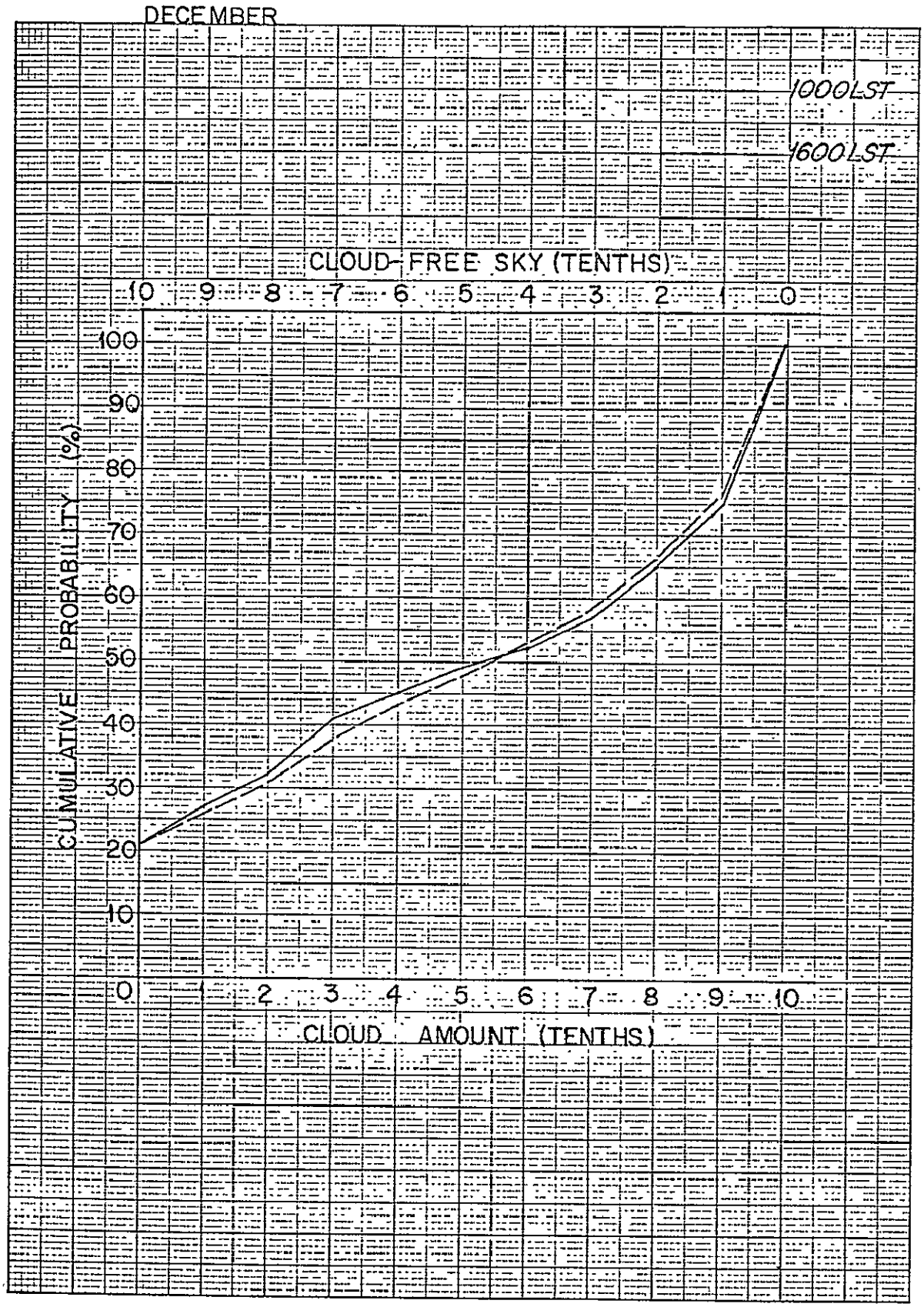
DECEMBER
1000 LST
1600 LST
CLOUD-FREE SKY (TENTHS)
10
9
8
7
6
5
4
3
2
1
0
100
90
80
70
60
50
40
30
20
10
0
CUMULATIVE PROBABILITY (%)
1
2
3
4
5
6
7
8
9
10
CLOUD AMOUNT (TENTHS)

COMPARISONS BETWEEN SATELLITE-OBSERVED AND GROUND-OBSERVED CLOUD COVER FOR THE SOUTHERN CALIFORNIA COASTAL AREA

Prepared by

Allied Research Associates, Inc.

Concord, Massachusetts

for

Scripps Institute of Oceanography

under

P. O. 706-30108-0

Introduction

Under Contract No. P. O. 706-30108-0, a Southern California Cloud Climatology has been developed, based largely upon conventional ground observations of cloud-amount and cloud-type. The results of this study have been submitted previously. They include:

1) Computer listings of cloud amount and cloud type for the San Clemente, San Diego, and San Nicolas stations.
2) Cumulative probability listings of cloud amount for the three combined stations for a 5-year period of overlap.
3) Cumulative probability graphs of cloud (and cloud-free) amount for the three combined stations at mid-morning and mid-afternoon.

Because these data are eventually to be used to estimate the probabilities of having a clear line of sight to the surface from a satellite camera, however, this report discusses potential discrepancies between satellite and ground observed cloud amounts for the Southern California coastal area.

Cloud Climatology Summary

The Southern California coastal area is basically a Desert Marine climate with predominantly stratiform cloudiness having small seasonal but large diurnal variations in cloud amount. The small seasonal variations in the cloud-amount frequency distributions at 1300 LST may be seen in Table 1. These data represent a 5-year composite (1961 through 1965) from the San Clemente, San Diego and San Nicolas stations. The diurnal variations are the smallest during the winter months, and reach their maximum in July. Figure 1 shows the cumulative probabilities of clear-sky amount for 0700 and 1600 LST for the three-station composite in July. Note, for example, that at 0700 there is only a 12% chance of a less than 50% cloud cover, while by 1600 this has increased to a 67% chance.

From Table 1 the strong U-shaped characteristics of the frequency distributions of cloud amount may be noted. This is typical of areas with predominant stratiform cloudiness where totally clear or overcast conditions predominate. Figure 2 represents a mean annual cloud-amount frequency distribution for the combined stations at 1300 LST. Again, the U-shaped characteristics are very evident.

TABLE 1

MONTHLY CLOUD-AMOUNT FREQUENCY DISTRIBUTIONS AT 1300 LST (in %) FOR SOUTHERN CALIFORNIA COASTAL AREA

	CLOUD AMOUNT										
	0	1	2	3	4	5	6	7	8	9	10
Jan	34	5	4	5	5	5	6	6	6	7	17
Feb	30	6	5	6	4	3	5	7	7	8	19
Mar	20	10	7	6	5	5	9	8	7	6	17
Apr	28	8	5	6	5	5	5	7	7	7	17
May	24	9	5	6	5	4	5	6	8	9	19
Jun	20	6	5	4	5	5	4	6	6	4	35
Jul	26	11	8	6	7	7	5	6	6	5	13
Aug	30	10	11	7	5	6	4	5	5	5	12
Sep	35	12	7	5	5	4	2	5	5	6	14
Oct	31	8	5	8	5	3	5	6	6	9	14
Nov	23	7	7	5	5	5	4	5	7	7	25
Dec	19	6	7	5	7	5	5	6	9	10	21

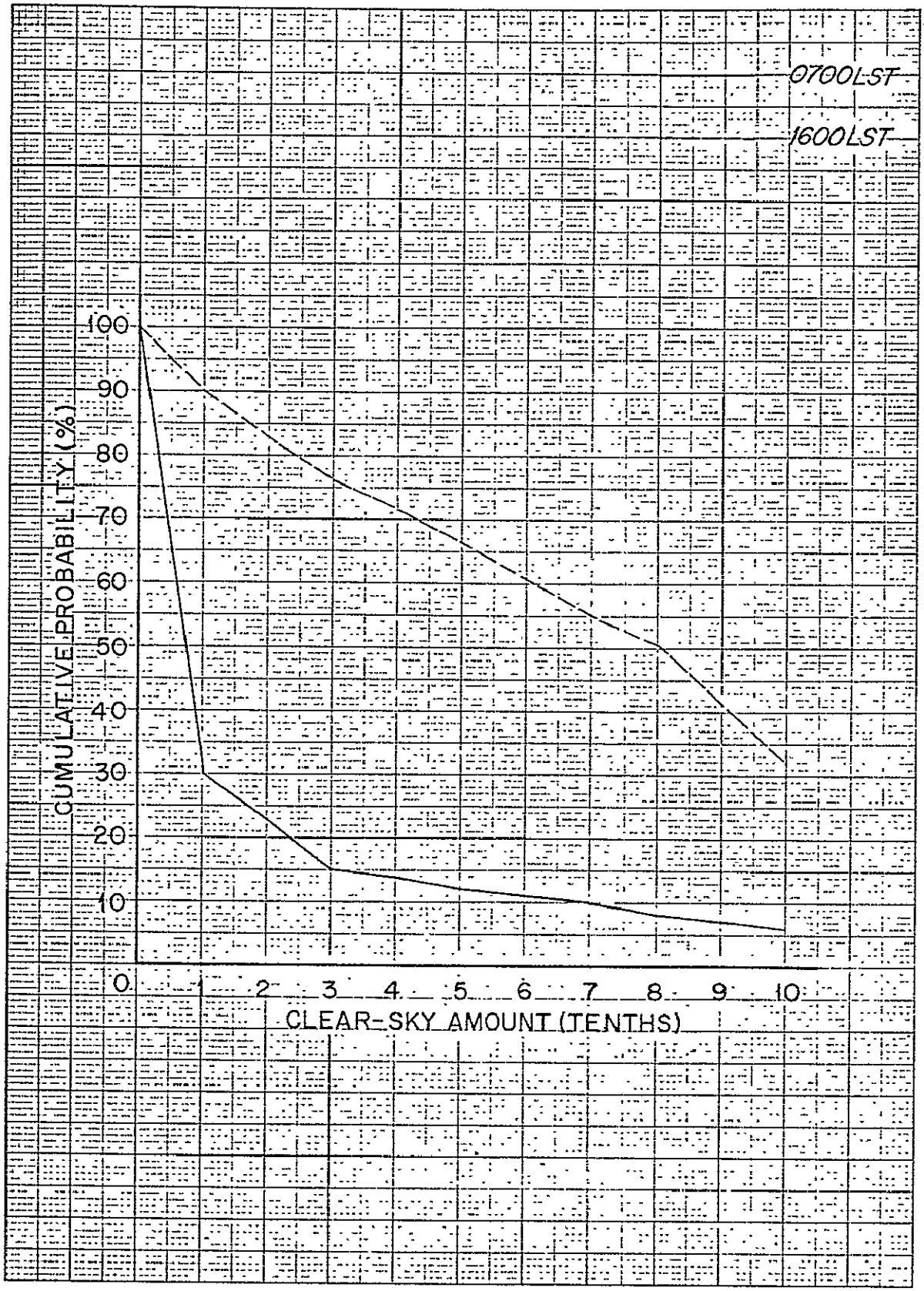

Fig. 1 Cumulative Distributions of Clear-Sky Amounts for July

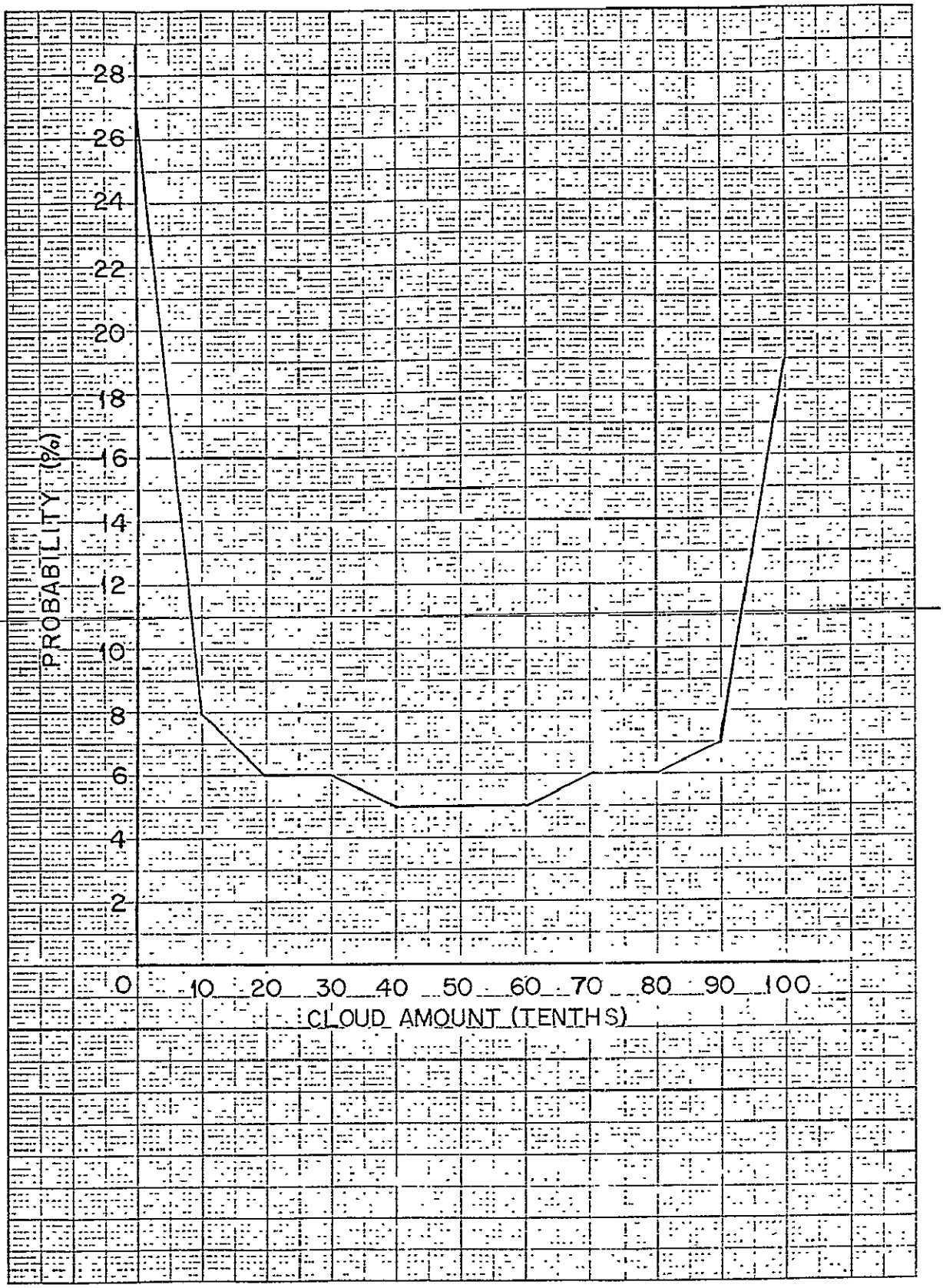

Fig. 2 Mean Annual 1300 LST Cloud-Amount Frequency Distribution

Throughout, both the cloud-amount and cloud-type data were quite similar from the three selected stations, indicating a relatively homogeneous cloud climatic region. (This area had in fact been designated as a separate cloud climatic category in a previous ARA study in which 29 cloud climatic regions were defined on a global basis, Reference 1.) Figure 3 shows cloud-amount frequency distributions for the three selected stations. These curves were drawn from a 10-year record (not simultaneous), and represent the 1000 LST distributions for the month of March (one of the times and month chosen at random for comparison). The greatest discrepancy occurs in the clear-sky category for the San Nicolas station, although this may be due in part to the different time frame of the San Nicolas data.

The predominance of stratiform cloudiness may be seen by examining the cloud-type computer listings mentioned as Item 1 in the Introduction. With reference to low cloudiness in particular, Table 2 presents the percentages of low stratiform cloudiness relative to all low cloudiness. (Due to the observer's inability to see higher levels of cloudiness in the presence of low overcasts, the statistics for the middle and high cloudiness are considerably less reliable.) As might be expected, the stratiform cloudiness reaches its peak in the early morning of the summer months. The island stations generally report more stratiform cloudiness than does San Diego.

As will be seen in the next section, the U-shaped distribution of cloud amounts plus the stratiform nature of the cloudiness is nearly ideal for close satellite/ground cloud-amount comparisons.

Satellite/Ground Cloud-Amount Comparisons

Estimates of the amount of cloud cover as observed from the ground and from a satellite generally differ. In certain circumstances these differences are considerable. There are several reasons that may account for these differences:

1) Small cumulus clouds may not be resolved in the satellite pictures. The satellite photograph may show an area as being clear when a small percentage of the sky is actually cloud covered. (Current cameras have a 2 to 5 n.mi. resolution capability.)

TABLE 2

PERCENTAGES OF LOW STRATIFORM CLOUDINESS

Station	0700 annual	1600 annual	0700 July	Daytime annual
San Clemente	88	83	99	87
San Diego	86	72	100	78
San Nicolas	91	87	98	89
All	88	80	99	84

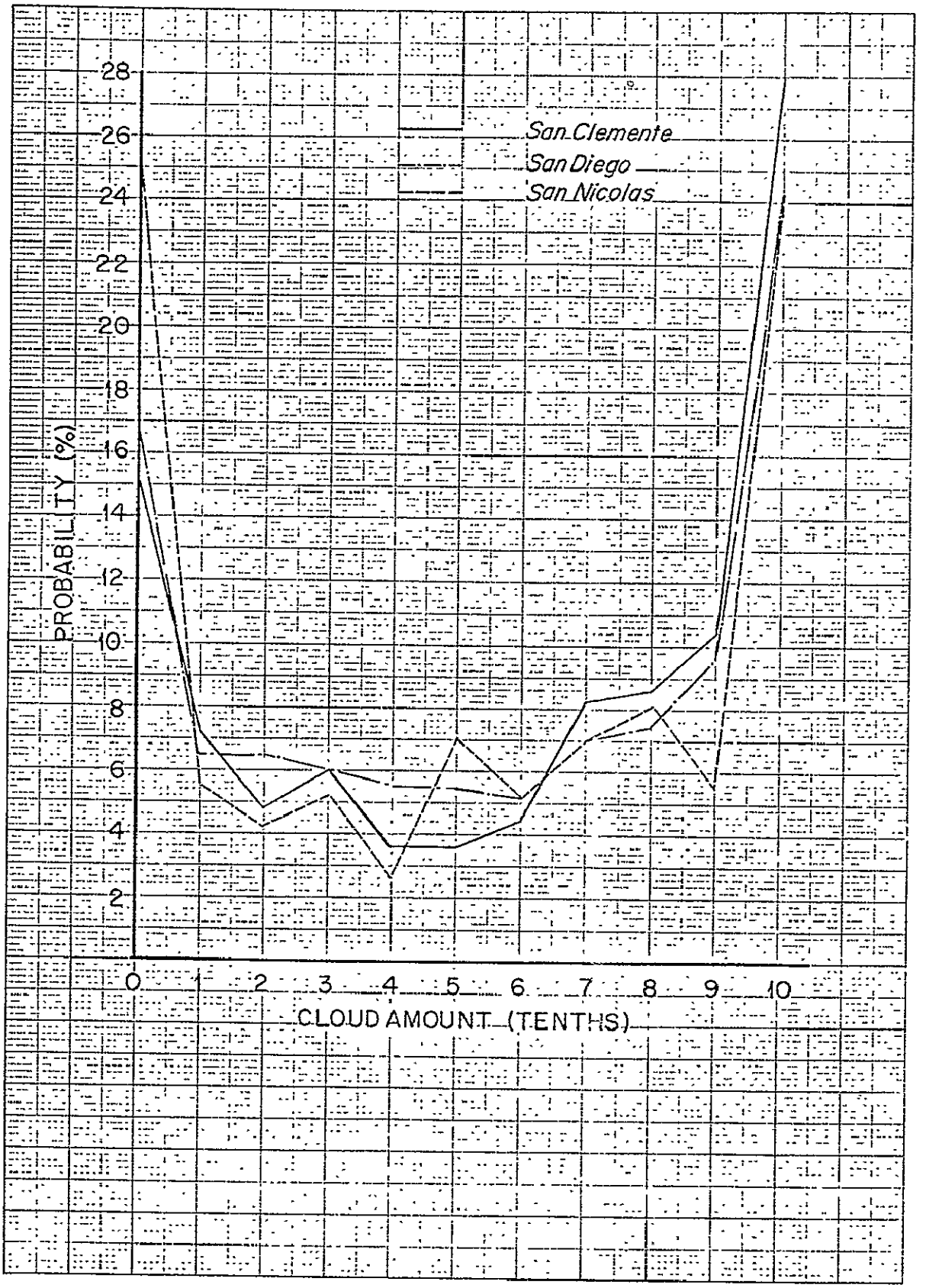

Fig. 3 March 1000 LST Cloud-Amount Frequency Distributions

2) The poorest overall agreement between satellite and surface observations of cloud amount occurs in the presence of cirrus-type cloudiness. A thin cirrus overcast noted by a ground observer may be completely negligible when determining clear line of sight probabilities from spacecraft altitudes.

3) Because half the sky dome, over which an observer integrates to get total sky cover, is less than 30° above the horizon, the observer's view is often blocked more by the sides of the clouds than by their bases. The result is an overestimation of cloud cover on the part of the ground observer, particularly in the presence of cumuliform cloudiness.

The net result of all of the above considerations is that the cloud amounts as determined by analyses of ground-based data sources will tend to be overly pessimistic in establishing clear lines of sight. The remaining question is the magnitude of the error, particularly for the Southern California area.

By reviewing the list of reasons above it can be seen that the discrepancies should be minimal for the Southern California area. The stratiform nature of the predominant cloudiness eliminates many of the problems involving both inadequate satellite camera resolutions and the tendency of ground observers to overestimate cloud amount due to the vertical structure of the cloudiness. Additionally, past studies (Reference 2) show that satellite/ground correlations are best when the reported cloud amount is "less than four or greater than seven tenths sky cover." The strong U-shaped cloud-amount distributions of the Southern California area cause over 76% of the observations to fall within this high correlation category. Particularly in the case of clear or overcast (other than cirrus) conditions, in which over 50% of the Southern California observations fall, the satellite and ground observations shall agree exactly.

One remaining problem, then, is the presence of cirrus overcast. A review of the cloud-type listings suggests an overall satellite/ground cloud-amount discrepancy of the order of 5% due to this cause alone. This is in agreement with a comparison which was carried out between the high quality Nimbus I noontime AVCS data and the 1300 LST ground observations for San Diego which showed an approximately 7% discrepancy due to all causes. A previous study (Reference 3) showed a 10% discrepancy for the San Diego area, although the authors have since come to feel that this figure is too high.

Conclusions

Our general conclusion is that for the same relative area sizes the Cloud Climatology developed for the Southern California area, using ground observations, is quite representative of the cloudiness amounts that would be encountered in a satellite experiment. (The typical ground observation is representative of an area of about 30 n. mi. in diameter. If the area to be monitored using satellite data becomes significantly larger than this, the basic distributions of cloudiness will tend to become more bell-shaped than U-shaped.) An overestimation of cloudiness amounts of 5 to 7% by the ground-based data is to be expected. The available data were inadequate to establish any seasonal or diurnal variations in these discrepancy figures.

REFERENCES

1. Sherr, P. E., A. H. Glaser, J. C. Barnes and J. H. Willard, 1968: World-Wide Cloud-Cover Distributions for Use in Computer Simulations, Final Report under Contract No. NAS 8-21040, Allied Research Associates, Inc., Concord, Mass.

2. Barnes, J. C. and D. Chang, 1968: Accurate Cloud Cover Determination and Its Effects on Albedo Computations, Final Report under Contract No. NAS 5-10478, Allied Research Associates, Inc., Concord, Mass.

3. Barnes, J. C., D. Beran, and A. H. Glaser, 1967: Cloud Observation of Apollo Landmarks Derived from Meteorological Satellite Observations, Final Report under Contract No. 11-B-222113, Allied Research Associates, Inc., Concord, Mass.